Faculdade de Ciências e Tecnologia
UNIVERSIDADE DO ALGARVE

Hydrodynamic and Sediment Fluxes through the Inlets of the Ria Formosa

André Miguel Duarte Pacheco

Dissertação apresentada à Universidade do Algarve para obtenção do grau de Doutor em Ciências do Mar, da Terra e do Ambiente, Ramo Ciências do Mar, especialidade em Oceanografia Física

FARO, 2010

Faculdade de Ciências e Tecnologia
UNIVERSIDADE DO ALGARVE

Hydrodynamic and Sediment Fluxes through the Inlets of the Ria Formosa

by

André Miguel Duarte Pacheco

Dissertação apresentada à Universidade do Algarve para obtenção do grau de Doutor em Ciências do Mar, da Terra e do Ambiente, Ramo Ciências do Mar, especialidade em Oceanografia Física

Tese Orientada por:
Óscar Ferreira (Universidade do Algarve)
Jonathan Williams (Universidade de Plymouth, Reino Unido)

FARO, 2010

UNIÃO EUROPEIA
FEDER

FCT
Fundação para a Ciência e a Tecnologia

Dedicado a Belmiro de Almeida e à Cheila, sua filha

À minha Família, pela vossa constante presença

"Life is one big road with lots of signs. So when you riding through the ruts, don't you complicate your mind: flee from hate, mischief and jealousy; don't bury your thoughts; put your vision to reality…Wake Up and Live"
(Survival Album, "Wake Up and Live", Bob Marley)

Acknowledgements

Above all, I would like to express my gratitude to my supervisor Óscar Ferreira. His character, comprehension, enthusiasm and friendship made this thesis possible. There aren't enough words to express gratitude for his support and I only hope that we can work together for the coming years. A very special thanks to my other supervisor Jon Williams for giving me the opportunities I had in Plymouth, for all that I learnt with him and, above all, his friendship. Thanks also to Jon, Lu and Diego for the dinners, the parties, the fantastic walks and the good moments we shared together.

A very special thanks to Ana Vila Concejo and Brad Morris, with whom I share the enthusiasm of doing what I do and from whom I learn so much. They both are, without doubt, two models of professionalism, dedication and good team spirit.

Thanks also to Alveirinho Dias for his support and scientific advice.

This thesis could not have been done without the financial support for the fieldwork given by the project IDEM-Inlet Dynamics Evolution and Management at the Ria Formosa, under contract POCI/MAR/56533/2004; and also the Parque Natural da Ria Formosa and the Instituto Portuário dos Transportes Marítimos, which were always extremely helpful on providing historical data.

Thanks to all my colleagues who helped me during the thesis. The fieldwork, data processing, ideas on how to interpret the results, scientific discussions, relaxing moments, fieldwork trips, the early hours and long sunny days, the cold water and the endless summer times…well everything that builds up a thesis! This outcome is also their work. Here goes a list (and I hope no-one is missing!)…thank you: Aitana Vazquéz, Amaia Alegria, Ana Matias, Ana Rita Carrasco, Anna Zacharioudaki, Ángela Bouzas, Beta Berlow, Bruno Simeoni, Carlos Loureiro, Dae Dawson, Dan Buscombe, Davis Paula, Erwan Garel, Franscisca Rosa, Gerd Masselink, Jamie Mitchell, Javier

Alcántara-Carrió, Juan Baztan, Júlio Cunha, Isabel Mendes, Margarida Ramirez, Mara Nunes, Maria Bezerra, Maria Suarez, Mihalis Vousdoukas, Nejema Zergaoui, Paula Salge, Piet Harens, Ricardo Sánchez, Saul Reynolds, Susana Costas, Tiago Garcia, Tim Scott, Umberto Andriolo, Veit Bachmann, and Yaris Quintana. In general, thanks to all the CIMA group. To Simon Connor for your friendship and for being always available for correcting my English! To Pedro Almeida, the colleague and friend who was always available for help and with whom I shared most of the fieldwork days. You deserve a special recognition! Also, not forgetting the boat skippers, thanks to: Marinho, Janaca and, of course, the great Esmeraldo.

A special thanks to the people I love the most, the best friends any one can have, for their support, for helping me on the bad moments over the last 4 years (one was to lose part of my data…), and for sharing the good ones (and they were so many!). Thank you: Veiga and Laura, for being always there for me; Diogo, Mariana, Luís, Tomás, my friends from Porto; Joni, Inês, Fred, Catarina, Ricardo "Congo", Roberto, Ponga, R1, Simon, Seve, Denis, Helena, Cláudia, Ana Luísa, Benjamin, Bea, for sharing such good moments in the Algarve, mainly the ones at "Fonte da Murta"; Gastone Biondini and Cláudio Geneli, for the fantastic holiday in Italy; Julien Barde and Jamie Mitchell, two of the most inspiring persons I met in the way; and finally, to Daniel, Margarida and the little Matilde…thanks really, you always made me feel at home.

Thanks to Cheila for your support, love and endless friendship…I could not have made it without you :-)! And to my day-to-day company…my dog Reggae. Thanks to my family: Pai Alberto, Mãe Ilda, Avó Lídia, Marta, Pedro, Tiago, Aude, Atílio, Cristina, Rodriguinho and little Thomas. No words can express my gratitude, just a big smile!

Abstract

Research into the consequences of engineering works on the long-term behaviour of inlet systems has been hindered by the absence of suitable datasets, the shortcomings of existing formulae when applied to different inlets, and the difficulties particular to multi-inlet situations. Cross-sectional channel areas adjust to hydrodynamics and sediment transport conditions. The impacts of a new inlet on the adjacent shoreline can be unpredictable and are difficult to quantify. The coupling of morphology and hydrodynamics analysis should therefore be extended to all inlets in order to infer the stability of the overall system based on the distribution of the tidal prism through time and the patterns of inlet circulation and sediment transport.

Within this thesis both historical and present-day hydrodynamic data collected using high frequency equipment are combined to analyse the recent evolution and equilibrium of a multiple-inlet system. Methods for calculating sediment budgets, analysing the evolution of inlet parameters and determining present hydrodynamic and sediment transport patterns are coupled together, with the aim of improving understanding and prediction of tidal inlet morphodynamics. The results augment existing knowledge about multiple-inlet systems and improve understanding of their short- to medium-term stability.

The findings indicate that combining sediment budget calculation and inlet parameter analysis is useful for understanding historical sediment pathways and magnitudes, as well as for analysing the evolution of an inlet, or multiple-inlet system, towards equilibrium. Existing formulae for inferring inlet stability that relate cross-sectional area to tidal prism should be revised with a view to including other external variables (e.g. stratigraphic controls) and making their application more flexible to cope with the range of different inlet conditions.

Although it is generally acknowledged that most multiple inlets are unstable and cannot co-exist, detailed measurements of hydrodynamic variables obtained over complete spring and neap tidal cycles in a multiple-inlet system in Southern Portugal (Ria Formosa) indicate that the two main inter-connected inlets servicing an embayment (Faro-Olhão and Arrmona inlets) can coexist, at least over a time scale of several decades. Their coexistence cannot be explained simply using empirical equilibrium relations or inlet hydraulics.

Residual flow between the inlets appears to play an important role in enhancing their stability. The morphology of the inner channels connecting the inlets can play an important role in inlet stability by controlling the interconnections between the inlets. The capacity to exchange large portions of the tidal prism, while maintaining independent behaviour for the majority of the neap-spring tidal cycle, can contribute to the stability of multiple inlets by altering residual flow and, consequently, transport capacity. This can be particularly important for tidal conditions in which inlets can drain each sub-basin independently.

However, it is the availability of sediment stored in the ebb-tidal deltas (and its capacity to be carried into the inlets during storm events) that ultimately dictates the overall equilibrium, independently of hydraulic flushing capacity. If littoral drift is strong, ebb shoals trap significant quantities of sand. During periods of increased wave activity, the tide may not have the capacity to transport material away from the inlet mouth area, and the inlet will accumulate sand due to the shoreward migration of the ebb shoal. Such movement of sediment leads to the obstruction of the inlet channels, thereby affecting the hydraulic efficiency and eventually leading to inlet closure over the long term. The long-term equilibrium of sediment storage in the ebb-tidal deltas

must therefore be considered when analysing the possible equilibrium of multiple-inlet systems.

Regarding the techniques used, a statistical evaluation of the best method for extrapolating velocity measurements to the unmeasured areas of a vertical profile is presented. To calculate cross-sectional discharge, mean velocities and bed-friction velocities, custom Acoustic Doppler Current Profiler (ADCP) software makes use of theoretical models (e.g. 1/6 power-law and logarithmic law) to reconstruct velocity profiles based on models calibrated and tested for fixed current-meters The aim of this work was to define the best method to extrapolate velocities when using boat-mounted ADCPs, allowing the accurate calculation of the tidal prism, as well as increasing the reliability of the sediment transport estimations. The results revealed the logarithmic law to be more robust across different velocities and channel morphologies.

Quantification of sediment transport in tidal inlets remains a fundamental requirement for developing both conceptual and numerical modelling of tidal inlet function and evolution. Well-established empirical formulae were used to estimate bedload, suspended load and total sediment transport rates. The results compared favourably with direct and indirect field observations of sediment transport rates. Although subject to a range of errors, the methods adopted have helped to quantify net accretion/erosion and enabled evaluation of both the flushing and bypassing capacity of tidal inlets in the system. The work has increased knowledge of sediment dynamics in multiple inlet systems and identified appropriate approaches for the prediction of sediment transport in these environments. They may therefore assist in identifying evolutionary trends for a single tidal inlet or a multi-inlet system.

The approach and methodology followed in this study could be applied to other multiple-inlet systems around the world in an attempt to “design with nature”,

combining an understanding of sediment movement in a region, development projects and regional sediment-management actions.

Resumo

Os sistemas de "ilhas barreira" caracterizam-se pela presença de barras de maré que constituem a conexão entre as zonas lagunares e o oceano. A complexidade dos processos nestes sistemas está associada à diversidade de morfologias, hidrodinamismo e padrões de transporte sedimentar. O conhecimento científico destes processos é essencial para uma correcta gestão das barras de maré e é particularmente complexo em sistemas de barras múltiplas, como é caso da Ria Formosa.

Avaliar os impactes de longo termo da abertura artificial de uma barra requer séries de dados específicas e são difíceis de quantificar. A presente tese propõe-se colmatar estas ausências de informação, recorrendo ao desenvolvimento de novas metodologias de análise, obtenção e processamento de dados. A determinação dos padrões de circulação e dos fluxos de transporte sedimentares foi efectuada com recurso a equipamentos acústicos de alta-frequência e a formulações empíricas. O recurso à análise integrada de balanços sedimentares históricos, de parâmetros morfológicos e dos padrões actuais hidrodinâmicos permitiu avaliar a estabilidade do sistema e prever a sua evolução futura.

Em particular, os resultados da presente tese indicam o sucesso da integração destas metodologias na compreensão dos padrões históricos e presentes de fluxos de transporte, quer de água quer de sedimentos. Estas metodologias provaram igualmente a sua utilidade na análise da evolução da estabilidade de sistemas individuais e múltiplos de barras de maré, e são aplicáveis a qualquer sistema com características semelhantes a nível mundial.

Do decurso da presente tese, conclui-se que as formulações de equilíbrio que relacionam a área de secção com o prisma de maré devem ser revistas, de forma a incluir outras variáveis externas (tais como o controlo estratigráfico e a deriva litoral,

entre outros), de forma a permitir uma aplicação mais geral e flexível de acordo com as diferentes características das embocaduras e zonas costeiras adjacentes.

De acordo com evidências sugeridas por diversos autores, adquiridas sobretudo com recurso à modelação numérica dos fluxos e à morfologia das áreas de secção, os sistemas de barras múltiplas são instáveis e não podem existir a longo-termo. Este facto deve-se sobretudo ao grau de conexão hidráulica das barras através dos canais interiores, que resultará na dominância de escoamento da barra principal e no fecho das barras secundárias a esta conectadas. As medições dos padrões hidrodinâmicos efectuadas para ciclos de maré completos em regime de maré-viva e maré-morta para todas as barras do sistema da Ria Formosa, indica que as duas barras principais do sistema, Faro-Olhão e Armona, estão sempre em conexão. A avaliação da morfologia de ambos os sistemas, bem como da linha de costa adjacente, indica estabilidade múltipla de ambas as barras, pelo menos para escalas temporais de médio a longo-termo.

De acordo com as evidências decorrentes do trabalho efectuado, a avaliação do equilíbrio de barras múltiplas não pode ser efectuada com recurso a formulações empíricas ou à avaliação da capacidade hidráulica de uma barra. O transporte residual desempenha um papel importante, ao contribuir para a estabilidade destes sistemas, traduzindo-se em assimetrias de fluxo e na dominância enchente/vazante das barras. No entanto, são as elevadas quantidades de sedimentos armazenadas nos deltas de vazante, e os processos que contribuem para o seu transporte, que contribuem principalmente para a estabilidade morfológica das embocaduras e linha de costa adjacente. O transporte esporádico de elevadas quantidades de sedimentos para os canais interiores em períodos de elevada agitação marítima, condiciona a capacidade hidráulica das barras de maré e pode levar, inclusive, ao seu encerramento. Portanto, e face ao exposto, a avaliação do equilíbrio de sistemas de barras de maré, individuais ou múltiplos, requer

o estudo da volumetria de equilíbrio dos deltas de vazante, independentemente da capacidade hídrica das correntes de vazante de transportarem o sedimento para o largo.

A avaliação das técnicas e metodologias utilizadas no decurso desta tese revela igualmente algumas conclusões importantes. O recurso a perfiladores acústicos com tecnologia Doppler, manuseados a bordo de embarcações, permite a aquisição rápida e de elevada frequência de dados de velocidade de corrente, assim como a aquisição em tempo real da batimetria e largura das secções medidas. No entanto, possui como desvantagem a não aquisição de dados em determinadas áreas da secção: zonas marginais, superficiais e junto ao fundo. Estas últimas são essenciais na determinação da velocidade de corte e indispensáveis no cálculo do transporte sedimentar. No sentido de resolver esta limitação, recorre-se a modelos de extrapolação, tais como a lei exponencial ou logarítmica. No decurso desta tese efectuou-se uma análise estatística dos resultados de ambos os modelos. Conclui-se que a lei logarítmica deve ser usada preferencialmente na extrapolação destas velocidades, revelando-se mais robusta para diferentes magnitudes e direcções de corrente, bem como para diferentes morfologias das secções analisadas.

Os resultados de transporte de fundo e de suspensão, estimados com recurso a formulações empíricas calibradas localmente com dados de alta-frequência, e tendo em conta os processos de interacção ondas-corrente e rugosidade do fundo, comparam favoravelmente com as observações directas e indirectas de transporte para o sistema. Apesar da sua aplicação generalizada estar sujeita a uma série de erros, e de decorrer de simplificações várias, o método permite determinar a capacidade hidráulica das barras e estimar a capacidade destas na transposição de sedimentos provenientes da deriva litoral.

O conhecimento histórico e actual do transporte de água e sedimentos associados às barras de maré, possibilita determinar quais as intervenções necessárias a efectuar (dragagens, abertura e localização de barras, realimentação de praias, transposição sedimentar entre sectores, entre outros). Desta forma, e com o objectivo de alcançar um equilíbrio dinâmico baseado no conhecimento científico do sistema, os resultados da presente tese contribuem para aprofundar o conhecimento do mesmo. Esta informação possibilitará aos gestores costeiros conhecimento base na gestão regional dos sedimentos recorrendo aos processos naturais.

INDEX

List of Figures

List of Tables

CHAPTER I

Introduction

I.1 MULTI-INLET SYSTEMS

Tidal inlets are located within barrier island systems and are found throughout the world in a variety of geologic and oceanographic settings, primarily on coastal plain shorelines (FitzGerald, 1988). An inlet is defined as a tidal inlet when the flow of water is dominated by the tide as opposed to river discharge (Escoffier, 1940). Despite being complex coastal systems and difficult to model, tidal inlets are of great importance as navigation routes, sediment sources for adjacent beaches, and conduits that allow exchange of nutrients between backbarrier systems and the coastal zone (FitzGerald 1996). Tidal inlets strongly influence the overall dynamics of barrier island shorelines because they interrupt the wave-induced transport of sediment along the coast, affecting both the supply of sand to downdrift shorelines and erosional-depositional patterns on adjacent beaches. The degree to which barrier islands are affected by inlet processes is dependent on the number of tidal inlets and their size (FitzGerald, 1988).

The origin, morphology, hydrodynamics and stability of tidal inlets are highly variable due to a wide range in physical settings such as wave and tidal energy, sediment supply, origin of the backbarrier, bedrock geology, sea-level history, storm occurrence and anthropogenic factors (FitzGerald, 1996). Hayes (1979) was the first to recognize the important influence that tidal range has on tidal inlets and barrier morphology and, through the tidal range classification proposed by Davies (1964), he identified five general categories of shoreline and established their relationship with the presence or absence of barrier island systems and tidal inlets. According to Hayes' (1979) classification, multiple tidal inlets can occur on microtidal coasts (mean tidal range < 1m), characterised by long, narrow, straight barriers with widely spaced inlets; whilst low mesotidal coasts (mean tidal range 1-2 m) are generally characterised by an increased number of small tidal inlets, normally wave dominated (FitzGerald, 1996),

and high mesotidal coasts (mean tidal range 2-3.5 m) may have abundant tidal inlets and the coast, although mixed-energy, is normally dominated by tidal processes. Along low-macrotidal (mean tidal range 3.5-5 m) and macrotidal coasts (mean tidal range > 5 m), barriers do not develop. According to FitzGerald (1988), there is a strong correlation between barrier islands and tidal range/wave energy, which also controls the size and number of tidal inlets.

The existence and persistence of multiple tidal inlets in coastal systems is fundamental for understanding issues such as flushing capability, navigability, and beach/barrier stability, as these depend on factors not found in single-inlet systems. According to Salles et al. (2005), multiple inlet systems should not be approached in terms of the stability of each inlet, but focus on their persistence through time.

Multiple tidal inlet systems, such as the Ria Formosa, are hydrodynamically connected, and therefore a morphological change in a given inlet will/should/could modify the hydrodynamic behaviour of other inlets and adjacent channels. These include changes to the tidal prism, generation of residual discharge and alteration of the non-linear tidal distortion signal (Salles et al., 2005). These changes are, in general, a function of channel hydraulics, i.e. tidal prism, which is a measure of the water exchange through the inlet. Thus, when a new inlet is opened and stabilised, its tidal prism will increase until it reaches equilibrium between its cross-section and the volume of water flowing through the inlet. Morphological changes can occur in areas adjacent to the new inlet over years to centuries, and coastal response to engineering stabilisation may extend far updrift and downdrift of the inlet. In a multiple tidal inlet system the changes can be more dramatic because the current field will change completely, inducing short- and long-term impacts on water circulation through the other inlets.

Lack of water oxygenation and nutrient fluxes, navigability constraints and coastal hazards are likely to occur as a result of human intervention.

I.2. THE RIA FORMOSA IN THE CONTEXT OF INTERNATIONAL RESEARCH ON TIDAL INLETS

The Ria Formosa is a highly dynamic multi-inlet barrier island system located in the Algarve region of Southern Portugal. Several economic activities take place in the system, e.g. aquaculture, salt production, fishing, shellfish culture, shipping, mining and tourism. Presently, the Ria Formosa's shellfish production represents 60 % of the Portuguese total . The combination of different and often competing economic activities makes management of the Ria Formosa a very difficult task for decision makers in the region.

The origin of the Ria Formosa is not clear, and several geological hypotheses for the system's genesis have been proposed (Dias, 1988; Pilkey et al., 1989; Bettencourt, 1994). Dias (1988) and Pilkey et al. (1989) followed the Hoyt (1967, cited in Pilkey et al., 1989) model, suggesting that the origin of the sand islands is related to changes in sea-level during and after the glacial period, i.e., the Ria's Holocene evolution fits within the classical shoreface transgression model.

The Ria Formosa system has been the subject of several PhD theses and scientific research papers, especially during the second half of the 20th century (Weinholtz, 1964; Dias, 1988; Pilkey et al., 1989; Andrade, 1990). Scientific interest in the Ria Formosa inlets is particularly related to the artificial relocation of the Ancão inlet in 1997 and the Fuzeta inlet in 1999. Inlet relocation is a novel coastal management tool that, when applied to a migrating inlet, consists of opening an inlet within the historic migration path of another inlet. These engineering interventions - the 3rd and 4th such relocations

in the world - and the subsequent publication of their implementation (i.e. Balouin, 2001; Morris et al. 2001, 2004; Salles, 2001; Salles et al., 2005; Vila-Concejo et al. 2002, 2003, 2004, 2006; Vila-Concejo, 2003; Williams et al. 2003a,b) made Portugal an international reference in tidal inlet studies. These publications are outcomes of the "Inlet Dynamics Initiative" (INDIA Project), supported by the European Commission (Contract MAS3-CT97-0106). INDIA's aim was to gain a better understanding of the interactions between tides, waves, currents and sedimentary processes at work in the European coastal zone to better predict change. In the Algarve, fieldwork activities centred on the Ancão Inlet, using state-of-the-art field equipment to study present-day processes (Williams et al., 2003a,b) and a range of numerical models to extend the spatial and temporal range of the measurements.

A doctoral thesis by Salles (2001) and a subsequent paper (Salles et al., 2005) are the two main studies on multiple inlet hydrodynamics and stability that focus on the Ria Formosa inlets. By combining a numerical simulation of inlet flow with a semi-empirical approach of inlet equilibrium, numerical simulations of the hydrodynamics of the Ria Formosa multi-inlet system were performed. These numerical simulations were mainly based on creating realistic physical disturbance (changes to inlet cross-sections) and analysing the hydrodynamic response of the multi-inlet system to those disturbances. The authors showed the importance of nonlinear processes in the hydrodynamics of multi-inlet systems, such as tidal distortion, ebb/flood dominance and residual flow patterns, and reinforced the need to consider these factors when analysing inlet stability in such systems. Whilst these works greatly contributed to understanding the importance of nonlinear processes in the hydrodynamics of multi-inlet systems, the modelling results were not validated by field measurements, or in terms of current or sediment transport. The tidal prism and sediment transport through the inlets (i.e. trends

and magnitudes), which would allow the estimation of the present and historic sediment budget, was not presented in the works of Salles. Moreover, Salles' scenarios for cross-sectional changes do not accurately reflect the historical evolution of the system; neither achieving a state of "dynamic equilibrium".

I.3 THESIS AIM

As demonstrated in the previous section, knowledge about the Ria Formosa inlets has improved through the last few years. There have been studies on the migration and current behaviour of some of the inlets of the Ria Formosa; however, data on the tidal prism and sediment fluxes is scarce. Scientific knowledge of these processes is considered to hold the key to correct management of inlets and surrounding areas.

As well as quantifying the sediment transport through the inlets, determining ebb or flood dominance for each inlet is another objective of the present thesis. This will enable sediment budgets to be determined and help predict the future evolution of these systems. The results are expected to show how dynamic equilibrium can be achieved, with potential applications for the formulation of integrated coastal management policies. Sediment budgets for coastal areas are an essential tool for determining the amount of sediment that can be removed from the system with minimal environmental impact. Additionally, the quantification of relationships between tidal prism and sediment fluxes in a multi-inlet system has never been previously attempted at this scale, and may therefore find application in other, similar systems worldwide.

The thesis includes an in-depth study of the Ria Formosa inlets, determining tidal prism distribution and circulation patterns, sediment fluxes and recent historical evolution in relation to anthrophic influence. The main chapters of this thesis correspond to scientific papers that were all submitted to international scientific

journals. The advantage of presenting a thesis by articles is that each chapter can be read independently; however, this format has the disadvantage of repeating certain details (e.g. study area description). While it is acknowledged that this repetition may hinder the flow of the text, the format has been maintained to preserve the integrity of the original scientific papers.

I.4 THESIS OUTLINE

Considering the importance of recent anthropogenic modifications in the Ria Formosa and the study of their impacts in the context of international research on inlet dynamics, the main objective of this thesis is to analyse evolutionary trends in the hydrodynamic and sediment fluxes of the system. The thesis comprises seven chapters:

- A brief introduction is given in Chapter I, referring to the socio-economic importance of the Ria Formosa System and providing a scientific justification for the work undertaken;
- Chapter II describes the various methods used to calculate sediment budgets on the basis of historical documents and gives an example of their implementation to the Faro-Olhão inlet, the main inlet of the Ria Formosa system. The work was published in Marine Geology on the 17th July 2007:

  Pacheco, A., Vila-Concejo, A., Ferreira, Ó., Dias, J.A., 2008. Assessment of Tidal Inlet Evolution and Stability Using Sediment Budget Computations and Hydraulic Parameter Analysis. *Marine Geology* 247, 104-127.
- Chapter III evaluates methods for extrapolating velocity measurements to the unmeasured areas of Acoustic Doppler Current Meter (ADCP) profiles, selecting the best method for accurate tidal prism values, as well as increasing the reliability

of the sediment transport estimations. The work was submitted to Continental Shelf Research and is currently under review:

Pacheco, A., Faísca, L., Almeida, L., Ferreira, Ó., Williams, J.J., Dias, J.A. (under review). A statistical evaluation of models for extrapolating current velocities from boat-mounted ADCP profiles. *Continental Shelf Research*.

- Chapter IV focuses on tidal prism distribution through the multiple-inlet system, based on detailed current measurements taken at all of the inlets of the Ria Formosa, through which residual flows and flood/ebb dominance could be determined. It was published in Marine Geology on the 15th March 2010:

  Pacheco, A., Ferreira, Ó., Williams, J.J., Garel, E., Dias, J.A., 2010. Hydrodynamics and equilibrium of a multiple-inlet system. *Marine Geology* 274, 32-42.

- Chapter V uses a combination of several transport models to estimate trends in net bedload, suspended and total transport, providing the basis for an annual sediment budget and a conceptual model. This work was recently submitted to Estuarine and Coastal Shelf Science, Elsevier, and builds on an earlier paper that was published in Journal of Coastal Research:

  Pacheco, A., Williams, J.J., Ferreira, Ó., Garel, E., Reynolds, S. (submitted). Application of Sediment Transport Models to a Multiple-Inlet System. *Estuarine and Coastal Shelf Science*.

  Pacheco, A., Williams, J.J., Ferreira, Ó., Dias, J.A., 2009. Evaluation of shear stress computation at a tidal inlet using different methods. *Journal of Coastal Research* 56, , 1385-1389.

- Chapter VI examines multiple tidal-inlet stability based on historical morphological changes–to infer the equilibrium state and future evolution of the system, with particular emphasis on the impact of engineering modifications. This work was recently submitted to *Earth Surface Processes and Landforms*:

  Pacheco, A., Ferreira, Ó., Williams, J.J. (submitted). Long-term Morphological Impacts of the Opening of a New Inlet on a Multiple Inlet System. *Earth Surface Processes and Landforms*.

- Chapter VII, the final chapter, presents the general conclusions of the study and proposes future directions for multiple tidal-inlet research, both nationally and internationally.

I.5 REFERENCES

Andrade, C. F., 1990. O Ambiente Barreira da Ria Formosa, Algarve-Portugal. PhD Thesis, Universidade de Lisboa. 627 p. (in Portuguese).

Balouin, Y., H. Howa, and D. Michel. 2001. Construction of the swash platform associated to an ebb-tidal delta during fair weather conditions, The Barra Nova inlet, South Portugal. *J. Coast. Res*. 17, 4784–791.

Davies, J.L., 1964. A morphologic approach to world shorelines. *Zeits Geomorphol.*, 8, 127-142.

Dias, J.M.A. 1988. Aspectos geológicos do litoral algarvio. Geonovas (Lisboa), 10, 113-128 (in Portuguese).

FitzGerald, D.M., 1988. Shoreline erosional-depositional processes associated with tidal inlets. In: Hydrodynamics and Sediment Dynamics of Tidal Inlets. Lecture Notes on Coastal and Estuarine Studies 29, 186-225.

FitzGerald, D.M., 1996. Geomorphic Variability and Morphologic and Sedimentologic Controls on Tidal Inlets. *J. Coast. Res.* SI 23, 47-71.

Hayes, M.O., 1979. Barrier island morphology as a function of tidal and wave regime. In Leatherman, S.P., (Ed.), Barrier Islands: From the Gulf of St. Lawrence to the Gulf of Mexico. Academic Press, New York, N.Y., 1-27.

Jarret, J.T., 1976. Tidal Prism-Inlet area relationships. GITI Report, vol. 3. U.S. Army Corps of Engineers, Waterways Experiment Station, Vicksburg, MS.

Morris, B.D., Davidson, M.A., Huntley, D.A., 2001. Measurements of the response of a coastal inlet using video monitoring techniques. *Mar. Geol*. 175, 251-272.

Morris, B.D., Davidson, M.A., Huntley, D.A., 2004. Estimates of the seasonal morphological evolution of the Barra Nova Inlet using video techniques. *Cont. Shelf. Res.* 24, 263-278.

O'Brien, M.P., 1969. Equilibrium Flow Areas on Inlets on Sandy Coasts. J. Waterw. Harb. Div. 95 (WW1), 43-52.

Pilkey, O.H., Neal, W.J., Monteiro J.H., Dias, J.M.A., 1989. Algarve Barrier Islands: a noncoastal-plain system in Portugal. *J. Coast. Res.* 5(2), 239-261.

Salles, P., 2001. Hydrodynamic Controls on Multiple Tidal Inlet Persistence. PhD Thesis, Massachusetts Institute of Technology and Woods Hole Oceanographic Institution, 272 pp.

Salles, P., Voulgaris, G., Aubrey, D., 2005. Contribution of nonlinear mechanisms in the persistence of multiple tidal inlet systems. *Estuar. Coast. Shelf. Sci.* 65, 475-491.

Vila-Concejo, A., 2003. "Sediment Dynamics and Tidal Inlet Relocation in Mixed-Energy Settings: The case of Ancão Inlet (Algarve – Portugal). PhD Thesis, Universidade do Algarve. 197p.

Vila-Concejo, A., Matias, A., Ferreira, Ó., Duarte, C., Dias, J.M.A., 2002. Recent Evolution of the Natural Inlets of a Barrier Island System in Southern Portugal. *J. Coast. Res*. SI 36, 741-752.

Vila-Concejo, A., Ferreira, Ó., Matias, A., Dias, J.M.A., 2003. The first two years of an inlet: sedimentary dynamics. *Cont. Shelf. Res.* 23, 1425-1445.

Vila-Concejo, A., Ferreira, Ó., Matias, A., Morris, B.D., Dias, J.A., 2004. Lessons from inlet relocation: examples from Southern Portugal". *Coast. Eng.* 51 (10), 967-990.

Vila-Concejo, A., Matias, A., Pacheco, A., Ferreira, Ó., Dias, J.M.A., 2006. Inlet hazard determination in the Ria Formosa barrier island system. *Cont. Shelf. Res.* 26 (9), 1045-1060.

Williams, J.J., Bell, P.S., Thorne, P.D., 2003a. Field measurements of flow fields and sediment transport above mobile beds. *J. Geophy. Res.* 108, NO. C4, 3109, doi:10.1029/2002JC001336.

Weinholtz, M.B., 1964. Contribuição para o Estudo da Evolução das Flechas de Areia na Costa Sotavento do Algarve. Separata do Boletim Trimestral de Informação do D.G.S.H. 14. (in Portuguese).

Williams, J.J., O'Connor, B.A.O., Arens, S.M., Abadie, S., Bell, P., Balouin, Y., Van Boxel, J.H., do Carmo, A.J., Davidson, M., Ferreira, Ó., Heron, M., Howa, H., Hughes, Z., Kaczmarec, L.M., Kim, H., Morris, B., Nicholson, J., Pan, S., Salles, P., Silva, A., Smith, J., Soares, C., Vila-Concejo, A., 2003b. Tidal inlet function: field evidence and numerical simulation in the INDIA project. *J. Coast. Res.* 19(1), 189-211.

CHAPTER II

Assessment of tidal inlet evolution and stability using sediment budget computations and hydraulic parameter analysis

Abstract

Research into the response of coastlines to the opening and stabilisation of inlets has been limited by the availability of suitable data, the shortcomings of existing formulae when applied to different inlets, and the difficulties particular to multi-inlet situations. Our appraisal of methodologies for studying inlet dynamics leads us to formulate a new approach for investigating inlet evolution and stability based on combining sediment budget computations (using best estimates and uncertainty analysis) and inlet hydraulic parameter analysis.

The approach developed is applied to a stabilised inlet, located within a multi-inlet system (Faro-Olhão Inlet, Ria Formosa, Southern Portugal), which was opened starting 1929 and has since been dredged periodically to maintain navigability. A series of digital maps was produced based on multi-year data acquired from charts, surveys, and aerial photos. The maps were used to compute sediment volumes for six coastal cells delineated on the basis of the morphological features of the inlet. Cell volumes and fluxes were calculated for three periods (1929-1962, 1962-1978, and 1978-2001), and overall sediment budgets were calculated for the latter two periods. Inlet hydraulic parameters measured included tidal prism, inlet channel cross-sectional area and hydraulic radius, and maximum depth of the inlet throat, and were tracked over 13 bathymetric surveys from 1947-2004. The computed budget reveals that the inlet is only at present reaching volumetric equilibrium. However, the analysis of channel cross-sectional area and radius indicates parameter stability around 1978-1985, 20-25 years before the inlet started to reach volumetric equilibrium. It is hypothesised that the observed stability in parameters for the

inlet post-1978 is related to the presence of fixed jetties and to a stratigraphic control that prevents further deepening, and not to the achievement of a dynamic equilibrium.

The findings indicate that the coupling of sediment budget computation and inlet parameter analysis is useful for understanding historical sediment pathways and magnitudes, and for analysing the evolution of an inlet towards equilibrium. Although the analysis of inlet parameter evolution is valuable for examining the locational/geometrical stability of an inlet, it needs to be used in conjunction with sediment budget computations in order to properly infer inlet equilibrium. Moreover, existing formulae used to infer inlet stability, which relate cross-sectional area to tidal prism, should be reviewed with a view to including other external variables (e.g., stratigraphic controls) and to making their application more flexible to cope with the range of different inlet conditions. For multi-inlet systems, the coupling of morphology and hydrodynamics analysis should be extended to all inlets in order to infer the stability of the overall system based on the distribution of the tidal prism through time and the patterns of inlet circulation and sediment transport.

Keywords: tidal inlet; equilibrium; tidal prism; cross-section area; volume computation; sediment budget

II.1. INTRODUCTION

Tidal inlets rate among the most dynamic of coastal features. The complex temporal and spatial interactions of waves, tides, and currents create and constantly modify the morphology and the sedimentary structure of tidal inlets. Quantification of the magnitudes, rates, and patterns of geomorphic change is central to sediment budget calculations, to the estimation of dredging requirements, and to the assessment of the extent to which inlet dynamics affect adjacent beaches (Stauble, 1998). Better understanding of the dynamics and evolution of inlets can be achieved by comprehensive investigations of sediment budgets, which are essential for understanding complex inlets whether in natural or engineered condition (Rosati and Kraus, 1999). However, the main constraint on performing sediment budget computations is the paucity of good quality datasets (comprising frequent observations over long periods) and site information, as well as the need to estimate best values and their associated uncertainties which derive from a number of error sources.

Research into the consequences of engineering works on the long-term behaviour of inlet systems has been hindered by the absence of such datasets. This paper investigates the importance of using sediment budget computation jointly with inlet parameter analysis in order to understand coastline changes resulting from the opening and stabilisation of tidal inlets. Existing methods used to examine inlet evolution are evaluated, and a new methodology is developed which is demonstrated with application to the artificially stabilised Faro-Olhão Inlet in Southern Portugal. The study applies new concepts developed by Rosati (2005) in order to compute a sediment budget, with an emphasis on uncertainty calculations. However, instead of using LST rates and computing several

"representative budgets," our approach is to consider the rate of longshore transport as incognito and immutable, coupling the obtained balanced budget with inlet parameter analysis in order to understand sediment pathways and accretion/erosion tendencies within each coastal cell.

II.1.1 Sediment Budgets

A sediment budget is a computation of sediment gains and losses, or sources and sinks, within a specific control volume (or cell) over a given time, and can be expressed by

$$\sum Q_{source} - \sum Q_{\sin k} - \Delta V + PL - R = \mathrm{Re}\,sidual \qquad \text{(II.1)}$$

where: Q_{source} and $Q_{\sin k}$ are the sources and sinks to the control volume, respectively; ΔV is the net change in volume within the cell; *PL* and *R* are the amounts of material placed into and removed from the cell, respectively; and Residual represents the degree to which the cell is balanced (Rosati, 2005). The accounting for uncertainties in the various components that comprise the sediment budget yields an indicator of the reliability of the budget, as well as bounds for judging the range of values that might be taken by the more uncertain quantities (Kraus and Rosati, 1999). Several studies of sediment budget computations have applied Eq. II.1 to estimate values of the best-known variables and solve the lesser-known terms. A detailed review of the various methods used for estimating best values in order to perform sediment budget computations is provided by Rosati (2005). Rosati has also constructed a personal computer-based program, the Sediment Budget

Analysis System (SBAS) (Kraus and Rosati, 1998; Rosati and Kraus, 1999), which enables sediment budget computations to be constructed and formulated within a georeferenced framework. The program relies on the importance given to the calculation of uncertainty, considered to be a central element of modern data treatment (Rosati, 2005).

Uncertainty enters through limited knowledge of changes in ebb- and flood-tidal delta sand volumes, and of the paths and relative magnitudes of longshore sediment transport (LST). When a new inlet is formed, sand is withdrawn from the longshore transport system until the ebb-tidal delta attains an equilibrium volume. Over long time scales, the total amount of sand stored in an ebb-tidal delta is reasonably constant if the inlet is in equilibrium. However, measuring variation in the quantity of sediment stored in an ebb-tidal delta over time requires historical datasets that are often either non-existent, unavailable, or unreliable. Sediment budgets often fail to present accurate values due to the difficulties in delimiting coastal cells and computing their volumes, assigning historical dredging and beach nourishment volumes and, most importantly, assigning values to Q_{source} and $Q_{\sin k}$, essential for determining rates of LST. Typically, the total (or gross) LST rate is computed using the Coastal Engineering Research Center (CERC) formula (SPM, 1984). However, the assumptions made in the development of the CERC formula, and its treatment of uncertainty, raise questions concerning its value for performing sediment budget computations.

II.1.2 Inlet Hydraulics and Stability

Tidal inlets display two types of stability: locational and geometrical (Mason, 1986). For inlets stabilised with two jetties, there is no migration and thus they possess locational stability. However, a stabilised inlet may have geometrical instability if its cross-sectional area (A_c), size, and shape change (O'Brien, 1969; Jarret, 1976). These geometrical changes are in general a function of variations in channel hydraulic parameters such as tidal prism (P), the volume of water exchanged between an estuary and the open sea during a tidal period. Several studies have presented empirical formulas relating A_c to P, including O'Brien's (1969) equation which relates the minimum equilibrium cross-section area with the volume of water flowing into or out of an inlet in response to tidal prism fluctuations. A more precise method of prism determination is the cubature method (Jarret, 1976), which takes into account the time required for a tide to propagate through a bay, rather than assuming a uniform rise and fall of the bay tide.

In the first analytical approach to inlet stability analysis, Escoffier (1940) proposed a diagram based on the plotting of two curves: the first being the maximum cross-sectionally averaged velocity (U_m) curve, produced by varying A_c; and the second the equilibrium velocity curve (U_E) (a stability criterion curve such as O'Brien's (1969) and Jarret's (1976) tidal-prism versus cross-section area relationship). These formulations are widely used for inlet stability evaluation and for engineering design projects.

Bruun (1978) considered tidal inlet stability as a function of tidal prism and sediment inflow capacity, including (for the first time) littoral drift in inlet stability analysis. Gao and Collins (1994a; 1994b) followed this with several analytical approaches that included the effect of independent variables (e.g. flood- and ebb-tidal durations, tidal prism, longshore

drift) and dependent variables (e.g. cross-sectional mean current speeds for flood- and ebb-tidal phases, width of the entrance channel) on equilibrium cross-sectional area.

An alternative approach to tidal inlet stability was taken by Van de Kreeke (1985), whose analysis was based on the shear stress value (τ_b). The approach characterised transport capacity as the maximum of τ_b during a tidal cycle, using this criterion for a stability analysis in which an equilibrium interval for the stable A_c was calculated. Van de Kreeke extended the approach to multiple inlet systems by considering the changes on the total tidal prism caused by the opening of a new inlet and adopting the closure curve method developed by Escoffier (1940).

II.1.3 Sediment Pathways in Tidal Inlets

The three main morphological features in tidal inlets are the inlet channel and the two adjacent sand bodies that form in the ocean and bay respectively. Sand transported into tidal inlets is moved seaward to ebb-tidal deltas by ebb-currents or landward onto flood-tidal deltas by flood currents. Ebb-tidal deltas can have a significant impact on the local coastal sedimentary budget, acting as valves on the coastal sedimentary supply, regulating the sand exchange between estuaries or lagoons and the open coast, and also trapping the longshore sediment transport (Hicks and Hume, 1997). The surface shape of an ebb-tidal delta determines how wave energy is focused on adjacent coastal beaches and how waves propagate into the inlet, and thus, influence shoreline evolution on the adjacent beaches and within the inlet (Buonaiauto and Kraus, 2003).

Whereas in general ebb-tidal deltas can be heavily modified by wave action, Walton and Adams (1976) showed that the tidal prism governs the volume of sand contained in the ebb-tidal delta. The same authors proposed an empirical equation, which was further validated for inlets in Florida by Marino and Mehta (1987). Walton and Adams' (1976) formula exhibits some scattering of data related to inaccuracies in the measurement of the delta volume (Mason, 1986) and it does not account for cyclic changes in the ebb-tidal delta volume that may occur at individual inlets (FitzGerald, 1996). Improvement of the formula will require the inclusion of natural volumetric variability of the ebb-tidal deltas, caused by many secondary external controls such as sediment supply, basin geometry, sedimentation history, and regional stratigraphy, all of which influence inlet behaviour (FitzGerald, 1996).

II.2 SEDIMENT BUDGET COMPUTATION AND INLET STABILITY ANALYSIS: METHODOLOGICAL CONSIDERATIONS

II.2.1 Data Acquisition and Processing for Sediment Budget Computation

In order to measure and evaluate how an inlet has evolved, both in its natural configuration and after the imposition of engineering structures, specific data sets are required. Several types of data can be analysed to determine the sediment budget on the inlet area: (1) existing plans, charts, and surveys since the time of the inlet opening until the present; (2) vertical aerial photographs; and (3) existing literature including published papers, theses, and technical reports. These datasets can be compiled using GIS software, which enables all data to be georeferenced to the same datum. The georeferenced information, in particular the topo-bathymetric maps, can be used to obtain digital contour maps for each year. Different budget cells are able to be defined and several operations

performed, including the computation of volume, the digitisation of the coastline, and the designation of individual areas of accretion/erosion between consecutive years.

II.2.2 Cell Compartments and Computation

Defining cell compartments in order to perform volume computations is dependent on the quality of information that may be available. Part of the main morphologic features of an inlet may be absent in some topo-bathymetric surveys and aerial photographs, making it difficult to properly identify its boundaries. GIS software can help to identify main cell compartments; however, in most cases, several methods need to be combined in order to compute volumes for a given period. Four areas corresponding to the main morphologic units of an inlet system can be distinguished: (1) the inlet channel; (2) the ebb-tidal delta; (3) the flood-tidal delta; and (4) the adjacent updrift and downdrift coastline.

A straightforward method to compute volume changes in cells is the difference map method (DMM) (Stauble, 1998). The DMM consists of subtracting the surface of one year from the surface of another year, thereby creating an elevation difference map between consecutive surveys. Several methods of surface gridding can be used to fit a rectangular gridded surface (or digital terrain model) to obtain digital bathymetric charts (Hicks and Hume, 1997). Such surfaces can be easily constructed using a software package such as SURFER® 8, following the quality control methods suggested by Hicks and Hume (1997), or using other programs such as MatLab® (The Mathworks, Inc). However, the full capability of using this method can be achieved only for cells that can be overlain (i.e., for cells whose geographic boundaries are the same from one year to the next). For example, the DMM method cannot be applied successfully to other cells of inlet systems, such as

tidal deltas, where the available information is, in most cases, scarce or non-existent. In this case, other methodologies need to be used and some values must be assumed or estimated, increasing the uncertainty of volume computations.

One of the main difficulties when computing the amount of sediment stored in both ebb- and flood-tidal deltas concerns the definition of their boundaries (landward, seaward, updrift, and downdrift). In most inlet systems, the boundaries of these morphological features change as the result of accretion/erosion processes, and therefore cannot be overlain. Standardised techniques to identify these boundaries do not exist. In the case of the ebb-tidal delta, the boundaries can be determined by analysing the deflection of the contours and the angle the contours make with the typically straight and parallel coastal bathymetry (Stauble, 1998), allowing the individualisation of an ebb-delta area. The delta volume (V_e) can be computed using the average thickness method (ATM), which involves multiplying the individual delta area by the average thickness of the ebb-tidal delta (Z_e):

$$V_e = [\int_{Ll}^{Sl} Ed(x) - Nd(x)]\, Z_e \qquad \text{(II.2)}$$

Where: *Nd(x)* represents a no-delta profile obtained from a bathymetric chart in an area where no delta exists (i.e., a representative beach profile from the beach berm/dune to the depth of closure); and *Ed(x)* represents the average ebb delta profile obtained within the area defined by the individualised boundaries (Fig. II.1) and the integral interval of *Ll* and *Sl*, the landward and seaward boundaries, respectively.

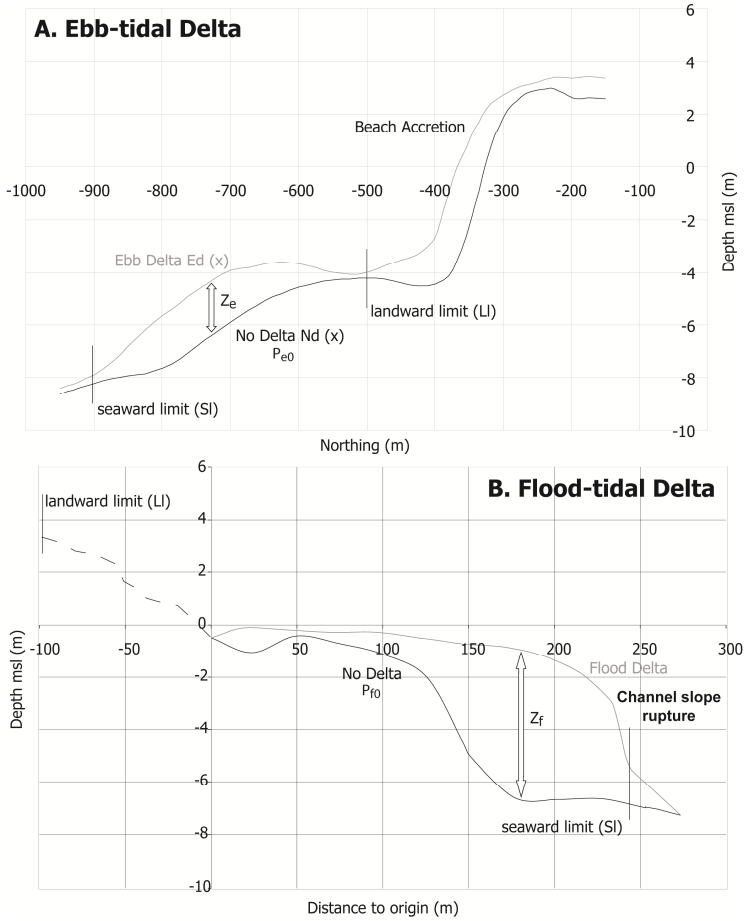

Figure II.1 Ebb- and flood-tidal delta boundaries used to perform volume calculations. Annotations include the landward limit (*Ll*), the seaward limit (*Sl*), the no-delta profile (*Nd*), the ebb-delta profile (*Ed*), and the average thickness of both deltas (Z_e and Z_f)

The computation of the volume stored in the flood-tidal delta is more difficult than in the ebb-tidal case, because these areas are not often fully bathymetrically surveyed (due to their partial supra-tidal extent). In addition, these areas are usually incompletely photographed during aerial surveys due to their location and extent. In such cases, GIS software can be extremely helpful in delimiting the boundaries, under which circumstances the ATM method used for the ebb-tidal delta volume computation can be employed to

determine the flood-tidal delta volume (V_f), by multiplying the area of the delta (A_f, extracted using GIS software) by the average thickness of the delta (Z_f):

$$V_f = [\int_{Ll}^{Sl} Fd(x) - Nd(x)]\, Z_f \qquad \text{(II.3)}$$

Where: *Nd(x)* represents a no-delta profile obtained from a bathymetric chart in an area where no delta exists (i.e. a profile representative of the normal channel slope without developing any flood delta); and *Fd(x)* represents the average flood delta profile obtained within the area defined by the individualised boundaries (Fig. II.1) and the integral interval of *Ll* and *Sl*, the landward and seaward boundaries, respectively.

Computation of the effects on the adjacent coast of opening an inlet is based on data taken from beach profile databases. However, in most cases these databases are incomplete due to deficient data storage or the complete absence of beach surveys. Rosati (2005) uses the active depth (A_D), which represents the part of the beach profile that is eroding or accreting during the time period under consideration, and is typically defined by the absolute sum of the berm crest elevation (B) and the depth of closure (D_c). However, there are several cases where even B values are absent or are difficult to identify using aerial photography analysis. In these cases, the feature selected to represent the position of the coastline can be the dune/beach limit, identified by the presence and density of dune vegetation. An arbitrary reference line following the orientation of adjacent dune fields can be established and several shore-normal transects defined. Using GIS software, different accretion and/or erosion polygons can be sketched between surveys and each polygon area computed which allows a coastline change area (C_a) to be obtained between two surveys.

The available topographic data can then be used to determine an average active elevation, Z_a, which represents the vertical extent of the beach profile that is facing erosion or accretion over the chosen period. The Z_a value is the absolute sum of the average height of the pre-existing dune field, h_d, and the depth of closure for the area, h_c.

The method assumes that any parcel added to or removed from each adjacent coastline during a given period would have a beach stock volume similar to the typical beach profile, defined in terms of the average height of the pre-existing dune field and the depth of closure. The adjacent coastline volume changes (V_c) can then be obtained by:

$$Vc = Z_a C_a \tag{II.4}$$

II.2.3 Engineering Activities

The quantification of historical sediment removal (R) from, and placement (PL) into, an opened inlet is problematic due to the usual lack of historical reports regarding locations, timings, and volumes of dredged and placed material. Kraus and Rosati (1998) and Rosati (2005) describe several methods for estimating sediment volumes and provide guidance for assigning associated uncertainties. The comparison of predredging and postdredging surveys can give accurate estimates, but when such surveys are not available for the whole period of interest, some assumptions can be made in the computation of sediment budgets. For example, a jettied inlet and its navigable channel require a particular annual dredging rate in order to prevent infilling processes which would otherwise cause navigation problems. In most cases, the annual dredging rate can be obtained from overlaying recent

surveys and computing volumetric variation. The value(s) can be then compared with the annual dredging report. Assuming that the infilling rate is constant through time, the annual dredging rate can be used to compute the value of *R*. The uncertainty of this method will decrease if several surveys and dredging reports can be analysed and an average value extracted. For determining *PL*, the same principles apply.

II.2.4 Best Estimate and Uncertainty Analysis

Sub-section II.2 presented examples of methodologies used to assign historical volumes to the main morphological features of an inlet system. An equally important issue regarding the estimation of the volume of a cell is to report its associated uncertainty. Measured or reported values entered into a sediment budget calculation consist of a best estimate (BE) and its uncertainty (Kraus and Rosati, 1998). If the quantity entering the budget is expressed as a product or quotient of independent variables as $X = xyz$ or as xy/z, then the maximum uncertainty (δX_{max}) and the root-mean-square (rms) uncertainty (δX_{best}) associated with the volume computation can be obtained (Rosati, 2005):

$$(\delta X / x)_{\max} = \partial x / x + \partial y / y + \partial z / z \qquad \text{(II.5)}$$

and

$$(\delta X / x)_{best} = [(\partial x / x)^2 + (\partial y / y)^2 + (\partial z / z)^2]^{0.5} \qquad \text{(II.6)}$$

The rms uncertainty treats the relative uncertainty of a product or quotient as being equal to the sum of the relative uncertainties of each term forming the product or quotient,

i.e., the individual uncertainties are independent and random. Thus, rms uncertainty based on the δX_{best} accounts for the uncertainty by presenting a value that is not an extreme such as δX_{max}. Further information about the rms treatment can be obtained in Kraus and Rosati (1998) and Rosati (2005).

Hick and Hume (1997) determined sand volumes and bathymetric change for an ebb-tidal delta by analysing the best surface gridding method and assessing the optimal survey line spacing and direction based on the surveyed topography. The methodology proposed by those authors should be followed to obtain digital bathymetric charts, using different grid-fitting methods (Kriging, Triangular, and Radial). The accuracy of the surface interpolation is determined by computing the difference between the elevation of the verification point and the elevation of the surface model at the same location (cross validation and residuals analysis). Various statistics computed for the errors can be used as a quantitative, objective measure of quality of the gridding method (i.e., the range, mean, standard deviation, standard error on the mean, skewness, and kurtosis), as proposed by Hicks and Hume (1997) and explained in the SURFER® 8.0 User's Guide (2002). Thus, residuals of the gridding processes should be analysed in order to define the best exact interpolator to represent the raw data.

After choosing the gridding method and grid spacing, the digital maps can be created. The DMM method, if it can be applied to a given cell, is computed with the cut/fill function using three different algorithms: Trapezoidal Rule, Simpson's Rule, and Simpson's 3/8 Rule (Hicks and Hume, 1997; SURFER® 8.0 User's Guide, 2002). Following Hicks and Hume (1997), the mean of the volumetric results yielded by the different algorithms is

taken as the BE of the true volume. The uncertainty volumes should enclose the vertical errors of the digitising process, the instrumental error of the survey (i.e., the boat movement induced by waves causing the pitch/roll error of the sounder), theodolite and/or GPS error, and the horizontal survey accuracy of the georeferencing process. In order to compute an error for the ATM method, an error area (xy) can be determined and then multiplied by the errors of the vertical variable (z). The error area can be computed by buffering the cell shape file using GIS software. Both maximum and rms errors should be determined as presented in equations II.5 and II.6, respectively. Both values should be presented separately for each cell and used for computing a final budget error when balancing all the cells. This procedure will both allow the identification of information gaps requiring the collection of further data for budget improvement, and indicate the level of confidence that should be used when interpreting the budget.

II.2.5 Using Inlet Hydraulic Parameters for Stability Analysis

Although inlet systems can be complex, for the purpose of hydraulic analysis inlet stability can be inferred from analysing key parameters which permit a simplified but useful analytical treatment of inlet hydraulics (e.g. Seabergh, 2006). Several parameters such as cross-sectional area (A_c), hydraulic radius (R_H), and average area over channel length (A_{avg}) can be easily determined from digital bathymetric maps. Other parameters such as average velocity in channel (V), maximum cross-sectionally averaged velocity during a tidal cycle (V_m), and the tidal prism (P), should also be determined but, in these cases, more intense fieldwork and processing tasks are required. These tasks may include the deployment of current meters, the completion of survey transects with an Acoustic

Doppler Current Profiler (ADCP), and the analysis of historical tide gauge records (where available). Several analytical or numerical models exist which can be used to compute these values (e.g. O´Brien, 1969; Jarret, 1976; Escoffier, 1977). However, despite good results for the particular surveyed inlets, there is no consistency in the application of these models to other inlets. Even so, the main constraint on the analysis of inlet dynamics and sediment patterns concerns the lack of field data on waves, tides, and currents. Therefore, linking sediment budget computation with inlet hydraulic parameter analysis should help to evaluate historical changes and to predict the movement of a stabilised inlet towards equilibrium, even if only a limited set of inlet parameters is used.

II.3 CASE STUDY: FARO-OLHÃO INLET

II.3.1 Introduction and Setting

The Ria Formosa is a multi-inlet barrier island system located in Southern Portugal (Fig. II.2). The system consists of five islands and two peninsulas separated by six tidal inlets: two artificially relocated inlets (Ancão and Fuseta inlets); two artificially opened and stabilised inlets (Faro-Olhão and Tavira inlets); and two natural inlets (Armona and Lacém inlets). The cuspate shape of the Ria Formosa system produces two areas differentiated in terms of exposure to wave action (Fig. II.2). The western flank, under the direct influence of the dominant SW wave conditions, is more energetic, while the eastern flank is directly exposed only to SE waves. According to Salles (2001), the Ria Formosa system can be divided into three hydrodynamically quasi-independent sub-embayments: (a) the western sub-embayment including Ancão, Faro-Olhão, and Armona inlets; (b) the central sub-

embayment, including Fuzeta and Tavira inlets; and (c) the eastern sub-embayment, including Lacém Inlet.

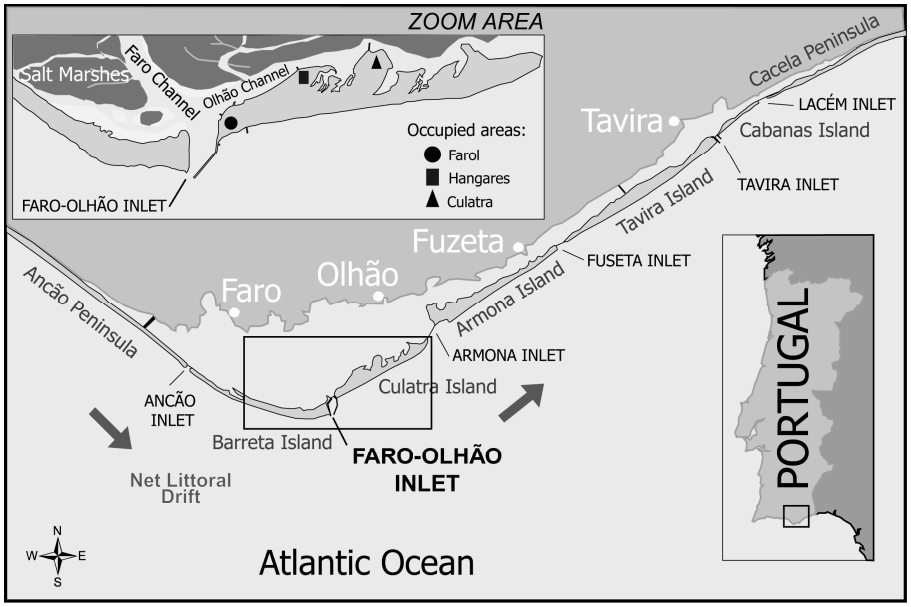

Figure II.2 Ria Formosa Barrier Island System, including the location of the Faro-Olhão Inlet and adjacent shoreline

The Ria Formosa system is characterised by large salt marshes, sand flats, and a complex network of natural and partially dredged channels, and covers 8.4×10^7 m^2 (Andrade, 1990). Tides in the area are semi-diurnal, with average ranges of 2.8 m and 1.3 m for spring and neap tides respectively, although ranges of 3.5 m can be reached. Wave climate in the area is moderate to high (Ciavola et al., 1997). Predominant wave directions are from the W-SW (approximately 70% of the time), while waves coming from the SE account for only 24% of the observations (Costa et al., 2001).

Faro-Olhão Inlet is the main inlet of the Ria Formosa system and was artificially opened progressively between 1929 and 1955. The objective of opening the inlet was to

ensure the maintenance of navigable depths in the access channel leading to the two main inhabited areas of the region, Faro and Olhão (Fig. II.2). Two jetties were constructed to protect the access channel from the prevailing west-to-east littoral drift and to improve navigational aspects, in particular the depth and orientation of the channel (Weinholtz, 1984; Esaguy, 1986). However, the distance between the jetties (160 m) proved to be too narrow and the inlet was not in equilibrium (Esaguy, 1986). As a consequence, erosion caused local depth reduction to about 40 m in the inlet gorge (Esaguy, 1986; Andrade, 1990). Furthermore, the flow was directed mainly towards the eastern jetty, leading to channel meandering (Esaguy, 1986; Pacheco et al., 2006, 2007). The opening of Faro-Olhão Inlet also had important effects on the littoral physiography and hydrodynamics of the Ria Formosa, as a consequence of the capture of a large tidal prism, the disruption of the net longshore transport pattern, and the erosion induced by the jet flow (Andrade, 1990; Salles, 2001). However, the hydrodynamic consequences of the opening and stabilisation of the Faro-Olhão Inlet were not of sufficient severity for the adjacent inlets to close (Vila-Concejo et al., 2002, 2006), probably because the opening was made in a former inlet position (Esaguy, 1986).

Faro-Olhão Inlet traps 60% of the total tidal prism of the western sub-embayment (Armona and Ancão inlets contribute 31% and 9%, respectively). Its flood-tidal prism is consistently larger than that of the ebb and thus the inlet is always flood-dominated, with the flood duration being consistently longer than the ebb duration (Salles, 2001). Currents near the inlet can attain average values of 2.2 m/s and 1.6 m/s during ebbing and flooding respectively (IH, 2000; Salles, 2001). The longshore currents and transport in this area run typically from west to east. Several estimates have been made of longshore sediment

transport (LST) rates using the Coastal Engineering Research Center (CERC) formula (Shore Protection Manual, 1984). Values obtained for the Faro-Olhão Inlet area range from a minimum of 1.0×10^5 m^3/year (Andrade, 1990) to a maximum of 2.0×10^5 m^3/year (Consulmar, 1989 in Bettencourt, 1994).

II.3.2 Sediment Budget Computation and Stability Analysis

II.3.2.1 Data Acquisition and Processing

Three types of data were analysed to determine the sediment budget for the inlet area: (1) existing plans, charts, and surveys since the time of the inlet opening (1927-1955) until 2004, (2) vertical aerial photographs between 1947 and 2001 and, (3) existing literature including published papers, PhD theses and technical reports. These datasets (Table II.1) were compiled using GIS software (ESRI ArcView^{TM} 8.3), which allowed all data and information to be georeferenced to the same datum. The digitised maps were used to obtain digital contour maps for each year, using *XYZ* data on bathymetry to fit a rectangular gridded surface (or digital terrain model).

Four main areas, corresponding to the main morphological units of the system (Fig. II.3), were defined, within which a total of six cell compartments were delineated for making sediment volume computations: (1) the inlet channel (the inner channel, cell V_i, and the offshore channel, cell V_o); (2) the ebb-tidal delta (cell V_e); (3) the flood-tidal delta (cell V_f); and, (4) the adjacent coastline (cell V_u and cell V_d, representing the variability in the vicinities of the updrift Barreta and downdrift Culatra islands, respectively). Table II.1 reports data availability for each cell.

Table II.1 Cell coverage, measured parameters, and types of data used in the sediment budget computation for Faro-Olhão Inlet

Year	Coverage	Parameters	Type of Data*
1947	V_u, V_d		AF
1955	V_i and part of V_o	A_c, R_H, A_{avg}, p, M_{depth}	IB
1958	V_u, V_d		AF
1962	V_i, V_o, V_e, V_f,	A_c, R_H, A_{avg}, p, M_{depth}	IB
1976	V_u, V_d		AF
1978	V_i, V_o, V_e, V_f, V_u, V_d	A_c, R_H, A_{avg}, p, M_{depth}	ICB
1985	V_i, V_o	A_c, R_H, A_{avg}, p, M_{depth}	ICB
1994	V_i, V_o	A_c, R_H, A_{avg}, p, M_{depth}	ICB
1996	V_u, V_d		AF
2001	V_u, V_d, V_i, V_o, part of V_f	A_c, R_H, A_{avg}, p, M_{depth}	ICB, AF
2002	V_i, V_o, part of V_f, V_u, V_d	A_c, R_H, A_{avg}, p, M_{depth}	ICB, AF
2003	V_i, V_o, part of V_f	A_c, R_H, A_{avg}, p, M_{depth}	ICB
2004	V_i, V_o, part of V_f	A_c, R_H, A_{avg}, p, M_{depth}	ICB

* AF – Aerial photo; IB – Inlet bathymetry; ICB – Inlet and channel bathymetry

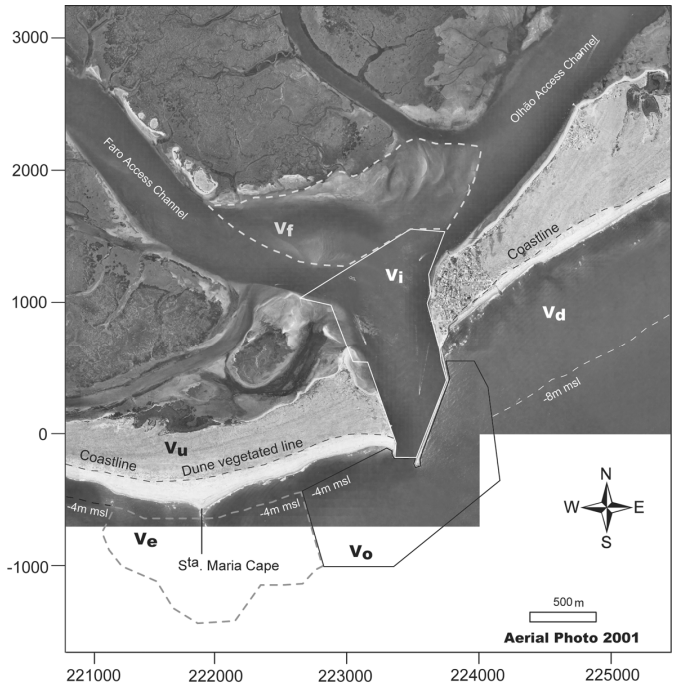

Figure II.3 Schematic representation of the compartments (cells) defined for volumetric computation. Co-ordinates refer to the Portuguese Military Grid

II.3.2.2 Inlet Channel

The volumetric evolution included individual quantitative calculations for each of the main morphologic features of the inlet (V_i, V_o) using the DMM. The bathymetric data used for this study (from 1962, 1978, and 2001) were analysed using the SURFER® 8 software package and following the methodology suggested by Hicks and Hume (1997). Although Faro-Olhão Inlet was opened during the period 1929 to1955, the first available bathymetry that includes both cells is from 1962. The DMM was used in order to determine V_i and V_o for the periods 1962-1978 and 1978-2001.

Channel evolution data (Table II.2) show that V_o and V_i eroded in both analysed periods (1962-1978 and 1978-2001). The V_o erosion rate was about 1.8 times higher in 1978-2001 than in 1962-1978 as a consequence of the offshore progression of the scouring process (Fig. II.4). In contrast, the V_i erosion rate was lower in 1978-2001 than in 1962-1978. The sum of both V_i and V_o volumes for each period resulted in an erosion rate increase of about 1.3 times for 1978-2001 compared with 1962-1978. The maximum values of uncertainty (δX_{max}) and rms uncertainty (δX_{best}) were determined by applying an error of 0.1 mm to digitising the chart (equivalent to an error of ±0.5 m for a 1:5,000 scale chart). The horizontal accuracy (xy) was 0.2 m for each independent variable (measured with a theodolite and/or GPS). The vertical error was 0.2±0.5 m, which encloses the survey instrumental error and the vertical pitch/roll error of the boat movement induced by waves. The δX_{max} and δX_{best} represent about 12 % and 10 % of the total computed cell volumes, respectively.

Table II.2 Best estimate (BE) values and uncertainties of the individual cells used to compute the sediment budget for the Faro-Olhão Inlet

Cell	Value	1929-1962	1962-1978	1978-2001
V_o	**BE**	N/a	-1.15×10^5	-2.01×10^5
	δX_{max}		$\pm 1.38 \times 10^4$	$\pm 2.41 \times 10^4$
	δX_{best}		$\pm 1.15 \times 10^4$	$\pm 2.01 \times 10^4$
V_i	**BE**	N/a	-7.86×10^4	-5.68×10^4
	δX_{max}		$\pm 9.43 \times 10^3$	$\pm 6.82 \times 10^3$
	δX_{best}		$\pm 7.86 \times 10^3$	$\pm 5.68 \times 10^3$
V_e	**BE**	5.30×10^4	4.58×10^4	ODC
	δX_{max}	$\pm 7.42 \times 10^3$	$\pm 7.79 \times 10^3$	
	δX_{best}	$\pm 5.30 \times 10^3$	$\pm 5.50 \times 10^3$	
V_f	**BE**	5.91×10^4	5.08×10^4	5.72×10^4
	δX_{max}	$\pm 1.83 \times 10^4$	$\pm 6.06 \times 10^3$	$\pm 1.77 \times 10^4$
	δX_{best}	$\pm 1.48 \times 10^4$	$\pm 4.57 \times 10^3$	$\pm 1.43 \times 10^4$
V_u	**BE**	1.09×10^5		1.46×10^4
	δX_{max}	$\pm 3.27 \times 10^4$		$\pm 4.38 \times 10^3$
	δX_{best}	$\pm 2.73 \times 10^4$		$\pm 3.65 \times 10^3$
V_d	**BE**	-4.52×10^4		-1.36×10^4
	δX_{max}	$\pm 1.62 \times 10^4$		$\pm 4.88 \times 10^3$
	δX_{best}	$\pm 1.35 \times 10^4$		$\pm 4.07 \times 10^3$

N/a – not available
ODC – out of data coverage

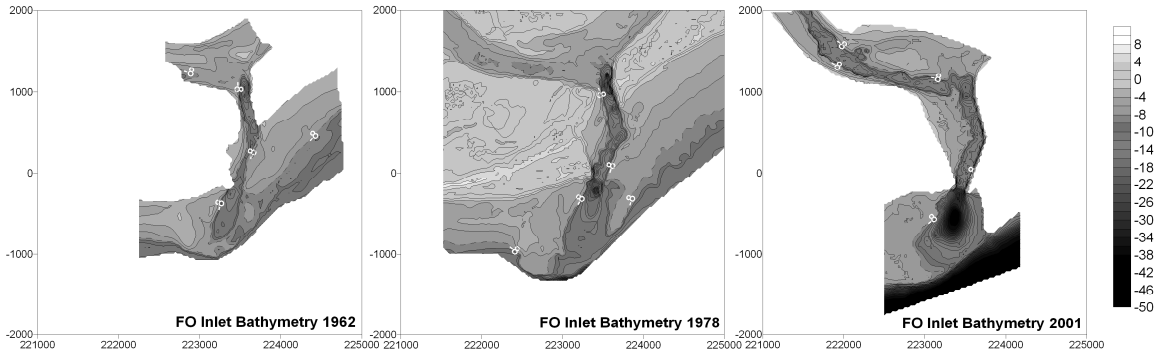

Figure II.4 Digital topo-bathymetric maps for 1962, 1978, and 2001. Co-ordinates refer to the Portuguese Military Grid. Elevation is referred to msl

II.3.2.3 Tidal-deltas

V_e could be determined only for 1962 and 1978 because the bathymetric chart of 2001 includes only V_o (Fig. II.3). Several cross-shore and alongshore profiles were plotted on the 1962 and 1978 maps (Fig. II.5), and were analysed together with the Profile P_{e0},

representative of a typical no-delta shaped profile (*Nd(x)*, Fig. II.1). Examination of the profiles' evolution allowed the boundaries of the ebb-tidal delta to be defined. After determining the ebb-tidal delta areas, the ebb-tidal volumes of 1962 and 1978 were computed by applying the average thickness method (ATM, Eq. II.2). The Z_e value was determined by creating different grids using the SURFER® 8 software package for every profile defined and for each year of analysis (Fig. II.5). The volumes and areas were computed between each profile for two different dates (e.g., transect PNS4 of 1962 and the no-delta typical shape profile, *Nd(x)* in Fig. II.1, represented by P_{e0} in Fig. II.5).

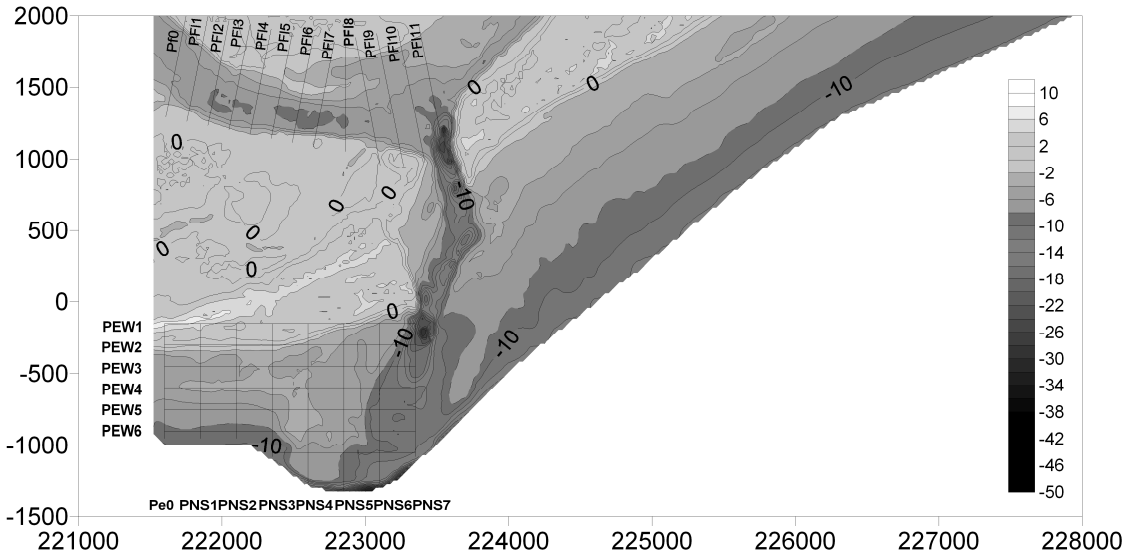

Figure II.5 Ebb-tidal delta profiles, both North-South (PNS1-7) and East-West (PEW1-6), and flood-tidal delta profiles (PFl1-14), plotted over the digital contour map of 1978. P_{e0} and P_{f0} represent the no-delta profiles. Co-ordinates refer to the Portuguese Military Grid. Elevation is referred to msl

The landward limit of the delta is the 4 m depth contour, whereas the seaward limit (the depth of closure of the ebb tidal data) is represented by the 8 m depth contour as beyond this point the computed profile cross sections do not show any appreciable change

(Fig. II.4). The updrift and downdrift limits were determined by analysing the deflection of the bathymetric contours away from their shore-parallel position where they reached the delta area. The determined value of Z_e was 3.66 m (1962) and 3.03 m (1978). V_e showed a relatively constant sediment accumulation rate through time. Thus, sediment stored in the ebb-tidal delta in 1978 was about 1.5 times higher than in 1962, implying a doubling of the ebb-tidal delta area. The ebb-tidal delta increased in area by being displaced towards the west in the direction of S^{ta}. Maria Cape (Fig. II.4).

Regarding volume uncertainties, errors were assigned to chart digitisation (±0.1 mm) and to digitising the delta area (±0.4 mm), which translates to ±0.5 m and ±2 m, respectively, for a 1:5,000 scale chart. The standard deviation of Z_e is about ±0.3 m and the instrumental vertical errors are ±0.2 m. These results produce maximum errors (δX_{max}) of about 14 % and 17 % of the total ebb-tidal delta volume computed for 1962 and 1978, respectively (Table II.2). The rms uncertainty (δX_{best}) represents about 10 % and 12 % of the total ebb-tidal delta volume for 1962 and 1978, respectively.

The amount of sediment stored in the flood-tidal delta (V_f) could be determined with a reasonable degree of accuracy only for 1978. To determine V_f for 1978, 14 profiles were sketched over the 1978 topo-bathymetric chart (Fig. II.5). Profile P_{f0} (Fig. II.5) was considered to be the profile representative of a no-delta area (*Nd(x)* in Fig. II.1). This profile was plotted against the 1978 profiles, and an average thickness (Z_f) of the flood-tidal delta was determined (Fig. II.1). The flood-tidal delta areas (A_f) were obtained using by combining analysis of the topo-bathymetric charts with aerial photography (for 1962, 1978, and 2001). The landward limit was considered to be fairly constant (*Ll* in Fig. II.1

approximates the salt marsh limit), and the seaward limit (*Sl* in Fig. II.1) was considered to be represented by the channel slope rupture in both channels' alignment (Faro and Olhão Access channels, Fig. II.3). After determining the flood-tidal delta areas, the flood-tidal volume was computed using Eq. II.3, assuming that Z_f determined for 1978 is representative of normal conditions.

V_f computations showed that between the 1929 opening of the inlet and 1978, the delta stored about 2.5×10^6 m^3 of sediment (a rate of approximately 5.6×10^4 m^3/year, Table II.2). Values of uncertainties δX_{max} and δX_{best} were determined for 1978, using an error of ±0.1 mm on digitising the chart, an error of ±0.8 mm on digitising the delta area (±0.5 m and ±2 m, respectively, for a 1:5,000 scale chart), a standard deviation of Z_f of ±0.3 m, and a vertical instrumental error of ±0.2 m. The obtained uncertainties (δX_{max} and δX_{best}) represent 13 % and 9 % respectively of the total sediment stored in the flood delta.

A_f was also obtained for 1962 and 2001 by analysis of aerial photos and bathymetric charts of Faro and Olhão channels. This allowed the delta areas to be digitised but did not enable an accurate value of Z_f to be determined. The horizontal error attributable to obtaining the delta area from rectified aerial photos is ±5 m, and the vertical error encloses the instrumental error (±0.2 m) and the error on determining Z_f (±1 m). The obtained values of δX_{max} and δX_{best} for 1962 and 1978 represent 31 % and 25 % of the total stored sediment, respectively (Table II.2). The accretion rate of the flood tidal delta for the three study periods was such that it produced a flood-tidal delta that was 1.4 times bigger in 1978 than it was in 1962, and 1.4 times bigger in 2001 than in 1978, bearing in mind however the sizeable uncertainties applying to volumes computed for 1962 and 2001. The relation

between V_f/V_e for 1962 and 1978 was computed based on the obtained data, resulting in an approximate value of 1.

II.3.2.4 Barrier Island Evolution

Aerial photos from 1947, 1976, and 2001 were georeferenced and used to digitise the coastline. The feature selected to represent the coastline position was the dune/beach interface which was identified by the presence/density of dune vegetation. An arbitrary reference line following the orientation of the barriers was established and shore-normal transects were defined every 250 m (Fig. II.6). Using GIS software, different accretion and/or erosion polygons were sketched between surveys and the area of each polygon computed, which allowed the coastline change area (C_a) to be computed for two periods: 1947-1976 and 1976-2001. The only detailed topography available (a 1978 survey of the Ria Formosa system, Table II.1) was used to determine the average active elevation, Z_a.

Because only beach profiles were available for 1978, the value of h_d was obtained for each 1978 shore-normal profile by reconstructing the dune field from the reference line to the digitised coastline. The values were used to obtain an average h_d value for each barrier. This method assumes that any parcel of beach added to or removed from each island during a given period would have a beach stock volume similar to the average 1978 typical beach profile, defined between the average height of the pre-existing dune field and the depth of closure. In essence, the 1978 typical beach profile was used as a reference with which to compute the values of accretion/erosion as indicated by offshore/onshore movements of the digitised coastline for other years.

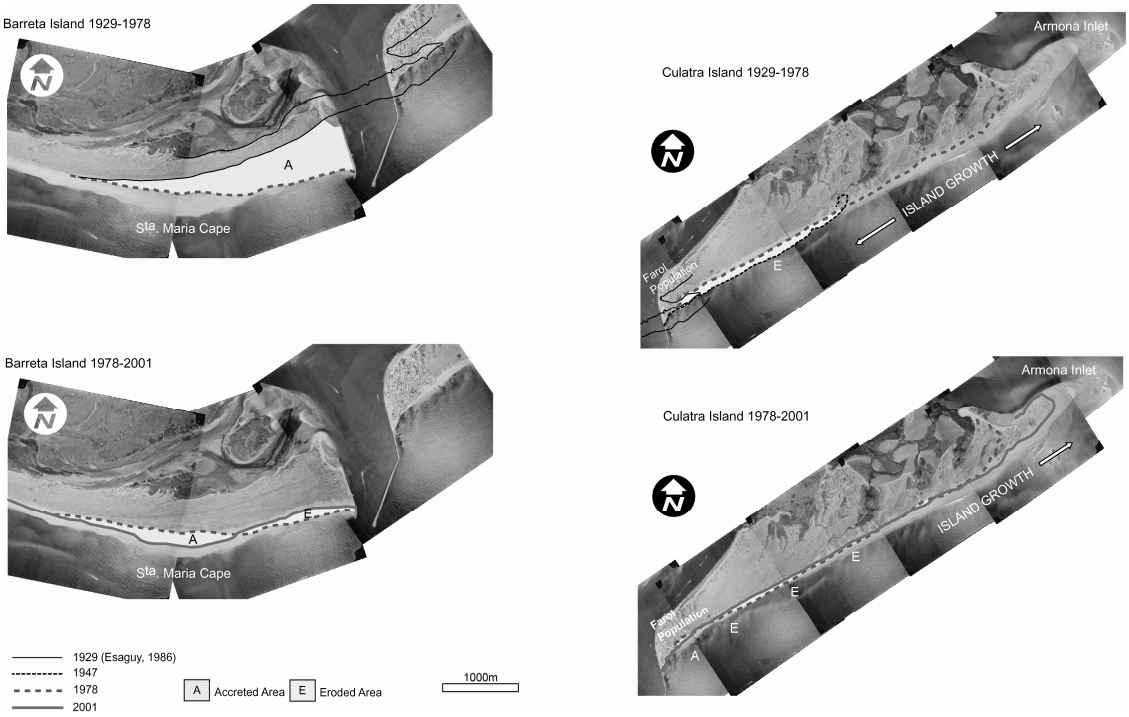

Figure II.6 Location of the shoreline normal profiles used to determine the shoreline evolution of the barrier islands

Several authors have analysed h_c in and around the study area. Andrade (1990) used formulations proposed by Hallermeier (1981) for estimating a standard h_c value for the Ria Formosa. Both Ferreira (2005) and Dolbeth et al. (in press) used a morphological approach, in which beach profiles were measured and used to compute beach volume changes and to calculate the depths of closure for Faro beach. The results of these authors were evaluated and compared to establish a value of h_c for the study area.

The barriers' changes in volume (V_u and V_d) were obtained separately using Eq. II.4, substituting in the formula the volume of the coastline (V_c) for each one of the variables, using 1978 as the reference year (i.e. V_{u2001}-V_{u1978}). Volume computations were made assuming h_c = -8 m for determining V_d (Culatra Island). For determining V_u, the seaward

limit is the landward boundary of the V_e cell established in Fig. II.3 (the bathymetric contour of 4 m depth). The h_c vertical error is ±2 m, which encloses the value determined by Andrade (1990) using the empirical equations and the range of season variability in h_c determined by Ferreira (2005) and Dolbeth et al. (in press). The average h_d was obtained from the 1978 topographic map and its standard deviation (±0.5 m) was used to determine volume uncertainties. The average h_d as obtained is 3.2 and 2.4 m (above msl) for Barreta and Culatra barriers, respectively. In determining uncertainty, the errors taken into account were the standard deviation of h_d, the instrumental (theodolite) error of ±0.2 m, and the error in horizontal position due to the interpretation of the coastline position in the aerial photos (±5 m).

The adjacent barrier islands exhibited general accretion updrift of the inlet and erosion downdrift of it (Table II.2 and Fig. II.7). Barreta Island accreted strongly during 1929-1976 and, after 1976, continued to accrete but in a more moderate way (the accretion rate during 1929-1976 was about 7.4 times higher than during 1976-2001). Between 1976 and 2001 the island underwent erosion mainly in the area between S^{ta}. Maria Cape and the western jetty, which resulted in a change in the island oceanic contour (Fig. II.7). Culatra Island underwent erosion along its western half, particularly strongly until 1976 (the erosion rate of 1929-1976 was about 3.3 times higher than during 1976-2001). From 1976 to 2001 the barrier eroded at lower rates, and showed some accretion in its western area as a result of the seawall/groin system (located 600 m from the East jetty, Fig. II.3) installed to protect the occupied township of Farol, located on Culatra Island (Fig. II.7). δX_{max} and δX_{best} represent 30% and 25% of the total volumes, respectively. The relation between the

absolute values of volumetric change (accretional/erosional) for both barriers $|V_u / V_f|$ was ≅2 for 1929-1976 and ≅1 for 1976-2001 (Table II.2). Finally, the eastern half of Culatra Island (to the east of the 14 profiles, Fig. II.6) has experienced significant accretion and eastward island growth (Fig. II.7). The island growth was maximal between 1929 and 1976, during which time the island doubled in size. After 1976, the island continued to increase in size but at lower rates. The accretion of Culatra Island's eastern end was not included in this budget, but is further discussed in sub-section II.3.6 below.

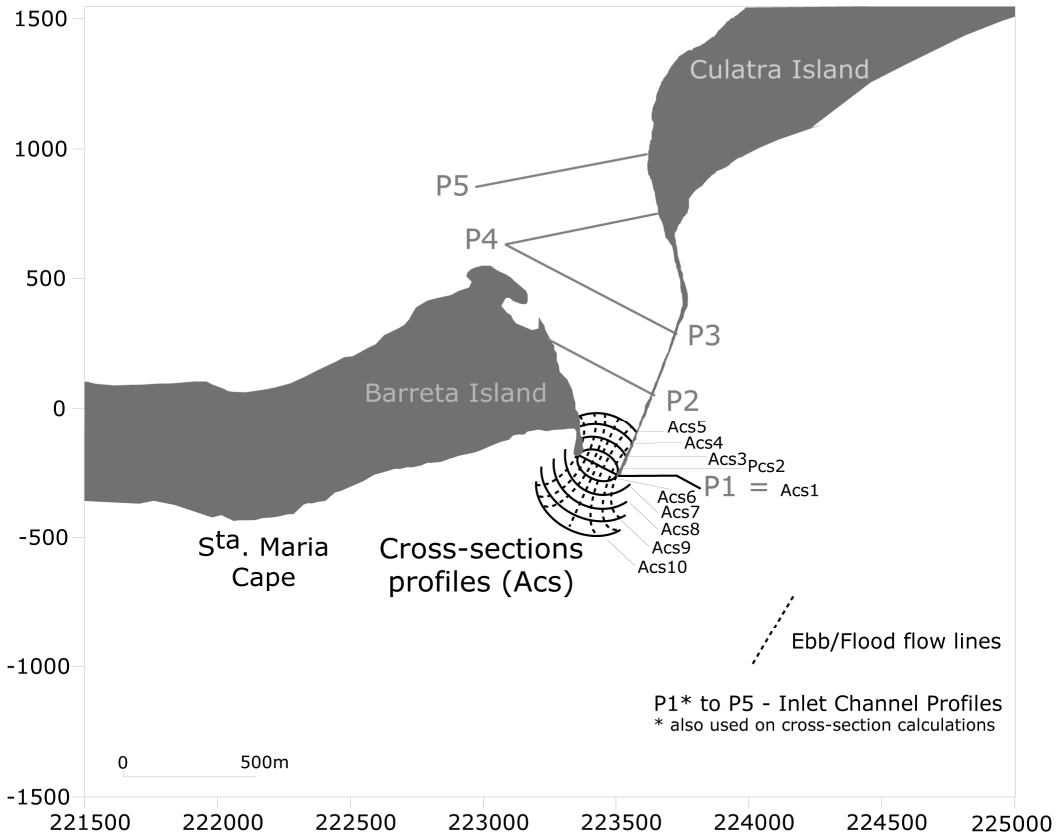

Figure II.7 Evolution of Barreta and Culatra islands between 1929 and 2001

II.3.3 Engineering Activities

The period between 1929 and 1947 corresponds to the opening of the Faro-Olhão Inlet and the first dredging in the Faro Access Channel, and therefore experienced significant dredged volumes (≅2.5 x10^6 m^3). The engineering works included the opening of the access channel, beach nourishment, and jetty construction; however, the data do not separate *PL* from *R* (Esaguy, 1986; ICN, 1999). Between 1947 and 1985 the volume dredged was ≅2.0 x10^6 m^3, although there is no information for the period 1956-1974. Again there is no distinction between *PL* and *R*, although available aerial photography (post-1947) does not show evidence of emplaced material within the boundaries used for the Faro-Olhão Inlet budget computation.

Data obtained from previous studies show that dredging intensified between 1985 and 2001 (≅4.6 x10^6 m^3). Pacheco et al. (2003, 2006) concluded that sediment entry into the system (i.e. the volume needed to be dredged in order to maintain channel navigability) is ≅1.4 x10^5 m^3/year. Between 1994 and 2001 the dredged volume was ≅3.7x10^5 m^3/year, implying an annual over-exploitation of 2.3 x10^5 m^3/year. The digital bathymetric maps (Fig. II.4) clearly demonstrate the increase in depth of the inner channel.

There is a considerable discrepancy in the values of *R* obtained for 1985-2001 (≅2.9 x10^5 m^3/year) and for 1929-1985 (≅7.0 x10^4 m^3/year). Considering that this is a navigable channel which must maintain navigable depths, we assumed that the same value applied to both periods. By assuming that the period from 1985-1994 was a period of normal dredging activity, the dredging rate is calculated to be ≅2.15 x10^5 m^3/year with a variability of about ±0.75 x$10^5$$m^3$/year (35 % uncertainty, based on the variability measured

from volumetric analyses of the 1985-2001 bathymetric charts). The dredging rate value was defined in order to fit the range of the maximum dredging rate and the sediment entry within the system, and takes into account the dredging needed to remove the sediment entry (preventing shoaling and navigation problems) and a dredging allowance (for over-exploitation of dredging sands). The assigned yearly dredging rate of the 1929-1985 period, also ≅2.15 x10^5 m^3/year, should approximate the value of sediment entry again on the basis of maintaining channel navigability.

II.3.4. Inlet Stability Parameters

A_c was determined for all existing bathymetric surveys (Table II.1) of Faro-Olhão Inlet, and was measured at the inlet gorge, which corresponds to the narrowest and deepest section of the channel. The method presented in the Coastal Engineering Manual (CEM) (Seabergh, 2006) was used to obtain the minimum cross-section area, whereby 10 equally spaced cross-section profiles were defined normal to the flow lines through the inlet (Acs1-Acs10, Fig. II.8). After the computation of the 10 minimum cross-section areas an average cross-sectional area below msl was obtained. In addition, other inlet parameters were calculated following Seabergh (2006): the average area over the channel length (A_{avg}), the wetted perimeter (p), and the hydraulic radius (R_H), all measured along the inlet channel (P1-P5, Fig. II.8); and the maximum depth at the inlet throat (M_{depth}) (measured at P1, Fig. II.8). These parameters were measured for all the inlet bathymetric surveys (Table II.1).

The computed values of R_H for each profile through time show that, in general terms, each analysed channel section reached stability between 1978 and 1985 (Fig. II.9). There are small variations in R_H after 1978, most notably to some inner channel sections (P4 and P5) that have been subjected to more intensive dredging. P1, located at the inlet throat (Fig. II.8), shows the greatest variation in R_H due to the scouring activity and because its wetted perimeter (p~160 m) is fixed by the distance between the two jetties.

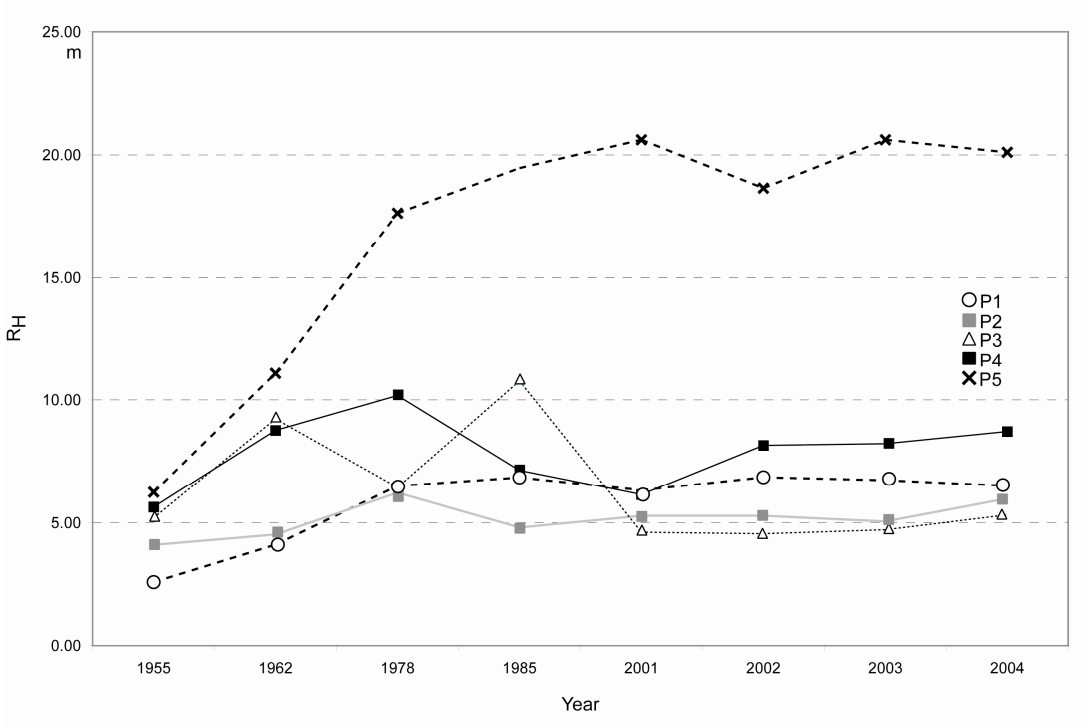

Figure II.8 Configuration of five cross-section profiles along the inlet channel (P1-P5) and 10 equi-spaced cross-section profiles normal to the ebb and flood flow lines (Acs1 – Acs10). Co-ordinates refer to the Portuguese Military Grid

The results show an increase in A_{avg} over time (mean A_{avg} curve, Fig. II.10), although there is little variation after 1985 except for the period 2001-2004. This most recent variation was related to emergency dredging at P5, in order to attenuate channel

displacement to the east, which had started to occur (Pacheco et al., 2006, 2007). Therefore, it is the A_c value at P5 that is responsible for raising the value of average A_{avg} during 2001-2004. The greatest variation in A_{avg}, however, occurred between 1978 and 1985, probably due to the effect of the increase in R_H at P5 (Fig. II.9), and can be explained by channel artificial enlargement/deepening for navigational purposes. M_{depth} at the inlet throat (P1) appeared to reach stability between 1978 and 1985 (~20-25 m, also showed by the computed A_c value for P1, Fig. II.10). However, A_c measured using the CEM method (Fig. II.10) exhibits higher variability between 1978-1985 and little variation between 1985 and 2004 (reaching an average value of about 4.5 x10^3 m^2).

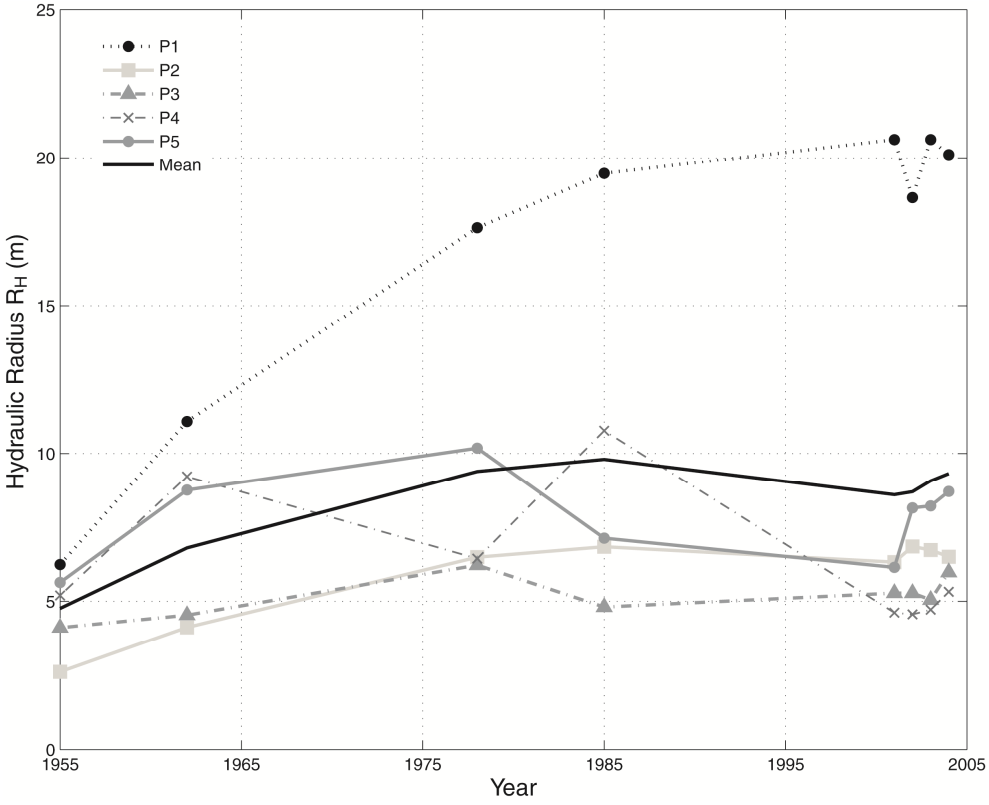

Figure II.9. R_H evolution for profiles P1 to P5 between 1955 and 2004

Comparing the values of A_c measured at P1 with the computed A_c (CEM method) it appears that, despite the inlet throat cross-section attaining stability sometime during 1978-1985, the scouring activity increased offshore (Fig. II.4). This suggests a stratigraphic control whereby a consolidated stratum prevented further deepening of the inlet and instead the scouring was displaced offshore.

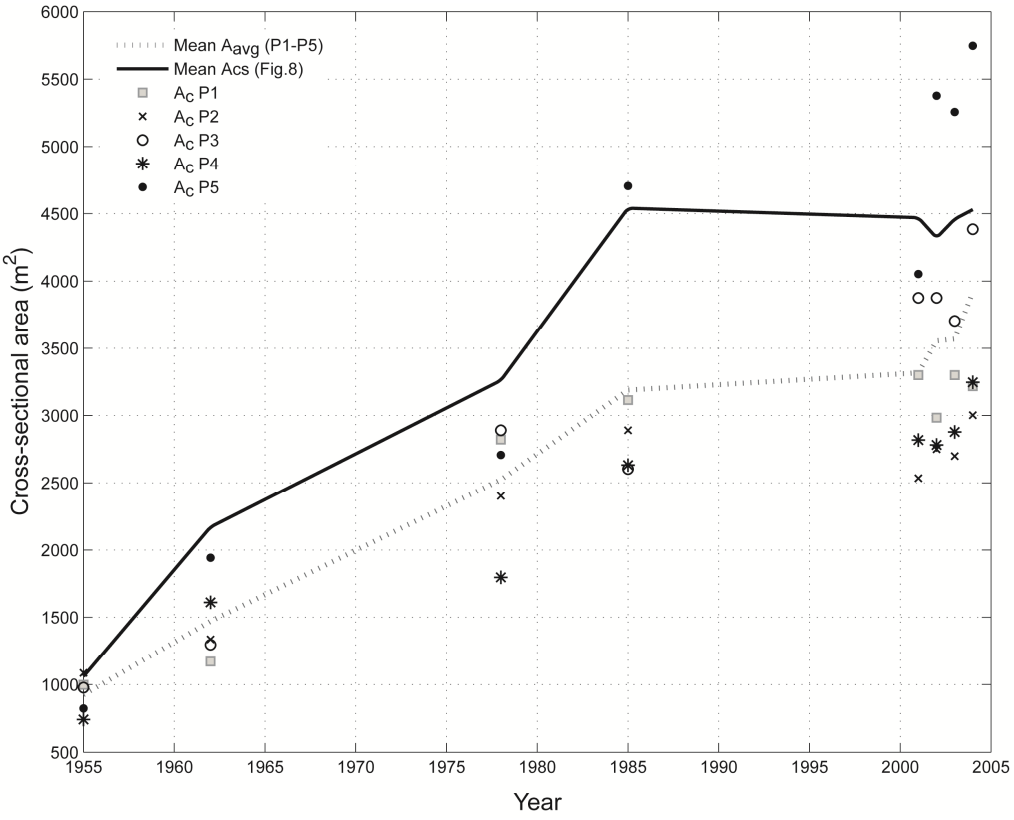

Figure II.10 Average cross-sectional area (A_{avg}) of inlet channel area (P1-P5) and minimum cross-sectional area (A_c) of Faro-Olhão Inlet measured using the CEM method, 1955-2004

II.3.5. Best Estimate and Uncertainty Analysis

The sediment budget equation (Eq. II.1) was used to calculate a balance for the inlet area for two periods, 1962-1978 and 1978-2001, considering a balanced cell (residual

equals zero) with the difference between ΣQ_{source} and ΣQ_{sink} as unknown. These parameters include LST rates, and also other variables that are expected to be less significant than LST such as aeolian transport, overwash events, and losses to the offshore area (e.g. rip and ebb-jet currents).The source and sink volumes of the inlet area could not be obtained accurately, thus Eq. II.1 was used to approximate the sediment balance using the computed data (Fig. II.11). The approach aimed to compute the balance between ΣQ_{source} - ΣQ_{sink} by making Eq. II.1 (ΣQ_{source} - $\Sigma Q_{sink} = \Delta V + R - PL$) equal to zero.

1962-1978: $\Delta V \cong$-0.4 x10^5 m^3/year (rms uncertainty, δX_{best}, of 40 %, Fig. II.11A). The relation between $V_e/V_f \cong 1$ and $|V_u/V_d| \cong 2$ (Table II.2), meaning that Barreta Island accreted double the amount of erosion that occurred at Culatra Island. The accretion at Barreta Island represents more than 50 % of the total accretion in the inlet. The inlet offshore area, inlet gorge, and channel are in an erosive state ($V_o/V_i \cong 1.5$, Table II.2). Assuming that the dredging rate $\cong$2.2 x10^5 m^3/year (rms uncertainty, δX_{best}, of 35 %), the balance between sources and sinks yields a final volume of 1.8 x10^5 m^3/year (rms uncertainty, δX_{best}, of 53 %). Thus, the ΣQ_{source} - ΣQ_{sink} budget of the Faro-Olhão Inlet for the period 1962-1978 ranges between a minimum of 0.85 x10^5 m^3/year to a maximum of 2.75 x$10^5$$m^3$/year (Fig. II.11A). It should be pointed out that in this case rms uncertainty results in an upper limit.

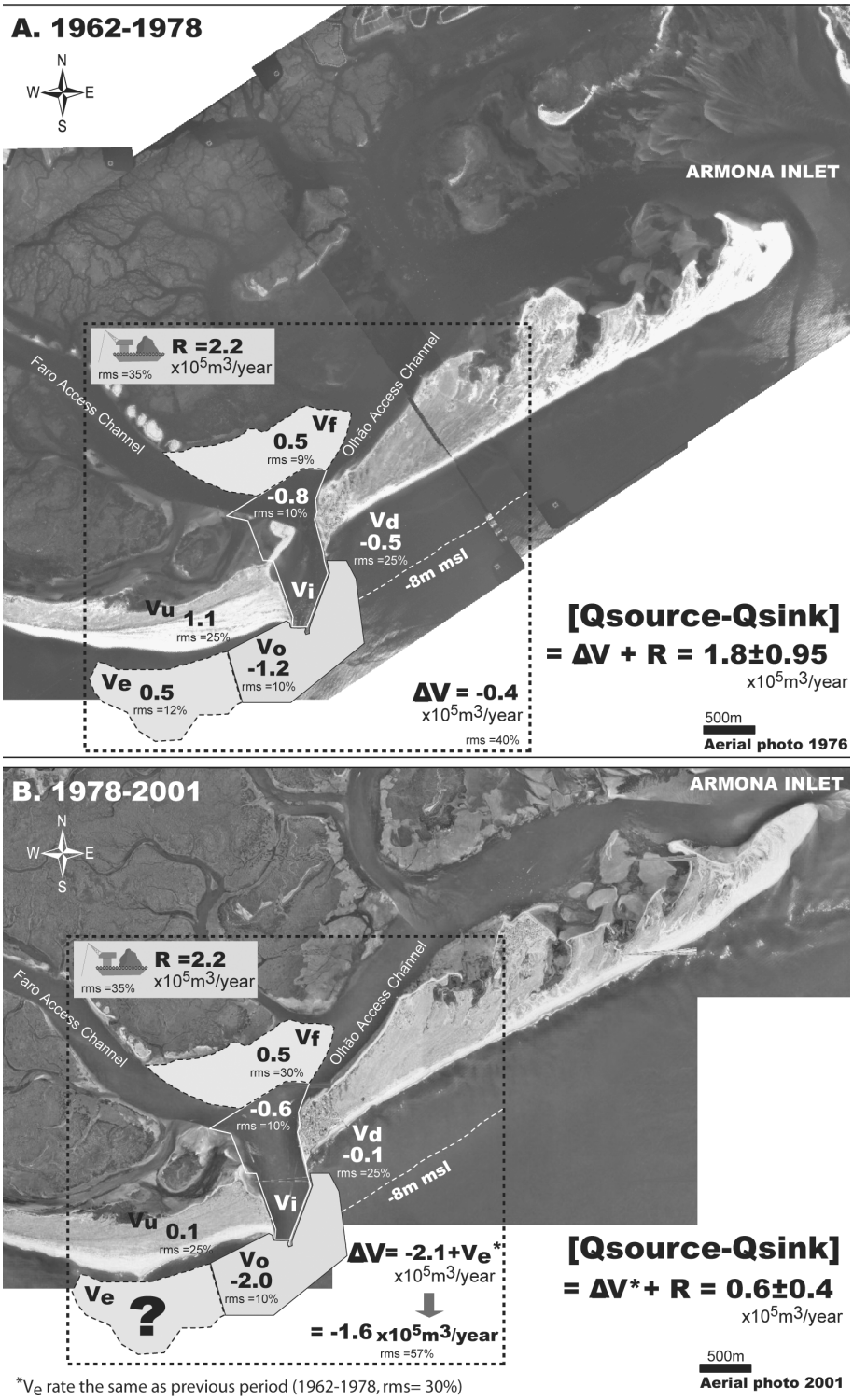

Figure II.11 Faro-Olhão Inlet budget and rms uncertainty of the ΣQsource - ΣQsink balance for two study periods: 1962-1978 (A) and 1978-2001 (B)

1978-2001: ΔV could not be obtained, since it was not possible to compute V_e accurately because in this period the ebb-tidal delta was forced to move westward by the offshore progression of scouring activity, and therefore the bathymetric data did not cover the whole of the ebb-tide delta area for 2001. However, the accretion trend of the ebb-tidal delta continued (Fig. II.11B). The computed V_u and V_d rates were drastically reduced compared with the previous period 1962-1978 (Table II.2). This indicates that both barriers are reaching equilibrium after the opening and stabilisation of the inlet (and its subsequent dredging). (V_o+V_i) increased with respect to the previous period (about 25 %). $V_o/V_i \cong 3.3$ (Table II.2), with the main contributor to this increase being the erosion at V_o, which was about 1.8 times higher than in the previous period. It was not possible to calculate V_e/V_f, although the V_f rate is similar to that of the previous period (Fig. II.11A) but with a higher uncertainty due to the methodology used in its computation (Table II.2). If it is assumed that the V_e yearly accumulation rate was similar to that of the previous period (and considering an rms uncertainty of about 30 %), then $\Delta V \cong$ -1.6 x 10^5 m^3/year (rms $\cong$ 57 %, using Eq. II.7) and a final balance between sources and sinks yields 0.6x10^5 m^3/year (rms $\cong$ 67 %, using Eq. II.7). Therefore, for the period 1978-2001, the balance between sources and sinks ranges between a minimum of 0.25 x 10^5 m^3/year to a maximum of 1.0 x 10^5 m^3/year.

II.3.6 Inlet Hydraulic Parameters and Stability Analysis

Several assumptions had to be made, such as the estimation of yearly dredging rates and h_c values. In order to avoid increasing the budget uncertainty it was decided to approximate

the balance by coupling cell evolution analysis with measurement of the inlet's A_c and other hydrodynamic parameters. The approach allows explanation of inlet evolution processes and the progression of the inlet toward dynamic equilibrium.

The results show that Faro-Olhão Inlet has been essentially dominated by three periods: (1) an initial process of sediment retention within the inlet area related to the opening stage (1929-1962). The inlet started to capture the LST in order to build both deltas, and channel scouring began in order to achieve an equilibrium A_c (Fig. II.10); (2) An intermediate stage (1962-1978), during which both deltas accumulated sediments at approximately the same rate (Table II.2) and the major modifications occurred in both barriers (V_u accreted significantly). Scouring activity also increased during this period; and (3) The stage characterised by the stabilisation of both coastlines with respect to the presence of the inlet and by the drastic intensification of scouring at the inlet gorge, in the period 1978-2001 (Table II.2). The A_c value reached equilibrium (Fig. II.10) and therefore the application of an A_c vs P relation (similar to several existing formulations for inlets around the world) would produce an equilibrium of the overall tidal prism. However, as discussed in sub-section II.3.4, although the inlet throat cross-section attained stability sometime during 1978-1985, this does not mean that the inlet itself reached equilibrium. The increase in current velocity at the inlet throat, caused by the stratigraphic control, and the subsequent increase of the scouring offshore, constitutes clear evidence of the inexistent equilibrium between P and A_c.

Based on the results, the ΣQ_{source} and ΣQ_{sink} balance was computed for 1962-1978 and 1978-2001 (Fig. II.11), assuming a yearly maintenance dredging rate for Faro Channel

navigability. The 1962-1978 period (Fig. II.11A) shows an inlet area accumulating sediment at an average rate of 0.85 x10^5 to 2.75 x10^5 m^3/year. For the 1978-2001 period it was not possible to compute V_e, and V_f contains large uncertainties; however, some assumptions were made in order to establish alternatives for the budget (Fig. II.11B). The results show a closer equilibrium between sources and sinks if the computed V_e and V_f (Table II.2) are considered. This final result could be explained by three possible hypotheses.

Hypothesis one proposes sediment bypassing the inlet, contributing to the growth of the eastern tip of Culatra Island (Fig. II.7) and to the narrowing of the Armona Inlet (Fig. II.11). However, judging by the observed increase of the scouring process in the offshore part of the inlet, and considering that the outer bar is located between 8 m and 10 m depth (Fig. II.4), it does not seem likely that significant bypassing is occurring. Thus, it seems more likely that the major sediment source for the eastward growth of Culatra Island must be the retreat of the Armona tidal deltas (Fig. II.11A), a direct consequence of tidal prism loss due to the Faro-Olhão Inlet opening (Salles, 2001). In order to better assess the effect of the Faro-Olhão Inlet on the narrowing of Armona Inlet, the sediment budget and A_c/P analysis would need to be extended to include both hydrodynamically connected inlets.

Hypothesis two proposes an increase in the scouring process (V_o value, Fig. II.11B), responsible for displacing the ebb-tidal delta towards the west and beyond the boundaries used to perform the sediment budget (i.e. an increase in the sink volume). The jet flow created a gorge (that reaches 40 m in depth) at the front of the inlet, extending offshore to the -10 m bathymetric contour (Fig. II.4), with the sediment load being exported to deeper

areas from which the return of sand to the littoral system is difficult. It should be noted that both barriers appear to have reached dynamic equilibrium. The readjustment of the Barreta coastline (Fig. II.7) also seems to be a result of the scouring activity, with erosion occurring between S^{ta}. Maria Cape and the Faro-Olhão Inlet western jetty and significant accumulation occurring in the frontal area of S^{ta}. Maria Cape.

Hypothesis three proposes a reduction in the source volume to the area for which the sediment budget was computed. In this case, V_e should be considerably higher and extend more towards the west and beyond the defined sediment budget boundaries. This hypothesis can explain the readjustment of the coast in the area of S^{ta}. Maria Cape, which is operating as a natural barrier to the source volume of LST and retaining the sediment load in V_e (not quantified).

An evaluation of the viability of hypotheses two and three can be made using information gained from the inlet parameters measured (Figs. II.9 and II.10). In general, R_H and A_c increased after the opening of the inlet, until 1978-1985. The increase in these parameters is related mainly to the hydraulic readjustment caused by the confinement of flow through the stabilised inlet and to the evolution of A_c until reaching equilibrium. Both parameters appear to have reached stability between 1978 and 1985 (Figs II.9 and II.10). In addition, M_{depth} at the inlet throat has not experienced significant variations since 1978. However, despite the fact that A_c reached stability, there was an increase in scouring activity extending offshore (Fig. II.4). Therefore, the present geometry represents either an equilibrium cross-sectional area for the average hydrodynamic conditions, or a configuration in which the inlet has a tendency to grow but is limited by the jetties and by other external controls. One such control was proposed by Salles (2001), who analysed

historical data and suggested that Faro-Olhão Inlet has a tendency to grow, and that the growth has stopped because the bottom of the inlet channel has reached a more consolidated stratum that prevents further deepening. This would explain the increase in A_c, despite the equilibrium reached at cross section P1 (Fig. II.10). Using the closure curve developed by van de Kreeke (1985), Salles (2001) also showed that the inlet would increase in size if the jetties were absent.

Due to the scouring activity caused by the confinement of flow, the offshore morphology of the inlet entrance provides a natural barrier to the littoral drift, conferring on the inlet a low sediment bypass capacity under fair-weather conditions. The ebb-tidal delta was displaced westward and at present is located in front of S^{ta}. Maria Cape (Fig. II.3), although its size does not seem to have increased. However, considering the evolution of A_c as well as the volumes computed for each cell, it seems more plausible that V_e annual accretion rates are approximately the same for the two analysed periods given that changes in yearly LST are not expected. Therefore the difference between both balanced periods is more likely to be related to the increase in sink volume due to the offshore progression of scouring activity (thereby supporting hypothesis two).

At present, Faro-Olhão Inlet appears to be reaching a dynamic equilibrium. About 50 years after its opening the inlet reached equilibrium with regard to the main inlet parameters (A_c, M_{depth}, and R_H); but only after 70 years since the opening has the inlet started to reach equilibrium in terms of the adjacent coastline. The evolution of V_o (offshore channel) is the major driver of the recent evolution of the inlet, and is directly related to the evolution of the inlet cross-section area in its progression towards geometric equilibrium. The evolution of this cell (with V_o) caused considerable disruption and redistribution of the

sediment load, affecting both sediment pathways and magnitudes, and is also related to the jetty configuration. As discussed, the current depth of the outer bar suggests that no significant bypassing is occurring to the downdrift coast. Therefore, either the outer bar will substantially increase its volume to achieve equilibrium between the LST and the inlet area (which would allow natural bypassing), or the status quo will persist, characterised by significant scouring activity exporting the sediment load to deeper areas offshore and maintaining a high ΣQ_{sink} volume.

II.4 DISCUSSION

In part of this paper, we analysed in detail cross-sectional/tidal prism relations for several inlets (Escoffier, 1940; O´Brien, 1969; Jarret, 1976) and also examined the wave-energy/ebb-tidal delta equation (Walton and Adams, 1972). Based on these analyses, we came to the conclusion that, despite the reasonable applicability of these formulae to some case studies, there remains a need to include other external controls as suggested by FitzGerald (1996) and as attempted in a few other studies (Bruun, 1978; Gao and Collins, 1994). In general, hydrodynamic parameters such as tidal prism and maximum velocity at the inlet throat are not known, which makes it impossible to analyse the viability of these formulae when applied to other case studies. In addition, even if these parameters were measurable using, for example, Acoustic Doppler Current Profilers (ADCP), their applicability to a multi-inlet system such as Rio Formosa is questionable because the increase of a tidal prism in one inlet would cause a decrease of it in others. Detailed A_c/P relations can be computed only by taking into consideration external controls, such as

regional stratigraphy or littoral drift, which are needed to perform detailed sediment budget computations. We recognise the utility of analysing inlet parameter evolution such as cross-sectional area and hydraulic radius, especially for understanding the major changes in the inlet channel. However, in order to properly infer inlet equilibrium, the inlet parameter analysis needs to be coupled with the sediment budget computations.

The opening of tidal inlets and the subsequent readjustment of the tidal prism are responsible for significant changes along adjacent coasts, especially in multi-inlet systems. The process is more evident when jetties are involved in inlet stabilisation, because they disrupt natural inlet migration patterns and impact the overall sediment budget of the coastal cells involved. Therefore, the analysis of inlet channel evolution and cross-sectional area with respect to the progression towards inlet geometric stability can be of great value in understanding sediment patterns. If the inlet cross-section is not in dynamic equilibrium, the cells comprising the inlet budget area are also not in dynamic equilibrium and therefore will undergo changes until equilibrium is achieved between the adjacent coast, deltas, and inlet channel area.

The Ria Formosa multi-inlet system, like other inlet systems, has been subjected to several anthropogenic activities with marked and/or unknown changes to the adjacent coast. The Faro-Olhão Inlet opening provides an informative case study of the associated and unpredictable effects of anthropogenic intervention, which in this example caused scouring processes and the narrowing of Armona Inlet which in turn caused the growth of Culatra Island. No convincing attempt has previously been made to develop inlet history based on sediment budget computations and to link this to inlet parameters. The results presented have allowed computation of the sediment budget and the associated rms uncertainty in a

stabilised inlet for two periods. The computed budget reveals that the inlet is only at present reaching equilibrium. The evolution of A_c showed constant values from around 1978-1985, about 25 years before the inlet started to reach volumetric equilibrium. It is hypothesised that the observed stability in A_c presented for Faro-Olhão Inlet (after 1978) is related to the jetties and to a stratigraphic control that prevents further deepening, and not to the achievement of a dynamic equilibrium. The intense scouring process occurring in the inlet offshore area continued after 1978, and was responsible for redistributing the sediments in the inlet area and adjacent coast. This redistribution implies several possible sediment transport paths. The most likely path, as interpreted from the sediment budget computations, appears to be the loss of sediment to the offshore area as a result of the offshore progression of the scouring process.

Elias and van der Spek (2006), studying the long-term evolution of an ebb-tidal delta (Texel Inlet, The Netherlands), concluded that the various conceptual models and empirical relationships that have been proposed to explain the variety in size, volume, and distribution of channels and shoals of the ebb-tidal delta, are focused on the relative importance of wave versus tidal energy and largely ignore other external controls as suggested by FitzGerald (1996). They also suggested that the dynamic coupling of the ebb-tidal delta, inlet, and basin is the key element of interest in analysing inlet evolution and behaviour, and thus it is possible to study inlet dynamics by analysing any one of those features. Previously, Dean (1988) had described the "sand sharing system" concept which recognised the interconnectivity and equilibrium of the sand bodies comprising the inlet, ebb-tidal delta, and adjacent shoreline. Essentially, the system attempts to reach a state of dynamic equilibrium for a specific set of hydraulic conditions. If the hydraulic conditions

are changed significantly, the system will attempt to attain a new state of dynamic equilibrium as dictated by the new conditions. Although circulation patterns are specific to each inlet and channel, particular characteristics may show commonality such as ebb or flood dominance, the use of preferred channels during ebb and flood tides, and jetty control of flow patterns.

The results of this study provide support for the "sand-sharing system" concept and for the useful coupling of sediment budget computation with inlet parameter analysis to understand inlet processes. In addition, the study has also shown how the analysis of even a single cell's evolution can explain significant aspects of inlet history (e.g., V_o), as suggested by Elias and van der Spek (2006). In most coastal areas affected by engineering activities, it is difficult to collect historical datasets in order to analyse coastline evolution and coastal engineering impacts. Inlet stability therefore is normally inferred from inlet hydraulics; however, most derived empirical formulae do not account for external controls, which can lead to erroneous interpretation of inlet hydraulics. Combining inlet hydraulic analysis with detailed sediment budget analysis can help to interpret sediment pathways and assign approximate values to their magnitudes, whereas the analysis of uncertainties plays an important role both in avoiding over-interpretation of data and in highlighting how the sediment budget could become better constrained in the future.

The method presented here should be applicable to other inlets, thereby increasing our knowledge of inlet evolution and how it may differ from case to case. The method implies there is a need to reconsider the use of empirical equations to infer stability. In addition, the method should be complemented with hydrodynamic measurements, especially of inlet tidal prism quantification and evolution and, in the case of a multi-inlet system, of the

distribution of the tidal prism. Our ongoing work is focussing on ADCP measurements along the entire tidal cycle (during both neap- and spring-tide conditions), which will allow us to compute the tidal prism, establish A_c/P formulations, examine ebb/flood dominance, and define prevailing sediment transport paths based on shear stress values (as proposed by Van de Kreeke, 1985). In the case of a multi-inlet system, the coupling of morphology and hydrodynamics should be extended to all inlets in order to infer the stability of the overall system based on the distribution of the tidal prism through time, and to understand inlet circulation patterns and their influence on the pathways and magnitude of sediment transport.

II.5 CONCLUSION

Sediment budgets for inlet areas are particularly difficult to formulate because the paths for sediment movement are complex and neither well known nor directly measurable (Kraus and Rosati, 1998). The complexity increases when determining ΣQ_{source} and ΣQ_{sink} because is difficult to measure or calculate LST rates. This paper has presented an approach for analysing a stabilised inlet that involves performing sediment budget computations in combination with analysis of inlet parameters. The approach chosen was based on estimating values for the best-known quantities and solving the less-well-known terms. Volume uncertainties, based on the definition of a maximum error area, were also determined. The results presented have allowed the estimation of annual rates of sediment flux for each inlet cell. Although the uncertainty of the budget calculated is large, it is fully representative of the complexities and difficulties associated with inlet sediment budget

computations. The maximum and rms volume uncertainties could be improved by considering most errors to be random, and therefore for a large number of data points, the errors would tend to cancel each other.

The coupling of sediment budget computation and inlet parameter analysis has been shown to be useful in understanding historical sediment pathways and magnitudes, and for analysing the evolution of an inlet towards equilibrium. The analysis has also highlighted that although the cross-section area evolution is a valuable parameter with which to analyse the locational/geometrical stability of an inlet, it should be complemented with analysis of other external controls. Existing formulae, widely used to infer inlet stability, relate cross-section area to the tidal prism and include terms to represent wave energy versus sediment storage on the ebb-tidal delta. Such formulae should be reviewed with a view to including other variables (e.g., stratigraphic controls) and to making them more adaptable in their application.

Appendix II: Notation

The following symbols are used in this paper:

τ_b = shear stress value

A_{avg} = average area over the channel length

A_D = active depth

A_c = cross-sectional area

A_f = delimited area of the flood-tidal delta

B = berm crest elevation

C_a = coastline change area of the barrier

h_c = depth of closure

h_d = average high of the dune field

H_s = significant wave height

Ll = landward limit of the tidal-delta

M_{depth} = maximum depth at inlet throat

PL = placement of sediment within sediment area

p = wetted perimeter

R = removal of sediment within sediment area

R_H = hydraulic radius

Sl = seaward limit of the tidal delta

P = tidal prism

V_E = equilibrium velocity

V_m = maximum cross-sectionally averaged velocity

V_d = individual cell representing the volume accreted/eroded on the downdrift shoreline

V_e = individual cell representing the volume stored at the ebb-tidal delta

V_f = individual cell representing the volume stored at the flood-tidal delta

V_i = individual cell comprising the inner inlet channel

V_o = individual cell comprising the inlet channel and offshore area

V_u = individual cell representing the volume accreted/eroded on the updrift shoreline

Z_a = average active depth of each barrier

Z_e = average thickness of the ebb-tidal delta

Z_f = average thickness of the flood-tidal delta

ΣQ_{source} = sediment flux entering a sediment budget area

ΣQ_{sink} = sediment flux exiting a sediment budget area

ΔV = volume change rate for sediment budget area

δX_{best} and/or rms = root-mean-square uncertainty

δX_{max} = maximum uncertainty

II.6 REFERENCES

Andrade, C. F., 1990. O Ambiente Barreira da Ria Formosa, Algarve-Portugal. PhD Thesis, Universidade de Lisboa. 627 pp. (in Portuguese).

Ballouin, Y., Howa, H., Michael D. (2001). Swash platform morphology in the ebb-tidal delta of the Barra Nova Inlet, Southern Portugal. J. Coast. Res.17 (4), 784-791.

Bettencourt, P., 1994. Les Environnements Sedimentaires de la Côte Sotavento (Algarve, Sud Portugal) et leur Évolution Holocéne et Actuelle, University Bordeaux I, (in French).

Bruun, P., 1978. Stability of Tidal Inlets. Elsevier, Amsterdam, 506 pp.

Buonaiuto, F.S., Kraus, N.C., 2003. Limiting slopes and depths at ebb-tidal shoals. Coast. Eng. 48 51-65.

Ciavola, P., Taborda, R., Ferreira, Ó., Dias, J.A., 1997. Field Measurements of Longshore Sand Transport and Control Processes on a Steep Meso-Tidal Beach in Portugal. J. Coast. Res. 13 (4), 1119-1129.

Costa, M., Silva, R., Vitorino, J., 2001. Contribuição para o estudo do clima de agitação marítima na costa Portuguesa. 2as Jornadas Portuguesas de Engenharia Costeira e Portuária in CD-ROM (in Portuguese).

Dean, R.G., 1988. Sediment Interaction at Modified Coastal Inlets: Processes and Policies, Hydrodynamics and Sediment Dynamics of Tidal Inlets. *Lecture Notes on Coastal and Estuarine Studies*, D.G. Aubrey and L. Weisher, eds., Vol. 29, Springer – Verlag, New York, NY, 1988, 412-439.

Dolbeth, M., Ferreira, Ó., Teixeira, H., Marques, J.C., Dias, J.A., Pardal, M.A., 2007. Beach morphodynamics impact on a macrobenthic community along a subtidal depth gradient. Mar. Ecol. Prog. Ser., 352: 113-124.

Elias, E.P.L., van der Spek, A.J.F., 2006. Long-term morphodynamic evolution of Texel Inlet and its ebb-tidal inlet (The Netherlands). Mar. Geol. 225, 5-21.

Escoffier, F.F., 1940. The stability of tidal inlets. Shore Beach 8, 114-115.

Esaguy, A.S., 1986. Ria de Faro, Barra de Faro-Olhão. Evolução 1955-1985. Direcção Geral de Portos Internal Report, 10 pp. (in Portuguese).

Ferreira, Ó., 2005. Depth of closure variability through time as a function of wave action. Book of Abstracts of the International Coastal Symposium 2005, Iceland, 77-78.

FitzGerald, D.M., 1996. Geomorphic Variability and Morphologic and Sedimentologic Controls on Tidal Inlets. J. Coast. Res. SI 23, 47-71.

Gao, S. and Collins, M., 1994a. Tidal inlet equilibrium, in relation to cross-sectional area and sediment transport patterns. Estuar. Coast. Shelf Sci. 38: 157-172.

Gao, S. and Collins, M., 1994b. Tidal inlet stability in response to hydrodynamic and sediment dynamic conditions**.** Coast. Eng. 23(1), 61-80

Hallermeier, R., 1981. Seward limit of significant sand transport by waves: and annual zonation for seasonal profiles. Coast. Eng. Tech. Aid U.S. Army Coast. Eng. Res. Cent. 81-2, 23p.

Hicks, D.M., Hume, T.M., 1997. Determining Sand Volumes and Bathymetric Change on an Ebb-tidal Delta. J. Coast. Res. 13 (2), 407-416.

ICN, 1999. Instituto da Conservação da Natureza. Estudo Ambiental do Projecto "Requalificação do Sistema Lagunar da Ria Formosa", Vol. 1, 223pp. (in Portuguese).

IH, 2000. Instituto Hidrográfico. Relatório de Progresso dos Trabalhos, Rel. PT. 0606/2000 – Monitorização Ambiental da Ria Formosa, 1999, Technical Report, 24pp. (in Portuguese).

Jarret, J.T., 1976. Tidal Prism-Inlet area relationships. GITI Report, vol. 3. U.S. Army Corps of Engineers, Waterways Experiment Station, Vicksburg, MS.

Kraus, N.C., Rosati, J.D. 1998. Estimation of uncertainty in coastal-sediment budgets at inlets. Coast. Eng. Tech. Note IV-16, 12pp.

Marino, J.N., Mehta, A.J., 1987. Inlet ebb shoal related to coastal parameters. Proc. Coastal Sediments'87, ASCE, 1608-1623.

Mason, J.E., 1986. Morphologic Evolution of a Relocated Mesotidal Inlet: Captain Sam's Inlet, South Carolina. Technical Report, Dept. Geol., University South Carolina, 149 pp.

O'Brien, M.P., 1969. Equilibrium Flow Areas on Inlets on Sandy Coasts. J. Waterw. Harb. Div. ASCE 95 (WW1), pp. 43-52.

Pacheco, A., Vila-Concejo, A., Ferreira, Ó., Dias, J.M.A., 2003. Recent bathymetric evolution of the Faro Channel (Algarve, Portugal), Special Volume on the 4th Symposium on the Atlantic Iberian Continental Margin, Thalassas 19(2b), 166-168.

Pacheco, A., Carrasco, A.R., Vila-Concejo, A., Ferreira, Ó. and Dias, J.M.A., 2006. Recent Evolution of the Faro Channel and its Association to Dredging Operations (Algarve, Portugal). J. Coast. Res. SI39, 572-577.

Pacheco, A., Carrasco, A.R., Vila-Concejo, A., Ferreira, Ó. and Dias, J.M.A., 2007. A coastal management program for channels located in backbarrier systems. Ocean Coastal Manage. 50, 119-143.

Rosati, J.D., Kraus, N.C., 1999. "Formulation of Sediment Budgets at Inlets". Coast. Eng. Tech. Note IV-15, 20pp.

Rosati, J.D., 2005. Concepts in Sediment Budgets. J. Coast. Res. 21 (2), 307-322.

Salles, P., 2001. Hydrodynamic Controls on Multiple Tidal Inlet Persistence. PhD Thesis, Massachusetts Institute of Technology and Woods Hole Oceanographic Institution, 272 pp.

Seabergh, W.C. 2006. Hydrodynamics of Tidal Inlets. In: Demirbilek, Z. (editor), Coastal Engineering Manual, Part II, Coastal Hydrodynamics, Chapter II-6, Engineer Manual 1110-2-1100, U.S. Army Corps of Engineers, Washington, DC.

Stauble, D., 1998. "Techniques for Measuring and Analysing Inlet Ebb shoal Evolution". Coast. Eng. Tech. Note IV-13, 12pp.

Shore Protection Manual, 1984. 4th ed., 2 Vol, U.S. Army Engineer Waterways Experiment Station, U.S. Government Printing Office, Washington, DC.

Surfer 8.0 User's Guide, 2002. Contouring and 3D Surface Mapping for Scientists and Engineers. Golden Software, Inc., 640pp.

Van de Kreeke, J., 1985. Stability of tidal inlets – Pass Cavallo, Texas. Estuar. Coast. Shelf Sci. 21 (1), 33-43.

Vila-Concejo, A., Matias, A., Ferreira, Ó., Duarte, C., Dias, J.M.A., 2002. Recent Evolution of the Natural Inlets of a Barrier Island System in Southern Portugal. Journal of Coastal Research SI 36, 741-752.

Vila-Concejo, A., Matias, A., Pacheco, A., Ferreira, Ó., Dias, J.M.A., 2006. Inlet hazard determination in the Ria Formosa barrier island system. Continental Shelf Research, Volume 26 (9), 1045-1060.

Walton, Jr., T.L., Adams, T.L., 1976. Capacity of Inlet Outer Bars to Store Sand. Proc. of the 15th Coastal Engineer Conference, ASCE, Vol. 2, 1919-1937.

Weinholtz, M.B., 1964. Contribuição para o Estudo da Evolução das Flechas de Areia na Costa Sotavento do Algarve. Separata do Boletim Trimestral de Informação do D.G.S.H. 14. (in Portuguese).

CHAPTER III

A statistical evaluation of models for extrapolating current velocities from boat-mounted ADCP profiles

Abstract

This paper presents a statistical evaluation of two theoretical fitting methods - logarithmic and power law - commonly used to extrapolate velocities to unmeasured areas of a vertical profile, such as near-bottom velocities. Analysis of covariance (ANCOVA) was used to test the models' performance when applied to velocity data collected with a boat-mounted Acoustic Doppler Current Profiler (ADCP) at the six tidal inlets of the Ria Formosa (southern Portugal) under spring- and neap-tide conditions. Results show that both models' goodness-of-fit is negatively correlated with velocity. Correlation also diminishes under ebb conditions, with no relation to velocity, but rather to transect depth. Both models consistently produce better simulations in inlets with a larger cross-sectional area, where turbulence scales are more attenuated due to spatial averaging. The logarithmic law model proved to be more robust across different velocities and channel morphologies and should be adopted as the preferred method for extrapolating velocity profiles when using boat-mounted ADCPs at confined channels and inlet entrances.

Keywords: Acoustic Doppler Current Profiler, statistical analysis, velocity profiles, bed friction velocity

III.1 INTRODUCTION

Increasingly, tidal inlet discharge is computed from data obtained using boat-mounted Acoustic Doppler Current Profilers (ADCPs). Although rapid data acquisition by boat-mounted ADCPs is attractive from a practical standpoint, there are some data limitations imposed by instrument operation (e.g. Gordon, 1996; SonTek, 2000; Simpson, 2001) and a range of measurement errors (e.g. Simpson and Oltman, 1993; Oberg et al., 2005; González-Castro and Muste, 2007).

Four regions can be identified when analysing raw ADCP velocity profile data: (1) the transducer draft, which relates to the distance from the acoustic beams to the water surface and therefore to the equipment position on the boat; (2) the blanking region, the distance that corresponds to electronic and transducer recovery time, where no measurements can be taken (Simpson, 2001); (3) the measurement region, with large spatial variability attributable to temporal variations associated with turbulent flows (Simpson, 2001; Dinehart and Bureau, 2005) and; (4) the side lobe region, emitted at 30-40º off the main acoustic beam (Muste et al., 2004), attributable to the direct reflection of the pulse from the boundary and to the reflection from side lobe energy taking a shorter path to the boundary (Simpson, 2001; González-Castro et al., 2002). The combination of transducer draft, blanking distance and side-lobe interference yields an incomplete profile of velocity through the water column (Fig. III.1). To compute cross-sectional discharge, mean velocities and bed-friction velocities, custom ADCP software makes use of theoretical models (e.g. 1/6 power-law and logarithmic law) to reconstruct the velocity profile in the unmeasured areas, based on models calibrated and tested for fixed current meters (i.e. using time-average profiles).

The structure of turbulent open-channel flow comprises a cascade of eddies varying in size and life-cycles. The wide range of interconnected flow structures is characterized

by a variety of spatial and temporal flow scales that in turn impose specific requirements on the measurement instruments and operational procedures (Muste et al., 2004). Instantaneous velocity profiles (e.g. ensembles) measured with a boat-mounted ADCP are incapable of smoothing out fluctuations induced by micro- and macro-turbulence and the potential effects of channel irregularities (e.g. proximity of coastal engineering structures, bank and bathymetric irregularities). This is because velocity profile is not an instantaneous feature of the flow, but a time-integrated one; hence individual ensembles cannot be used to characterise mean flow properties. In turn, fixed ADCP velocity measurements clearly show that there is good agreement between measured and theoretical velocity profiles if the data is collected over an extended time-span (Barua and Rahman, 1998).

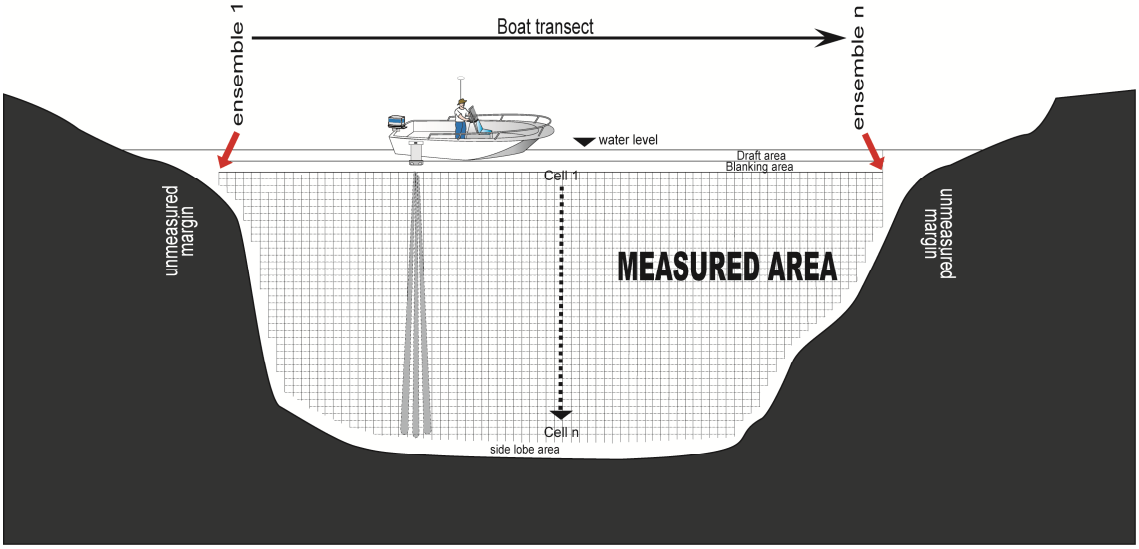

Figure III.1 Schematisation of the ADCP measurement along a transect course, with explanation of the recorded ensembles, draft, blanking, sidelobe areas, and unmeasured and measured areas

Inadequate sampling time is a major source of data scatter when using either stationary or boat-mounted ADCPs, resulting in ensembles strongly affected by turbulence and channel irregularities (Muste et al., 2004). However, boat-mounted ADCPs can successfully estimate discharge, despite this scatter (Muste et al., 2004).

This is because of the inherent spatial averaging applied to the raw velocity profiles as the boat moves along the transect. Micro- and macro-turbulence are smoothed out through a process similar to time-averaging, such that the output discharge equally samples the whole range of velocity fluctuations.

The present study aims to identify differences between two theoretical models used to extrapolate velocities to the unmeasured areas of velocity profiles collected with boat-mounted ADCPs, such as near-bed velocities, which can then be applied to estimate bed-friction velocities used in sediment transport formulae. Both models are used in commercial ADCP software and were reproduced in a MatLab environment for the present study (*The MathWorks, Inc.*®). ADCP data from twelve tidal cycles measured at the inlets of the Ria Formosa (Southern Portugal, Fig. III.2) were analysed in order to compute cross-sectional velocities using raw data and model reconstructions. Analysis of covariance (ANCOVA) will be used to test the models' performance in computing cross-sectional velocities.

The Ria Formosa is a multi-inlet barrier island system with five islands and two peninsulas separated by six tidal inlets: two artificially reopened inlets (Ancão and Fuseta), two artificially stabilised inlets (Faro-Olhão and Tavira) and two natural inlets (Armona and Lacém). The large embayment located behind the barrier islands is occupied by salt marshes, sand flats and a complex network of natural and partially dredged channels, covering 8.4×10^7 m^2 (Andrade, 1990). Tides in the area are semi-diurnal with average ranges of 2.8 m for spring tides and 1.3 m for neap tides. A maximum tidal range of 3.5 m can be reached. Harmonic analysis performed by Salles et al. (2005) revealed M_2 as the dominant component. Tides inside the lagoon are strongly distorted (in general, the growth of the M_4/M_2 ratio is significant, Salles et al., 2005). Wave climate in the area is moderate to high (offshore mean annual wave height

H_s ~ 1 m and peak period T_p of 8.2 s). The lagoon is generally well mixed vertically, with no evidence of persistent haline or thermal stratification (Newton and Mudge, 2003). Due to reduced freshwater inputs and elevated tidal exchanges, salinity values are usually close to those observed in adjacent coastal waters (Newton and Mudge, 2003). The prevailing winds are moderate (average 3 ms^{-1}) and predominantly westerly (Andrade, 1990). Salles et al. (2005) conducted a variance analysis of the lagoon's tidal and non-tidal signals, showing that meteorological and long-term water-level variability explained less than 1% of total variance. The authors concluded, with reference to Kraus and Militello (1999), that wind plays a minor role in governing water circulation patterns. Information on inlet survey parameters, characteristics and evolution can be found in Table III.1 as well as in Vila-Concejo et al. (2002, 2006) and Pacheco et al. (2008).

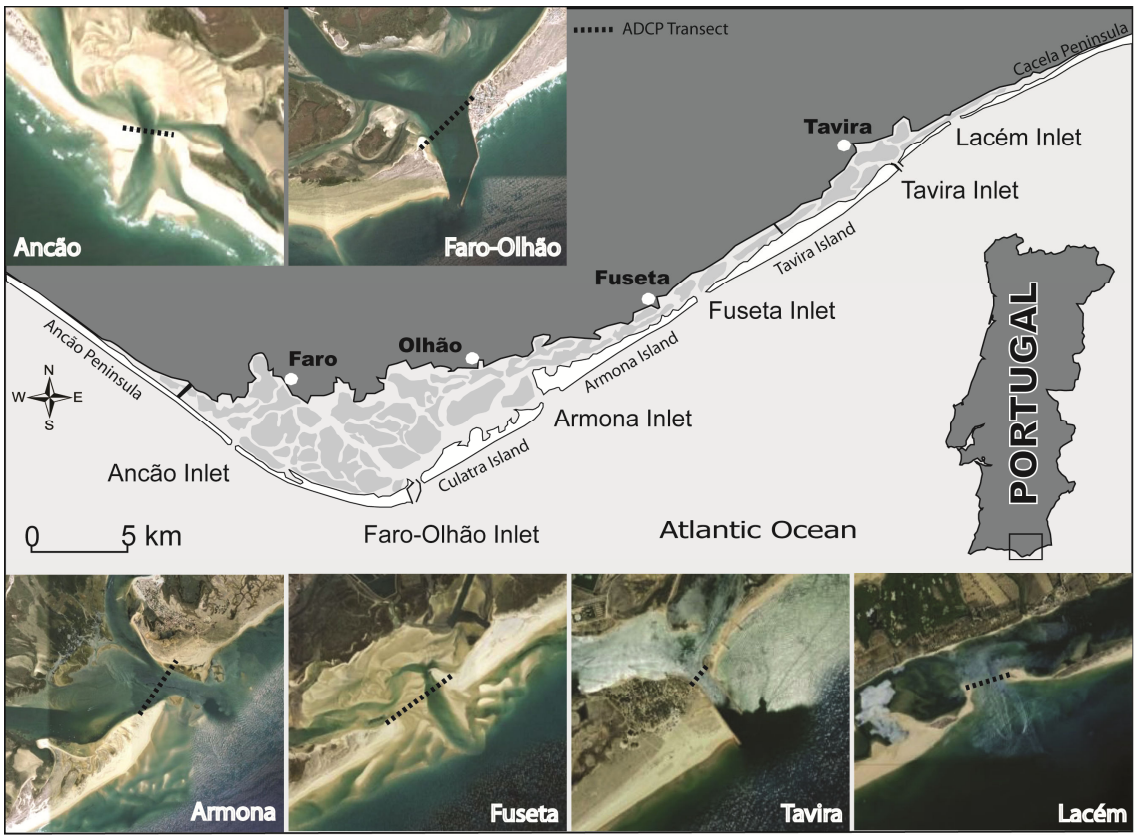

Figure III.2 The Ria Formosa multi-inlet lagoon system (Southern Portugal)

Table III.1 General inlet characteristics and mean survey parameters: cross-section (A_c), channel depth (D), channel length (L), transect travel time (Tt) and collected ensembles per transect (Ens)

INLET	General Characteristics	Mean (Survey Parameter) ± σ				
		A_c (m^2)	D (m)	L (m)	Tt (s)	Ens (N)
Ancão	Artificially relocated. Cyclic eastward migrating inlet. Stable A_c while migrating.	420	3.8	110	55	11
Faro-Olhão	Artificially open and stabilised (dual jetty). Main inlet of the system. Intense scouring at inlet gorge.	5290	9.0	620	310	62
Armona	Natural inlet. Stable location through recent centuries. Losing hydraulic efficiency since Faro-Olhão opening.	2950	5.2	560	280	56
Fuseta	Artificially relocated. Cyclic eastward migrating inlet. Presents channel infilling and meandering.	280	3.4	84	42	8
Tavira	Artificially open and stabilised (dual jetty). Intensively dredge to be maintained open.	970	10.2	95	48	10
Lacém	Natural inlet that can open over a wide area. Cyclic eastward migrating inlet. Presents channel infilling & meandering	200	1.6	100	50	10

III.2 METHODOLOGY

III.2.1 Data acquisition and post-processing

Current velocity profiles were measured during spring and neap tides at the six tidal inlets of the Ria Formosa system using a boat-mounted 1500 kHz ADCP with bottom tracking. The equipment was mounted port-side in the middle of the boat and synchronized with a global positioning system (RTK-DGPS, *DSNP Scorpio 6001 SK/MK*) connected to a navigational interface running hydrographic survey software (*Hypach®Max 4.3a Gold, Coastal Oceanographics, Inc.*). Measurements were taken along a fixed transect across each channel (c. 13 profiles per inlet) every hour during a 12h30' tidal cycle. The range cell/bin spacing was set to 0.5 m and the number of cells was set to an appropriate resolution for the given water depth. Blanking distance and ADCP transducer draft were both set to 0.5 m. The instrument was run in continuous mode and the ADCP profile/ensemble interval was set to the same value as the

averaging interval (c. 5 s). Boat speed was maintained at ~2 m/s, except is strong currents occasionally encountered around flood/ebb peaks. Velocity data were collected following guidelines for assuring data quality (Simpson and Oltman, 1993; Simpson, 2001; Oberg et al., 2005). The first step on pos-processing was to compute the speed of sound using temperature and salinity values at Ria Formosa, based on the values given by Newton and Mudge (2003). The ADCP uses a compass to define the North direction, which results in velocities referenced to magnetic North instead of true North. Both values of speed of sound and magnetic declination were given as input to the software used on data collection to (1) convert the Doppler shift to output water velocities and (2) to correct velocity measurements so that they are referred to true North.

The signal-to-noise ratio (SNR) threshold was set to 5 to remove invalid data below the ambient noise level. A uniform weighting filter (3-point interpolation) was applied horizontally and vertically. The box filter was chosen due to it simplicity and common use on reducing random noise. At the boundaries, i.e. margins and bottom and, the filter only uses points at one side of the calculated output sample. Through the cross-section, when the number of available samples is higher than three, the filter works symmetrically, i.e., choosing points from one side and the other of the computed output value. The lowermost 10 % of the raw velocity data were discarded due to side-lobe interference. Data were rotated and individualised across- and along-flow relative to transect orientation.

III.2.2 Computation of cross-sectional velocity

Depth average velocity ($\overline{U}$) is obtained for each 5 s ensemble using the following formula (Soulsby, 1997),

$$\overline{U} = 1/h \int_0^h U(z)dz \tag{III.1}$$

where h is water depth, $U(z)$ is along-flow current speed at height z. The ensemble depth is the bottom-track depth plus the transducer draft and blanking distance; therefore the depth-average velocity (Eq. III.1) represents the entire velocity profile and is approached by the trapezoidal integration method of Soulsby (1997),

$$\overline{U} = 0.5/h \left[\left(\sum_{i=1}^{n} [(u_i + u_{i+1})(z_{i+1} - z_i)] \right) + (u_{n-1} + u_n) + 2u_n(h - z_n) \right] \tag{III.2}$$

where *i* and *n* represent the first and last measured cell, respectively, h is the total water depth and, u_1, u_2,..., u_n are current velocity measurements at heights z_1, z_2,…, z_n.

Velocity distributions along each velocity profile, i.e. depth, were obtained using the 1/6 Power Law (PL: Cheng, 2007, Eq. III.3) and Logarithmic Law (LL: Soulsby, 1997, Eq. III.4).

Power Law

$$\frac{u}{u_{\max}} = \left(\frac{z}{h} \right)^{1/m} \tag{III.3}$$

where u is the streamwise, time-mean flow velocity, $u_{\max}$ is the maximum flow velocity taken at the free surface ($z = h$), z is the bed-normal distance measured upwards from the profile datum, h is the flow depth, and $1/m$ is referred to as the power-law exponent.

Logarithmic Law

$$u = (u_* / k) \ln(z / z_0) \tag{III.4}$$

where u_* is the bed friction velocity, κ the von Kárman constant and z_0 the bed roughness length. The bed friction velocity and apparent roughness (z_a) can be estimated by a linear regression of $u(z)$ on $\ln(z)$,

$$u_* = mk \tag{III.5}$$

$$z_a = \exp(-c/m) \tag{III.6}$$

where c and m are the intercept and gradient of the regression line, respectively. The value of z_a, expressing both grain roughness and form drag, replaces z_0 in Eq. III.3. Ensemble depth-average velocity using theoretical velocity distributions predicted by the models was computed using Eq. III.1.

The cross-section depth-average velocity (U_{cs}) was then computed for raw ADCP data and the two models:

$$U_{cs} = [\sum_{i=1}^{n} (\overline{U}_i + \overline{U}_{i+1})/2]/n \tag{III.7}$$

where i represents the ensemble number from 1 (transect start) to the total n of measured ensembles (transect end) across the channel.

III.2.3 Statistical analysis

Coefficients of determination (R^2) were used to evaluate the relationships between U_{cs} values determined using raw ADCP velocities and U_{cs} values predicted by the two theoretical models (LL and PL). Two bifactorial ANCOVA tests were carried out to test the fit of each theoretical model to empirical data. In the first test, model performance was assessed by the correlation (i.e. outcome variable) between real and modelled U_{cs},

with tide (neap vs. spring, 2 groups) and inlet (Ancão, Faro-Olhão, Armona, etc, 6 groups) as independent variables. In the second ANCOVA test, inlet and tide were again the independent variables, but now the difference between R^2 from both models (LL-PL) was used as an outcome variable to evaluate their performance. In this comparison, positive values mean better goodness-of-fit for the logarithmic model, while negative values indicate a better fit for the power law. In both ANCOVA tests, two covariates were used separately: (1) U_{cs} raw data (expressing the velocity and direction of water flow) and, (2) U_{cs} raw modulus (expressing the velocity of water flow alone). The two covariates control for differences arising from flow direction (e.g. flood vs. ebb) and magnitude. Both test runs were made using 156 U_{cs} values, representing twelve tidal cycles at six tidal inlets, on both spring and neap-tide conditions (i.e. 13 transects per inlet * 6 inlets * 2 tidal cycles).

ANCOVA determines the differences between groups while controlling the effect of one or more continuous predictor variables, known as covariates. The covariate is controlled (e.g. U_{cs} in the first test), allowing the effect that each independent variable (i.e. tide condition or different inlet) has on the outcome (R^2 values between raw and model computed U_{cs}) to be analysed. ANCOVA thus tests whether certain factors have an effect on the outcome variable after removing variance contributed by the covariates. Additionally, if a variable used as a covariate varies systematically with any of the independent variables, ANCOVA can be used to identify and eliminate this confounding influence.

Prior to performing ANCOVA, the assumption of homogeneity of slopes was checked. The effect of the covariates on the outcome seems to be equal for all inlet and tide conditions ($p > 0.122$), except in one situation: the effect of raw U_{cs} on both

logarithmic and power law model fit seems to be different for Fuseta Inlet at neap tide. Since we cannot assume homogeneity of slopes in this case, Fuseta Inlet was excluded from analysis in this situation (tests using U_{cs} raw data as a covariate and R^2 values as outcome variables).

III.3 RESULTS

Typical instantaneous velocities distribution obtained by the ADCP for three cross-sections can be observed on Fig. III.3, which corresponds to slack water (A), peak flood (B) and peak ebb (C). At peak ebb/flood the maximum velocities occurred at the central channel for flood, and better distributed through the cross-section at ebb. Typical ensembles for three instantaneous moments of the flow can be also observed on Fig. III.3, as well as the adjustment of both models from the first to the last cell, discarding 10% of the values obtained at the sidelobe area.

Values of frictional velocity and roughness length scale obtained by the logarithmic law profile adjustment to the raw data were compared with values obtained using the Reynold Stress method (RS) applied to data collected with an ADV (Pacheco et al., 2009). The obtained values are within the same order of magnitude and agree well with results presented by Voulgaris and Trowbridge (1997). The RS presents slightly higher values, as expected, since the measurements relate to a specific point where the form drag component of stress can be more accurately determined, while the log profile from the ADCP depends on the average cross-section values. The results are also in agreement with the detailed measurements made by Williams et al. (2003) for the study area.

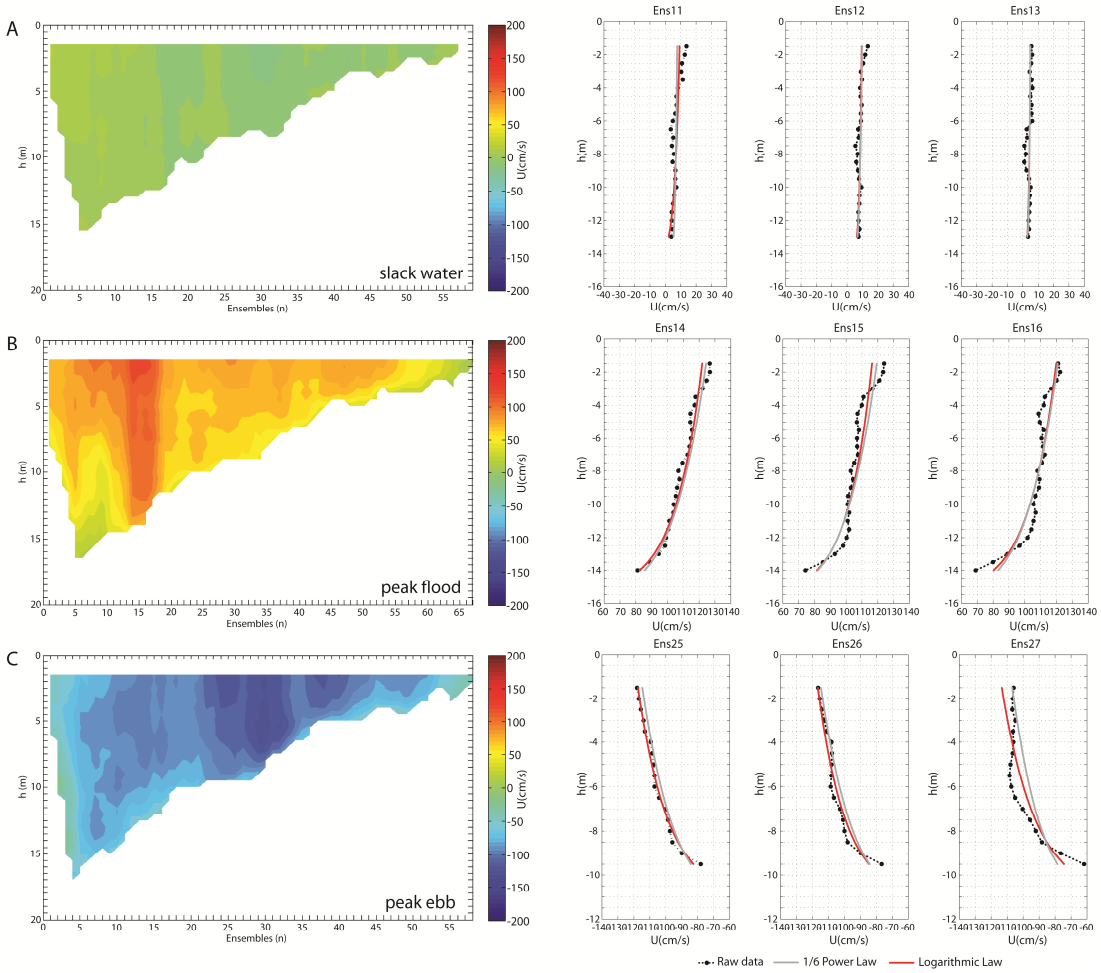

Figure III.3 Instantaneous velocity distribution of the flow structure through a cross-section at slack water (A), flood peak (B) and ebb peak (C) and adjustment of the 1/6 power and logarithmic law for three consecutive ensembles at each of the cross-sections

The overall correlation between U_{cs} computed using raw ADCP velocities and U_{cs} predicted by each theoretical model (PL and LL) is very strong (high R^2 values) for different tidal conditions and inlets (Fig. III.4). Fig. III.5 plots R^2 values for both models against velocity, U_{cs} and D (average cross-sectional depth) for flood/ebb conditions. It was not possible to identify variations in R^2 for different U_{cs} and D values for the two methods: the dispersion of R^2 values seems not to be linearly or curvilinearly related to either U_{cs} or D.

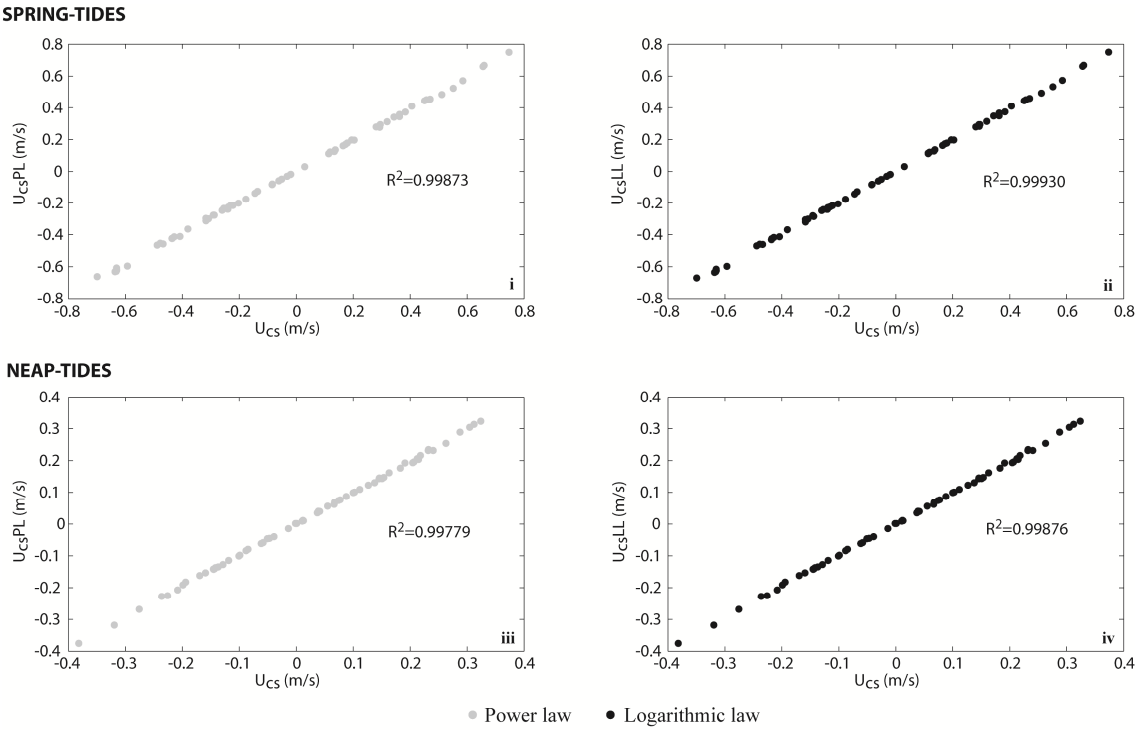

	Spring-tides		Neap-tides	
	PL (R^2)	*LL (R^2)*	*PL (R^2)*	*LL (R^2)*
1. Ancão	0.9999	0.9999	0.9999	0.9999
2. Faro-Olhão	1.0000	1.0000	0.9999	1.0000
3. Armona	0.9999	0.9999	0.9999	1.0000
4. Fuseta	0.9999	1.0000	0.9994	0.9998
5. Tavira	0.9997	0.9997	0.9997	0.9997
6. Lacém	0.9995	0.9998	0.9994	0.9995

Figure III.4 Coefficient of determination (R^2) between computed cross-sectional velocities (U_{cs}) using the raw data and both theoretical models for the six inlets, under both neap and spring tide conditions

A series of bifactorial ANCOVA tests was performed in order to understand whether model performance is dependent on tide or inlet. In the first tests, using R^2 values of the logarithmic law as outcome variables and U_{cs} raw data as covariates, there were no statistically significant effects. However, when U_{cs} raw modulus was used, significant effects were found for covariate – $F(1, 156) = 24.9$, $p < .001$ – as well as for inlet – $F(4, 156) = 3.3$, $p < .01$. Neither tide nor the inlet * tide condition interaction were significant. Similar results were found when R^2 values from the power law were used as outcome variables: no significant effects with raw U_{cs} data as a covariate. However, when U_{cs} raw modulus was used as a covariate, significant effects of

covariate – $F(1, 156) = 17.8$, $p < .001$– as well as inlet – $F(4, 156) = 3.0$, $p < .05$ – were found. In both models, the regression slope for the raw U_{cs} modulus covariate is negative, suggesting that PL and LL goodness-of-fit diminish with flow velocity. The effect of different inlets resulted in both models performing better for Armona and Faro-Olhão inlets, compared to the other inlets, especially Fuseta (*post hoc* comparisons with Bonferroni's correction).

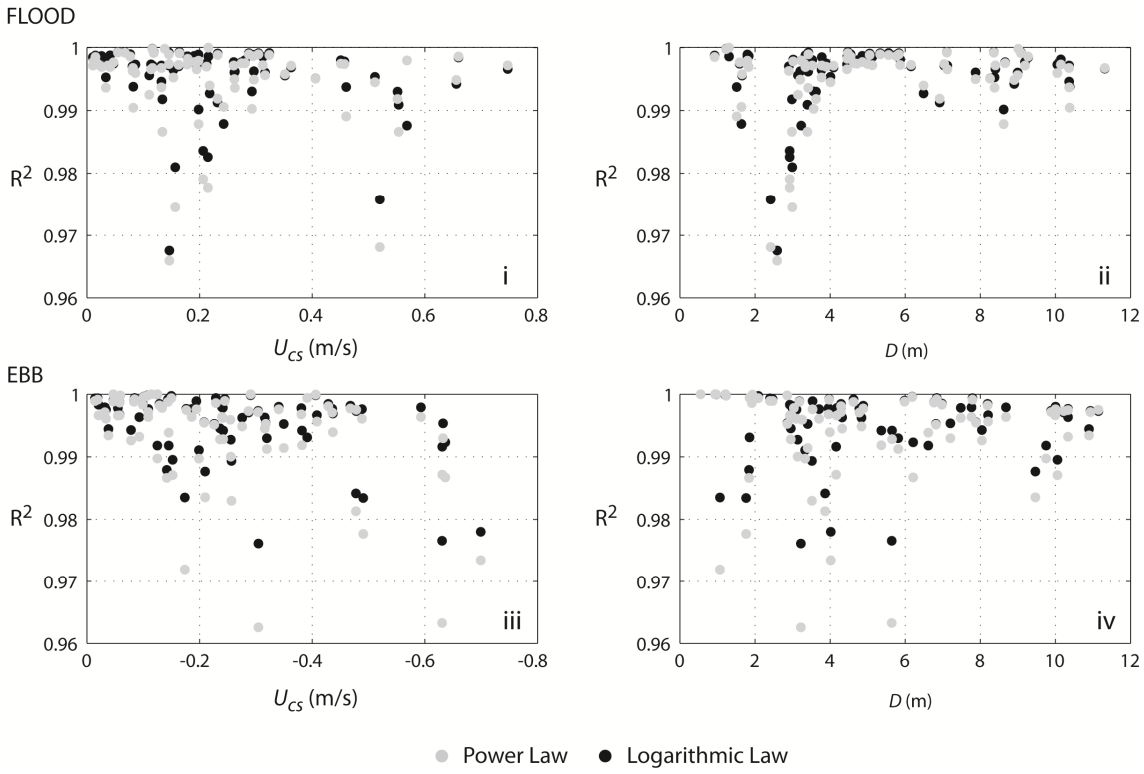

Figure III.5 Distribution of coefficient of determination values (R^2) comparing theoretical models and raw cross-section velocity (U_{cs}), versus U_{cs} magnitude and depth (D), for flood/ebb flow, for the six inlets

In the second ANCOVA test, the outcome variable expresses differences in performance between the two models. Testing the significance of ANCOVA intercept allows us to evaluate the difference between the levels of fit provided by both models. Since the ANCOVA intercept is significant and above zero – $F(1, 156) = 36.6$, $p < .001$ - we can conclude that LL seems to show, on average, a better fit (higher R^2) than PL. In

this analysis, U_{cs} raw data covariates have a significant effect – $F(1, 156) = 8.1$, $p < .01$ – suggesting that the velocity and direction of water flow contributes to the LL model's superior performance. No other effect was significant – once raw U_{cs} is controlled, differences between tides or between inlets are too small to be statistically significant.

III.4 DISCUSSION

The covariates used on the ANCOVA tests performed were the U_{cs} raw and U_{cs} raw modulus, which represent sources of variation that affect the response variable (R^2 values), but were not controlled during the study, i.e., the flow raw velocities across transect are direct measurement of the equipment. The first ANCOVA results show that R^2 values for each model in computing U_{cs} are not affected by raw U_{cs} but by its modulus, i.e. the effect of the tidal signal (positive for flood, negative for ebb) is negligible. It is the increase in U_{cs} magnitude that causes decreased performance in both models. When this effect is excluded from analysis, differences between inlets are highlighted: both theoretical models showed poorer fit in inlets with a small cross-sectional area, especially Fuseta Inlet. The effect is not so evident at Lacém Inlet, the inlet presenting the shallower depths. However, this could be attributed to the technical difficulty of obtaining velocity measurements at Lacém, resulting in an artefactual increase in R^2 values (i.e. regression based on only one or two bin/cells). Considerably better adjustments were obtained for Armona and Faro-Olhão, the largest inlets of the system (Table III.1). Because boat-mounted ADCPs operate on a multi-transmit mode, with a measurement volume proportional to boat speed (Muste et al., 2004), if near-constant velocity is assumed, the number of ensembles used in the spatial integration method ultimately depends on the transect/channel length.

The second ANCOVA test revealed the better overall performance of the LL model. This advantage is particularly evident at flood tide, characterised by deeper average transect depths *D*, compared to ebb. The use of two different covariates, raw U_{cs} and modulus U_{cs} (with significance found only for raw U_{cs}), seems to indicate that both velocity and direction of the flow contribute to the LL model's superiority over PL in computing U_{cs}. This advantage seems to be less related to velocity and more to other, independent factors, such as water depth (*D)* and channel length (*L*) (Table III.1). Our data suggest that the LL method for extrapolating velocities across channels better responds to the potential effects of channel irregularities (e.g. channel banks, irregular bathymetry).

Based on the present evidence, and using velocity profiles measured with boat-mounted ADCPs, the LL model fits the raw U_{cs} with the greatest statistical significance. It should therefore be adopted as principal method for extrapolating velocity in unmeasured areas of the current profile, and used to estimate bed-friction velocities commonly used in sediment transport formulae.

III.5 CONCLUSION

A statistical analysis of the performance of two velocity distribution models showed strong correlations between modelled and real cross-sectional velocities. More detailed analyses, using ANCOVA tests, showed that the fit of both models is negatively correlated with velocity. Comparing the two models, the logarithmic law (LL) model is less influenced by this effect and therefore more robust than the power law (PL) model. The study also showed a general decline in both models' performance during ebb situations, related not to velocity, but to channel depth. Performance of the logarithmic law model was again less affected, indicating its greater adaptability to different channel

morphologies. Both models present consistently better responses at inlets with a large cross-section compared to those with smaller cross-sectional area, where turbulence scales are less attenuated. The authors reinforce that the results of this study applies to confined channels and inlets. More tests should be done on the future at open waters.

III.6 REFERENCES

Andrade, C., 1990. O Ambiente Barreira da Ria Formosa, Algarve-Portugal. PhD Thesis, Universidade de Lisboa. 627 pp. (in Portuguese).

Barua, K.H., Rahman, K.H., 1998. Some aspects of turbulent flow structure in large alluvial rivers. J. Hydr. Res. 36(2), 235-252.

Cheng., N., 2007. Power-law index for velocity profiles in open channel flows. Advances in Water Resources 30, 1775–1784.

Dinehart, R.L., Burau, J.R., 2005. Repeated surveys by acoustic Doppler current profilers for flow and sediment dynamics in a tidal river. J. Hydrol. 314, 1-21.

González-Castro, J.A., Ansar, M., Kellman, O., 2002. Comparison of discharge estimates from ADCP transect data with estimates from fixed ADCP mean velocity data, in: Proceedings of the ASCE-IAHR Hydraulic Measurement & Experimental Methods Conference, Estes Park, CO (CD-ROM).

González-Castro, J.A., Muste, M., 2007. Framework for Estimating Uncertainty of ADCP Measurements from a Moving Boat by Standardized Uncertainty Analysis. J. Hydraul. Eng., 133(12), 1390-1410.

Gordon, R.L., 1996. Acoustic measurements of river discharge. J. Hydraul. Eng. 115(7), 371-389.

Kraus N. C., and A. Militello, 1999: Hydraulic study of multiple inlet system: East Matagorda Bay, Texas. J. Hydraul. Eng., 25, 224–232.

Muste, M., Yu, K., Spasojevic, M., 2004. Practical aspects of ADCP data use for quantification of mean river flow characteristics; Part I: moving-vessel measurements. Flow Measurements and Instrumentation 15, 1-16.

Newton, A., Mudge, S.M., 2003. Temperature and salinity regimes in a shallow, mesotidal lagoon, the Ria Formosa, Portugal. Est. Coast. Shelf Sci. 57: 73-85.

Oberg, K.A., Morlock, S.E., Caldwell, W.S., 2005. Quality-Assurance Plan for Discharge Measurements Using Acoustic Doppler Current Profilers. US. Geological Survey, Scientific Investigation Report 2005-5183, Reston, Virginia, 35pp.

Pacheco, A., Vila-Concejo, A., Ferreira, Ó., Dias, J.A., 2008. Assessment of Tidal Inlet Evolution and Stability Using Sediment Budget Computations and Hydraulic Parameter Analysis. Mar. Geol. 247, 104-127.

Pacheco, A., Williams, J.J., Ferreira, Ó., Dias, J.A., 2009. Evaluation of shear stress computation at a tidal inlet using different methods. J. Coast. Res. 56, *Proceedings of the 10th International Coastal Symposium*, 1385-1389.

Salles, P., Voulgaris, G. and Aubrey, D., 2005. Contribution of nonlinear mechanisms in the persistence of multiple tidal inlet systems. Estuar. Coast. Shelf. Sci. 65, 475-491.

Simpson, M.R., Oltman, R.N., 1993. Discharge-measurement system using an acoustic Doppler current profiler with applications to large rivers and estuaries, US Geological Survey Water-Supply Paper 2395, Denver, CO, 32pp.

Simpson, M.R., 2001. Discharge measurements using a broad-band acoustic Doppler current profiler, Open-File Report 01-1, US Geological Survey, Sacramento, CA, 123pp.

SonTek, 2000. Acoustic Doppler Profiler, Technical Documentation, San Diego, CA, SonTek/YSI, Inc. San Diego, CA, USA, 160pp.

Soulsby, R.L., 1997. Dynamics of marine sands. A manual for practical applications. HR Wallingford Report SR 466, 142pp.

Vila-Concejo, A., Matias, A., Ferreira, Ó., Duarte, C., Dias, J.M.A., 2002. Recent Evolution of the Natural Inlets of a Barrier Island System in Southern Portugal. J. Coast. Res. SI 36, 741-752.

Vila-Concejo, A., Matias, A., Pacheco, A., Ferreira, Ó., Dias, J.M.A., 2006. Inlet hazard determination in the Ria Formosa barrier island system. Cont. Shelf. Res. 26 (9), 1045-1060.

Voulgaris, G., Trowbridge, J.H., 1997. Evaluation of the Acoustic Doppler Velocimeter (ADV) for Turbulence Measurements. J. Atmos. Oceanic. Technol. 15, 272-289.

Williams, J.J., Bell, P.S., Thorne, P.D., 2003a. Field measurements of flow fields and sediment transport above mobile beds. J. Geophy. Res. 108, NO. C4, 3109, doi:10.1029/2002JC001336.

CHAPTER IV

Hydrodynamics and Equilibrium of a Multiple-Inlet System

Abstract

Although it is generally acknowledged that most multiple inlets are unstable and cannot coexist, there is evidence to suggest that such inlets can indeed be stable over decadal time scales. Multiple-inlet systems servicing a single embayment, in contrast to single-inlet systems, confer particular hydrodynamic characteristics such as the potential existence of residual discharges and currents between the inlets. This paper presents detailed measurements of hydrodynamic variables obtained over complete spring and neap tidal cycles in a multiple-inlet system in Southern Portugal (Ria Formosa). The results indicate that the two main inter-connected inlets servicing an embayment can coexist, at least over a time scale of several decades. However, their coexistence cannot be explained simply using empirical equilibrium relations or inlet hydraulics. Although residual flow between the inlets appears to play an important role enhancing their stability, it is the availability of sediment stored in the ebb-tidal deltas (and its capacity to be carried into the inlets during storm events) that ultimately dictates the overall equilibrium, independently of the flushing capability provided by the hydraulics. Such movement of sediment leads to the obstruction of the inlet channels, thereby affecting the hydraulic efficiency and eventually leading to inlet closure in the long term. The results augment existing knowledge concerning multiple-inlet systems and improve understanding of their short- to medium-term stability.

Keywords: tidal inlets, dynamic stability, tidal prism, Ria Formosa, Portugal

IV.1 INTRODUCTION

A requirement to artificially open or maintain multiple tidal inlets serving a single embayment can arise in order to establish safe navigable routes or to increase water exchange between the open sea and a back-barrier lagoon system. Multiple-inlet systems servicing a single embayment, in contrast to single-inlet systems, impart particular hydrodynamic characteristics such as the potential existence of residual discharges and currents through the inlets. It is recognised that residual circulation, which can be regarded in terms of either the mean (Lagrangian) velocity or the mass transport (discharge), has direct control on the net transport of material through the inlet, especially suspended material (Liu and Aubrey, 1993; Bakker and de Vriend, 1995; de Vriend and Ribberink, 1996). If multiple tidal inlets are hydrodynamically connected, a morphological change in a given inlet can modify the hydrodynamic behaviour of other inlets and adjacent channels, and therefore lead to changes in the tidal prism (P), the generation of residual discharge, and an alteration of the non-linear tidal interaction of the offshore tidal constituents (Boon and Byrne, 1981; Speer and Aubrey, 1985; Friedrich and Madsen, 1992; Salles, 2001; Pendleton and FitzGerald, 2005; Salles et al., 2005). Because P is the quantity of water flowing through the inlet cross-section (A_c), changes in P induce changes in sediment transport, thereby affecting the equilibrium of channel A_c and hence causing inlet instability (O'Brien and Dean, 1978; Bruun, 1978).

Most investigations of multiple inlets have concluded that such inlets are unstable with respect to water exchange rates, critical inlet cross-section, and sedimentation regimes. However, several studies have presented evidence to show that multiple inlets can be stable over time scales of decades to centuries. The first such investigation was that of Escoffier (1977), whose work in Gasparilla Sound indicated that some bays

which communicate with the sea via two or more inlets can be stable. Such bays are normally expanded and shallow, thus giving rise to significant variations in tidal phase and amplitude throughout the bay. Subsequent studies [e.g. Chatham (Friedrich et al., 1993; Liu and Aubrey, 1993); Wadden Sea (Louters and Gerritsen, 1994); and Ria Formosa (Salles et al., 2005)] have since supported the idea of multiple-inlet stability.

Some authors have examined aspects of multiple tidal inlets (e.g. van de Kreeke, 1985, 1990) by using semi-empirical approaches to analysing single-inlet system equilibrium, combining Escoffier's curve (1940) and O'Brien's (1969) equilibrium relationship between P and A_c. For example, in a study of the equilibrium of a two-inlet bay system, van de Kreeke (1990) found that the equilibrium curves did not intercept in their stable equilibrium sections and concluded that neither of the inlets was stable. The assumptions in the combined semi-empirical approach include: the walls of the basin are vertical; there is no inflow of streams; there are no density currents present; and tidal fluctuations are given by a sine curve. The analysis also assumes equilibrium between the fraction of littoral drift that enters the inlet and the sediment transport by ebb tidal currents, where maximum velocity is a measure for the sediment transport capacity of inlet currents, as given by the equilibrium relation between P and A_c (O'Brien, 1969).

Subsequently, van de Kreeke et al. (2008) pointed out that these assumptions might be too restrictive, using the example of the Wadden Sea, where the backbarrier lagoon consists of a series of basins separated by topographic highs, rather than one single basin. The different topographic highs limit (but do not exclude) the exchange of water between the sub-basins, whereby the equilibrium of the multiple-inlet system depends on the degree of connectivity between the basins. For basins that are connected by a large, wetted cross-section opening over the topographic high, approaching the situation of a single basin, there are no stable equilibriums. In contrast, a set of equilibrium cross-

sectional areas can coexist for basins that are weakly coupled, approaching a two single-inlet bay configuration. For intermediate wetted cross-sections, the results become more complex, i.e., depending on the length and friction factor of the inlet channels there can be stable configurations. The causes and conditions that determine the number of stable equilibriums are not clear and must be better studied. However, the work of van de Kreeke et al. (2008) demonstrates the importance of topographic highs on the stability of multiple-inlet systems.

Complex intertidal areas are common in shallow embayments, which can result in large variations in bay surface slopes and friction coefficients throughout the tidal cycle (i.e., the development of strong non-linearities) (Liu and Aubrey, 1993; Salles et al., 2005). When analysing the stability of a single-inlet system in which fresh water input is negligible, tidal distortion can be used directly as an indicator for flow dominance and net sediment transport arguments (Aubrey and Speer, 1983). The conventional interpretation concerning tidal duration asymmetry (the unequal rise and fall of the tide) is that bays with shorter flood than ebb durations lead to flood dominance by producing shorter, stronger flood currents (flood-dominated) and subsequent infilling of the bay; whereas shorter ebb durations lead to strong ebb currents (ebb-dominated), enhancing sediment flushing, and promoting long-term inlet stability (Boon and Byrne, 1981). In such an approach, the peak velocities of flood and ebb are used as a first indicator for the preferred direction of movement for the coarse sediment fraction. However, this measure takes no account of the duration of such peak velocities. According to Dronkers (1986), flood or ebb dominance does not necessary lead to deposition or erosion; instead, the asymmetry of the flood and ebb extension of the tidal velocity curve, and in particular the length of high water slack period compared to the low water slack, appear to control the net sediment budgets of intertidal areas.

Strong non-linear distortion in water surface elevation and velocity fields can lead to situations where the directions of maximum velocity and net near-bed sediment transport operate in opposite directions (van de Kreeke and Robaczewska, 1993). The flood/ebb dominance relationship with prevailing sediment transport is not sufficiently uniform to assume that duration and velocity asymmetries within an entire inlet and backbarrier system are always consistent and in the same direction (Pendleton and Fitzgerald, 2005). The explanation is related to the friction-dominated behaviour of these shallow systems and the production of non-linearities associated with friction and time-varying channel depths and bay widths (Friedrichs et al., 1993). The process is even more complex for multiple inlets, where the duration of flood or ebb is not a determining factor for flow dominance due to the existence of strong residual flow between inlets.

Salles et al. (2005) analysed the long-term stability of a multiple-inlet system (Ria Formosa, Southern Portugal) by forcing variations on A_c and analysing its effects on tidal distortion, residual current, and net sediment transport. Through combining a numerical simulation of the flow with a semi-empirical approach of inlet equilibrium, simulations showed that a longer flood (ebb) may be associated with flood (ebb) dominance due to the existence of strong residual circulation between inlets. The direction of net sediment transport (flood or ebb) is dependent not only on the direction of the averaged velocity, but also on the shape (distortion) of the velocity, and on the flood to ebb maximum velocity ratio. The shape of the velocity curve depends on friction, bathymetry and channel geometry, and non-linear interactions within the water motion, and is described by the relative phases between tidal constituents. Salles et al. (2005) also showed that tidal distortion is inversely proportional to transport dominance, i.e., an increase in cross-sectional area at any given inlet translates to an

increase in tidal distortion at that same inlet, but the prevailing net near-bed sediment transport capacity decreases. No definitive explanation has been given as to why the water surface and tidal velocity distortions exhibit opposite responses to changes in A_c, but Salles et al. (2005) suggest that the water surface and tidal velocity phase are not, in most cases, reliable diagnostic indicators of flow dominance.

In the context of the aforementioned background, this present investigation focuses on hydrodynamic measurements obtained during a complete spring and a complete neap tidal cycle in the Ria Formosa, a multiple tidal inlet system located in southern Portugal. Analyses of the resulting tidal prism and flow velocity data are used to establish the circulation patterns inside the backbarrier area (flood/ebb dominance) and the interdependencies between the hydrodynamically connected inlets. The results add to previous knowledge (Salles, 2001; Salles et al., 2005) by quantifying discharge, residual flow, and residual velocities, under different tidal conditions. The findings contribute to our understanding of the long-term stability of multiple inlets and reveal the complexity of hydrodynamic interactions in such situations.

IV.2 STUDY AREA

IV.2.1 General characteristics

The Ria Formosa is a multiple-inlet barrier island system located in Southern Portugal (Fig. IV.1). It comprises five islands and two peninsulas, separated by six tidal inlets: two artificially relocated inlets (Ancão and Fuseta inlets); two artificially opened and stabilised inlets (Faro-Olhão and Tavira inlets); and two natural inlets (Armona and Lacém inlets). The large embayment located behind the barrier islands is characterised by salt marshes, sand flats, and a complex network of natural and partially dredged channels, covering 8.4 x10^7 m^2 (Andrade, 1990). The tides in the area are semi-diurnal

with typical average ranges of 2.8 m for spring tides and 1.3 m for neap tides. A maximum tidal range of 3.5 m can be reached on equinoctial tides, and over 3.8 m with surge setup. The lagoon is generally well mixed vertically, with no evidence of persistent haline or thermal stratification (Newton and Mudge, 2003). Due to reduced freshwater inputs and elevated tidal exchanges, it is basically euryhaline with salinity values usually close to those observed in adjacent coastal waters (Newton and Mudge, 2003).

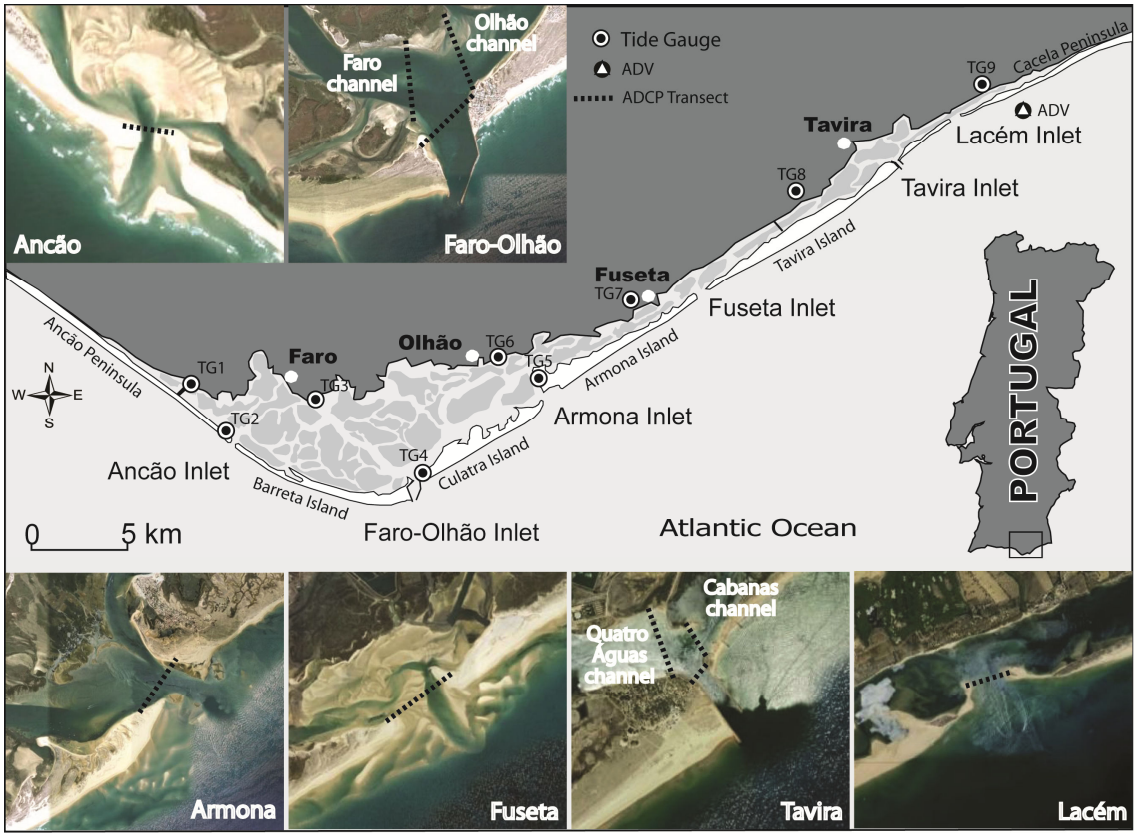

Figure IV.1 The Ria Formosa multiple-inlet system. Tide gauges and ADV location (adapted from Salles, 2001) and ADCP survey transect locations are shown

Wave climate in the area is moderate to high (offshore annual mean wave height $H_s \sim 1$ m and peak period T_p of 8.2 s, with storms characterised by H_s>3 m). Approximately 71% of waves are from the W-SW, with about 23% approaching from the E-SE (Costa et al. 2001). The cuspate shape of the Ria Formosa system leads to

differences in exposure to wave action, with the western region being dominated by the more energetic wave conditions and the eastern region being directly exposed only to E-SE waves. The wind is on average moderate (3 ms^{-1}) and predominantly from the W (Andrade, 1990). Salles et al. (2005) performed a variance analysis of the tidal and non-tidal signals, which showed that the meteorological and long-term water level variability explained less than 1% of the total recorded variance. The authors concluded, by comparison with the study of Kraus and Militello (1999), that the role of wind on water circulation in the area is minimal.

IV.2.2 Recent evolution of the inlets

Analysis of the area's historic and recent evolution dating from the 14th century shows that although the system has responded historically to both natural and artificial disturbances, with significant changes in overall morphology, it has always maintained between 4 and 7 inlets (Salles, 2001). A summary of inlet characteristics is presented in Table IV.1. The most recent major change to the system resulted from the opening of Faro-Olhão Inlet, which captured a large tidal prism from Armona Inlet, formerly the dominant natural inlet in the system. Sediment budget analysis since the opening of the Faro-Olhão Inlet (Pacheco et al., 2008) indicates that the inlet reached equilibrium with regard to its cross-section 50 year after its opening (Fig. IV.2A). The Escoffier's (1940) curve for Faro-Olhão Inlet, using the linear method to approach Keulegan's (1967) analytical solution for the dynamic equation (in Dean and Dalrymple, 2002), shows that the inlet is reaching the equilibrium point (Fig. IV.2B). However, it has taken around 70 years to approach equilibrium with the adjacent coastline, and has led directly to a greatly reduced width of the Armona Inlet (Fig. 2C; Vila-Concejo et al., 2002, 2006).

Table IV.1 General characteristics of Ria Formosa inlets

General characteristics	Further references
1. Ancão Artificially relocated (open year 1997); Cyclic eastward migrating inlet (90 m/year, about 1000 m since its opening); Inlet maintains a stable A_c while migrating	Vila-Concejo et al., 2002; Vila-Concejo et al., 2004; Williams et al., 2003 Pacheco et al., 2007
2. Faro-Olhão Artificially open & stabilised (dual jetty) (open year 1929-1957); Main inlet of the system; Strong ebb jet flow. Intense scouring at inlet gorge	Andrade, 1990; Salles et al., 2005; Vila-Concejo et al., 2006; Pacheco et al., 2008
3. Armona Natural inlet; Stable location through recent centuries; Losing hydraulic efficiency since Faro-Olhão opening	Andrade, 1990; Dias, 1988; Pilkey et al., 1989; Vila-Concejo et al., 2002
4. Fuseta Artificially relocated (open year 1999); Cyclic eastward migrating inlet; Presents channel infilling & meandering	Andrade, 1990; Dias, 1988; Pilkey et al., 1989; Vila-Concejo et al., 2002
5. Tavira Artificially open (1927) & stabilised (dual jetty) Intensively dredge to be maintained open	Andrade, 1990; Dias, 1988 Pilkey et al., 1989; Vila-Concejo et al., 2006
6. Lacém Natural inlet that can open over a wide area (open year 2003). Cyclic eastward migrating inlet. Presents channel infilling & meandering	Andrade, 1990; Dias, 1988; Pilkey et al., 1989; Vila-Concejo et al., 2002

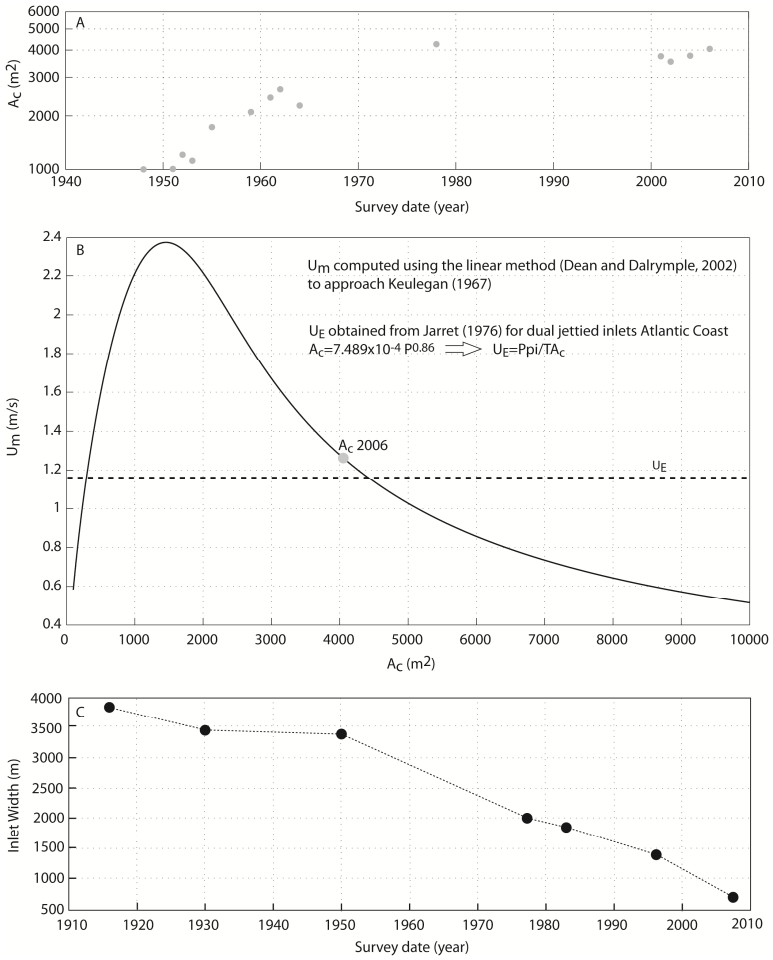

Figure IV.2 (A) Faro-Olhão inlet cross-section evolution (adapted from Pacheco et al., 2008); (B) Faro-Olhão Inlet Escoffier Curve; and (C) Armona Inlet width evolution (adapted from Andrade, 1990)

IV.2.3 Ria Formosa hydrodynamics

Salles (2001) analysed water surface elevation records to derive the amplitude and phases of the primary tidal constituents, which allowed the tidal distortion inside the lagoon to be examined. The tidal data were obtained from 9 Pressure Transducers (PTs) deployed inside the lagoon and one Acoustic Doppler Velocimeter (ADV) deployed offshore (Fig. IV.1, Table IV.2). The full results for the dominant tidal constituents and their corresponding overtides and compound tides can be found in Salles (2001) and Salles et al. (2005).

Regarding the amplitudes of the relevant tidal constituents, there is no definite trend in the tidal distortion as a function of distance from the station to the closest inlet for any of the constituents, as has been observed for single-inlet systems in other studies (Aubrey and Speer, 1985). Strong distortion of the tide within the lagoon was recorded, resulting in the reduction of the tidal amplitude and in the creation of phase lags. The decay of M_2 is generally small, with the exception of the stations of Cacela and Fuseta, which are close to the small, shallow inlets. The M_2 phase lag is consistently positive for all the stations and ranges from 8 to 26º. In addition, the semi-diurnal components show larger decay rates than the diurnal components for some stations. For all the stations, there is a significant growth in the amplitudes of MN_4, M_2, MS_4 and M_6, which are the dominant high frequency components in Ria Formosa. The six-diurnal tide M_6 is one order of magnitude smaller than M_4, and therefore the major contributor to tidal distortion is M_4.

A large difference between flood and ebb durations occurs during spring tide (Table IV.2), and this difference becomes small (and even reversed in some stations) during neap tide, similar to the findings of Aubrey and Speer (1985). This indicates that the

non-linear distortion varies considerably throughout the monthly tidal cycle, which in turn can lead to considerable variability in patterns of sediment transport.

Table IV.2 Tide gauges and ADV deployment duration, data return, and average flood and ebb durations at each station for a complete lunar cycle (adapted from Salles, 2001)

Tide Gauge (PT Levels)	Location	Distance to inlet (m)	Duration (days)	Data return (%)	Flood duration (h)	Ebb duration (h)
TG1	Faro Beach	3500	38	100	6:39	5:38
TG2	Ancão Inlet	160	39	100	6:32	5:55
TG3	Faro Channel (harbour)	7700	38	100	6:45	5:42
TG4	Faro-Olhão Inlet	1250	37	62	6:30	5:58
TG5	Armona	900	37	100	6:17	6:10
TG6	Olhão	5700	37	68	6:23	6:03
TG7	Fuseta	850	34	100	5:41	6:45
TG8	Tavira (Santa Luzia)	5450	24	100	6:25	6:02
TG9	Cacela	2600	24	100	4:15	8:13
ADV	Cacela (offshore)	N/A	9	100	N/A	N/A

***note:** sixteen sample bursts were taken at a rate of 2Hz and then averaged to provide a single average data point for each six-minute sampling interval (240 samples/day)

IV.3 METHODS

IV.3.1 Current and cross-section measurements

A boat-mounted Acoustic Doppler Current Profiler with bottom tracking (1500 KHz ADCP) was used to measure current velocity profiles at each inlet of the Ria Formosa system during neap and spring tide conditions, during fair weather conditions (Table IV.3). The ADCP was mounted port-side in the middle of the boat and synchronized with a global positioning system (RTK-DGPS, *DSNP Scorpio 6001 SK/MK*) connected to a navigational interface running hydrographic survey software (*Hypach®Max 4.3a Gold, Coastal Oceanographics, Inc.*). Measurements were made every hour during a full tidal cycle (c. 12,5h) along a transect across each inlet, yielding 14 surveys for each transect (Table IV.3). The location of the transect in each case (Fig. IV.1) corresponded to the minimum cross-section area at the inlet mouth, except for Faro-Olhão Inlet where measurements were made further up the inlet due to the intense currents at the inlet gorge. For the adjacent channels of the stabilised inlets (Faro and Olhão channels at

Faro-Olhão Inlet and Quatro Águas and Cabanas channels at Tavira Inlet), measurement surveys were made across transects extending from the inner barrier margin to the inlet's flood delta.

The software Current Surveyor v4.5 was used to record hydrodynamic data and to measure the cross-section shape and dimensions (Fig. IV.3). The cell size, blanking distance, and ADCP transducer draft were all set to 0.5 m, and the number of cells set to an appropriate number that accounted for the maximum depth of each profile. The instrument was programmed to run in continuous mode (average interval c. 5 s). In order to determine the discharge in the channel margins, topo-bathymetric measurements were made along each inlet for computing the respective cross-sectional areas (A_c), mean depths, and lengths within the unmeasured margins.

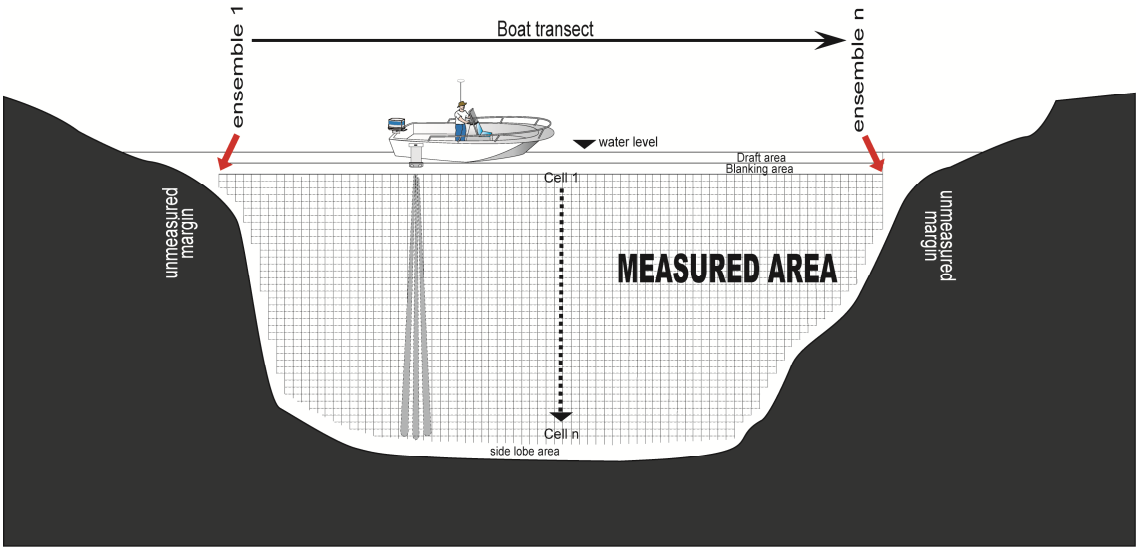

Figure IV.3. Hydrodynamic data sampling scheme

Table IV.3 Tide conditions for the survey days

Cross-section	Tidal regime	Date	Transects	Tide conditions	Max. Amplitude
Ancão Inlet	ST	02-06-2004	14	08h32 (0.6) 14h51 (3.4) 20h56 (0.5)	2.9 m
Ancão Inlet	NT	05-05-2006	14	09h43 (2.4) 15h31 (1.6) 22h03 (2.6)	1.0 m
Faro Channel	ST	11-07-2006	14	09h23 (0.8) 15h49 (3.3) 21h56 (0.6)	2.7 m
Faro Channel	NT	23-07-2007	14	09h46 (2.5) 15h41 (1.5) 22h15 (2.5)	1.0 m
Faro-Olhão Inlet	ST	11-07-2006	14	09h23 (0.8) 15h49 (3.3) 21h56 (0.6)	2.7 m
Faro-Olhão Inlet	NT	23-07-2007	14	09h46 (2.5) 15h41 (1.5) 22h15 (2.5)	1.0 m
Olhão Channel	ST	11-07-2006	14	09h23 (0.8) 15h49 (3.3) 21h56 (0.6)	2.7 m
Olhão Channel	NT	23-07-2007	14	09h46 (2.5) 15h41 (1.5) 22h15 (2.5)	1.0 m
Armona Inlet	ST	01-06-2007	14	09h15 (0.9) 15h49 (3.2) 21h43 (0.9)	2.3 m
Armona Inlet	NT	06-09-2007	14	04h58 (1.5) 11h24 (2.7) 17h59 (2.7)	1.2 m
Fuseta Inlet	ST	26-05-2006	14	08h35 (0.7) 14h56 (3.3) 21h00 (0.6)	2.7 m
Fuseta Inlet	NT	22-03-2006	14	06h49 (2.6) 12h54 (1.4) 19h29 (2.6)	1.2 m
Quatro-Águas Channel	ST	23-06-2006	14	07h29 (0.9) 13h51 (3.1) 19h59 (0.9)	2.2 m
Quatro-Águas Channel	NT	04-07-2006	14	09h39 (2.5) 15h32 (1.5) 21h52 (2.6)	1.1 m
Tavira Inlet	ST	23-06-2006	14	07h29 (0.9) 13h51 (3.1) 19h59 (0.9)	2.2 m
Tavira Inlet	NT	04-07-2006	14	09h39 (2.5) 15h32 (1.5) 21h52 (2.6)	1.1 m
Cabanas Channel	ST	23-06-2006	14	07h29 (0.9) 13h51 (3.1) 19h59 (0.9)	2.2 m
Cabanas Channel	NT	04-07-2006	14	09h39 (2.5) 15h32 (1.5) 21h52 (2.6)	1.1 m
Lacem Inlet	ST	11-09-2007	14	09h07 (0.7) 15h32 (3.4) 21h32 (0.6)	2.8 m
Lacem Inlet	NT	04-09-2007	14	08h30 (2.8) 14h28 (1.2) 21h13 (2.7)	1.6 m

ST-Spring-tides;NT-Neap-tides

IV.3.2 Data assimilation and processing

Transect surveys were analysed through View ADP v.4.03 and Current Surveyor v.4.5 software. The signal-to-noise ratio (SNR) was set to 3 dB to remove invalid data below the ambient noise level, resulting in a standard deviation of $\sigma = \pm 0.04$ m/s, assuming a sound velocity of c. ~1486 m/s (Sontek, 2000). Temperature and salinity were adjusted to values measured inside the Ria Formosa system, as well as to the magnetic declination and equipment draft.

Data were rotated and individualised on across- and along-flow components relative to the transect angle orientation. The vertical average velocity for each 5 s ensemble ($\overline{U}_{ens}$) was then evaluated using:

$$\overline{U}_{ens} = 1/h \int_0^h U(z)\, dz \qquad \text{(IV.1)}$$

(Soulsby, 1997), where *h* is the water depth, and *U(z)* is the current speed at height *z*.

The vertical average velocity was then integrated over the width of the cross section resulting in the cross-section average velocity ($\overline{U}_{cs}$) using:

$$\overline{U}_{cs} = [\sum_{i=1}^{n-1} (\overline{U}_{\{ens,i\}} + \overline{U}_{\{ens,i+1\}})/2]/(n-1) \qquad \text{(IV.2)}$$

where $\overline{U}_{\{ens,i\}}$ represents each vertical average velocity determined from Eq IV.1 from transect start (*i=1*) to transect end (*i=n*).

The boat travel distance made good (D_{mg}) along the transect, as well as the cross-section mean depth (h_{cs}), were given by Eq. IV.3 and IV.4, respectively:

$$D_{mg} = D_{mg}\ (n) \qquad \text{(IV.3)}$$

$$h_{cs} = [\sum_{i=1}^{n-1}(h_{\{ens,i\}} + h_{\{ens,i+1\}})/2]/(n-1) \quad \text{(IV.4)}$$

The discharge through the measured cross-section area ($Q_{measured}$) in m^3/s was then obtained by:

$$Q_{measured} = \overline{U}_{cs}\ D_{mg}\ h_{cs} \quad \text{(IV.5)}$$

The flow in the intertidal side banks of channels was obtained during post-processing using the simplified triangular *ratio interpolation method* (Fulford and Sauer, 1986, *in* Simpson, 2001) where the estimated velocity at the margin ($\overline{U}_e$) is given by:

$$\frac{\overline{U}_e}{\sqrt{h_e}} = \frac{\overline{U}_m}{\sqrt{h_m}} \quad \text{(IV.6)}$$

where *e* is a location midway between the edge and the first or last ADCP-measured subsection, $\overline{U}_e$ is the estimated mean velocity at location *e* (m/s), $\overline{U}_m$ is the measured mean velocity at the first or last ADCP-measured subsection (m/s), h_e is the depth at subsection *e*, and h_m is the depth at the first or last ADCP-measured subsection *m*. Assuming a triangular discharge area between the subsection *m* and the bank, Eq. IV.6 reduces to $\overline{U}_e = 0.707\overline{U}_m$ (considering $d_m = 2d_e$). The discharge at each margin is then given by:

$$Q_{m\,\mathrm{arg}\,in} = \frac{0.707\,\overline{U}_m L\ h_m}{2} \quad \text{(IV.7)}$$

where L is the distance to the margin from the first or last ADCP measured subsection n. Finally, total discharge through the cross-section transect (Q_{total}) was given by:

$$Q_{total} = Q_{measured} + Q_{Rm\,\mathrm{arg}\,in} + Q_{Lm\,\mathrm{arg}\,in} \quad \text{(IV.8)}$$

Data obtained for all transect surveys were then integrated through the c. 12.5 h tidal cycle. Hourly transect surveys were interpolated to obtain estimates of the flood (P_{Flood}), ebb (P_{Ebb}), and residual ($P_{\mathrm{Re}\,sidual}$) prisms, the mean flood ($\overline{U}_{Flood}$), mean ebb ($\overline{U}_{Ebb}$), and residual ($\overline{U}_{\mathrm{Re}\,sidual}$) velocities, and the flood (T_{Flood}) and ebb (T_{Ebb}) durations, using trapezoidal area computations of discharge and velocity curves, for spring and neap tides (for each inlet). Therefore, $\overline{U}_{Flood}$ and $\overline{U}_{Ebb}$ represent the magnitude of the velocity field across flood and ebb tides, respectively. There are slight differences in the tidal amplitude at the time of the surveys (Table IV.3), as well as in the time lag between them; thus residuals should be analysed as general tendencies and not as absolute values.

IV.3.3 Best estimate and error analysis

Discharge estimates determined by averaging measurements from independent transects assume that the flow is horizontally homogeneous; an assumption valid in two-dimensional flow fields (González-Castro et al., 2002). The method followed in our study allowed the best estimates of tidal prism, velocity, flood/ebb duration, and residual discharge/velocity values to be derived. Streamwise velocity profiles in open channels with quasi-2D flow fields can be accurately estimated from relatively long records collected with a fixed ADCP (González-Castro et al., 2002). Those authors

compared such estimates with the discharge measurements obtained by boat-mounted ADCPs, and concluded that streamwise velocity data from independent transects give a rather poor representation of the long-term mean flow, but that the deviations of single-ping data with respect to the time mean velocities seem to compensate each other in space. This latter point was considered by those authors to explain the small differences between the discharge estimates from transect data and fixed data and therefore the accuracy of discharge estimates.

The uncertainty of the method used in this study is related to the accuracy of the velocity measurements. Errors in ADCP measurements are attributable to instrument error (e.g. transducer ringing, side lobe interference), operator error (e.g. site selection, boat manoeuvring), and environment error (e.g. moving bed, noise). Simpson (2001) and Oberg et al. (2005) provide detailed descriptions concerning such errors. A rigorous methodology for estimating ADCP discharge measurement uncertainty which follows current engineering standards for uncertainty analysis is not yet available (González-Castro and Muste, 2007), and therefore the uncertainties on the discharge measurements cannot be presented. The results represent best estimates and can be used to assess general tendencies. Because boat velocity was constant while performing the measurements (at 2 m/s), the number of instantaneous velocities is higher for larger than for smaller cross-sections. Therefore the discharge accuracies will be greater for larger cross-sections.

IV.4 RESULTS

A summary of the Ria Formosa multiple-inlet hydrodynamics for spring- and neap-tides is presented in Table IV.4.

Table IV.4 Ria Formosa multiple-inlet system hydrodynamics (spring- and neap-tide conditions). Positive values refer to flood conditions and negative to ebb. A_c is cross-shore channel area; P is tidal prism; U is velocity; and T is duration

	Ancão		**Faro-Olhão**		**Armona**	**Fuseta**		**Tavira**		**Lacem**
SPRING-TIDES	Inlet Channel	Faro Channel	Inlet Channel	Olhão Channel	Inlet Channel	Inlet Channel	Quatro-Águas Channel	Inlet Channel	Cabanas Channel	Inlet Channel
Flood P (m^3)	8.28E+06	3.41E+07	6.64E+07	2.49E+07	2.11E+07	2.85E+06	2.46E+06	4.29E+06	1.87E+06	1.34E+06
Ebb P (m^3)	-8.93E+06	-3.37E+07	-6.19E+07	-2.20E+07	-2.59E+07	-1.39E+06	-3.38E+06	-5.60E+06	-2.14E+06	-1.39E+06
Residual P	-6.53E+05	3.69E+05	4.48E+06	2.98E+06	-4.74E+06	1.46E+06	-9.27E+05	-1.31E+06	-2.65E+05	-4.10E+04
Flood U (m/s)	0.58	0.23	0.50	0.34	0.31	0.46	0.11	0.21	0.17	0.33
Ebb U (m/s)	-0.80	-0.24	-0.52	-0.28	-0.43	-0.25	-0.14	-0.24	-0.22	-0.29
Residual U (m/s)	-0.23	-0.01	-0.02	0.06	-0.12	0.21	-0.03	-0.03	-0.05	0.033
Flood T (h)	6.6	6.4	6.4	6.2	6.4	5.4	6.1	6.3	5.7	4.1
Ebb T (h)<	5.9	6.1	6.1	6.3	6.1	7.1	6.4	6.2	6.8	8.4
NEAP-TIDES										
Flood P (m^3)	**1.85E+06**	**1.03E+07**	**1.98E+07**	**1.06E+07**	**1.56E+07**	**1.72E+06**	**1.88E+06**	**2.02E+06**	**3.12E+05**	**4.76E+05**
Ebb P (m^3)	-1.56E+06	-1.56E+07	-1.77E+07	-3.34E+06	-1.76E+07	-1.43E+06	-2.19E+06	-2.31E+06	-3.26E+05	-3.96E+05
Residual P	2.85E+05	-5.32E+06	2.02E+06	7.29E+06	-2.00E+06	2.90E+05	-3.06E+05	-2.90E+05	-1.37E+04	8.04E+04
Flood U (m/s)	0.20	0.07	0.17	0.16	0.23	0.18	0.09	0.09	0.03	0.15
Ebb U (m/s)	-0.27	-0.11	-0.15	-0.09	-0.21	-0.18	-0.08	-0.10	-0.03	-0.17
Residual U (m/s)	-0.07	-0.03	0.02	0.07	0.02	0.00	0.02	0.00	0.00	-0.02
Flood T (h)	7.4	5.8	6.3	8.4	5.6	7.1	5.5	6.1	5.5	6.5
Ebb T (h)	5.1	6.7	6.2	4.1	6.9	5.4	7.0	6.4	7.0	6.0

IV.4.1 Spring-tides

During spring-tides, Ancão and Armona inlets are ebb-tide dominated. The mean ebb is higher than the mean flood velocity through the tidal cycle, presenting a shorter ebb duration (Fig. IV.4A, B, and D; Table IV.4). The maximum U_{cs} velocity in the tidal cycle always occurs during the ebb, with maximum values of -1.25 m/s and -0.7 m/s for Ancão and Armona inlets, respectively (Fig. IV. 4B). The corresponding residual ebb prisms (Fig. IV.4C) are c. -6.5×10^5 and c. -4.8×10^6 m^3, respectively, with residual U values (Fig. IV.4D) of c. -0.23 and -0.12 m/s, respectively. The Faro-Olhão Inlet has a residual prism oriented landward of c. 4.5×10^6 m^3 (Fig. IV.4C). The mean ebb/flood velocities are approximately the same (c. 0.5 m/s), with a negligible residual velocity integrated through time of c. -0.02 m/s, directed offshore (Fig. IV.4D). The maximum U_{cs} velocity (c. 0.72 m/s) occurs at flood (Fig. IV.4B). Within the Faro-Olhão Inlet, measurements were also made across the two main adjacent navigable channels (Fig. IV.1), and show that both the Faro and Olhão channels present a landward directed residual flow (higher flood prism). Faro Channel presents almost equal mean flood/ebb velocities (c. 0.24 m/s, Fig. IV.4B), with a negligible residual velocity of c. -0.01 m/s, offshore directed, and a longer flood duration (Table IV.4), and thus is an ebb-dominated channel. Olhão Channel presents higher mean flood velocities (c. 0.34 m/s, Fig. IV.4C) and shorter flood duration (Table IV.4), and is clearly a flood-dominated channel, with a landward residual velocity of c. 0.06 m/s (Fig. IV.4B). Faro-Olhão Inlet presents a higher mean ebb velocity associated with shorter ebb duration.

Thus, from a conventional view point regarding flood/ebb velocity and duration, the Ancão, Faro-Olhão, and Armona inlets are ebb-dominated inlets. Analysing the differences in flood/ebb prism (i.e., residual flow, Fig. IV.4C), these inlets reveal a strong hydrodynamic interconnection, with the residual flow of Faro-Olhão Inlet being

directed to the Ancão and Armona ebb-tide dominated inlets. The three inlets can therefore be viewed as a hydrodynamic sub-system, in which the excess flood prism at Faro-Olhão Inlet ebbs through the Ancão and Armona inlets. This evidence indicates that Faro-Olhão Inlet, although presenting a higher ebb velocity and shorter ebb duration (i.e. ebb dominance under a conventional interpretation), develops a considerably lower prism during the ebb, as is therefore flood dominated.

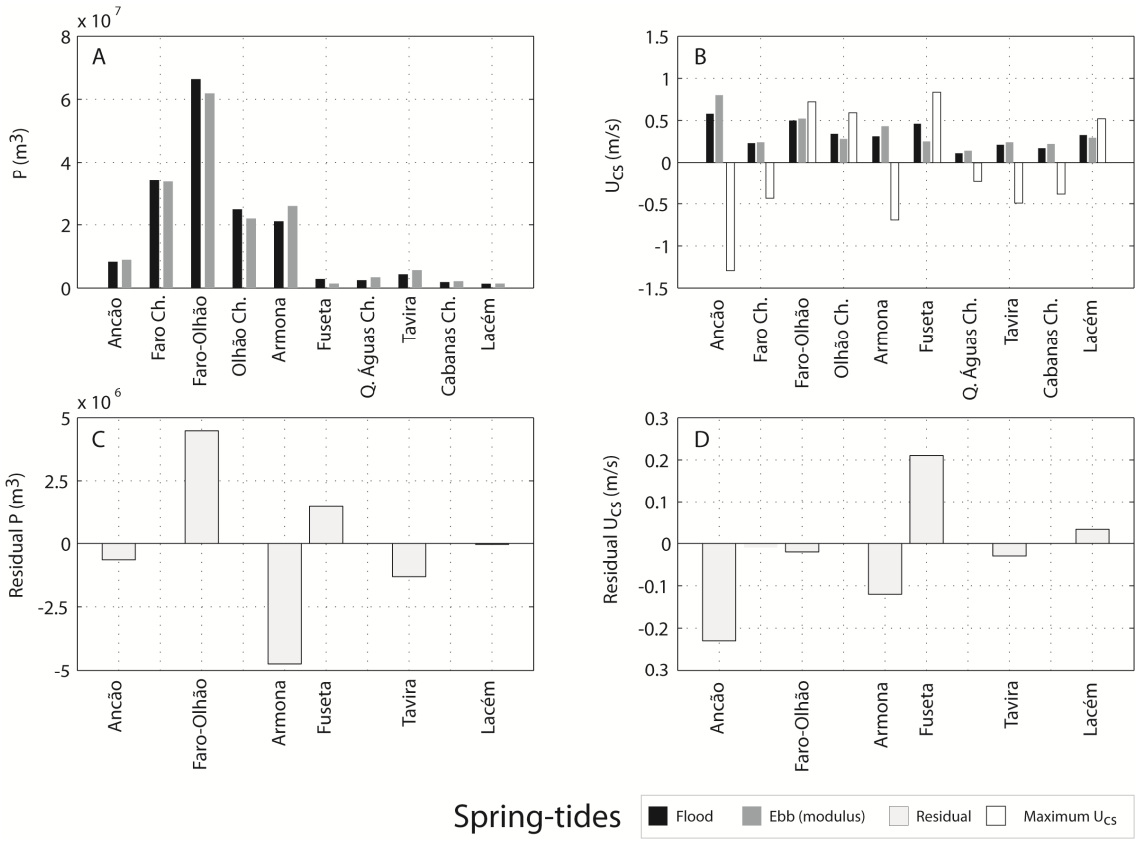

Figure IV.4. Ria Formosa inlets at spring-tides: (A) tidal prism; (B) mean cross-section velocities; (C) residual discharge; and (D) mean residual velocity. In all cases, positive values refer to flood and negative to ebb

Fuseta and Tavira inlets appear to present some connection at spring-tides (Table IV.4, Fig. IV.4A and C), with Fuseta Inlet being flood-dominated (higher mean flood velocity, shorter flood duration), and Tavira Inlet being marginally ebb-dominated (higher mean ebb velocity, shorter ebb duration) (Table IV.4 and Fig. IV.4B). Maximum U_{cs} presents the same pattern: 0.83 m/s for Fuseta Inlet and -0.49 m/s for

Tavira Inlet. As in the case of the stabilised Faro-Olhão Inlet, measurements were made across the main channels of the stabilised Tavira Inlet (Fig. IV.1 and IV.4A). Quatro-Águas Channel presents higher ebb *P*, longer duration, and higher mean ebb velocity. From the data provided in Fig. IV.4A and Table IV.4, a residual of c. $5.5x10^5$ m^3 flows from Fuseta to Tavira, which agrees with the offshore residual flow at Fuseta Inlet (c. $6x10^5$ m^3). The residual flow between the inlets explains why a higher mean ebb velocity is associated with longer ebb duration, where the excess flow through the flood-dominated Fuseta Inlet exits through the ebb-dominated Tavira Inlet.

The residual flow values (Fig. IV.4C and Table IV.4) suggest some residual flow from Fuseta to Armona Inlet (Fig. IV.4C). Although possessing lower residual flow values, Armona, Fuseta, and Tavira inlets demonstrate an interconnection similar to that identified between Ancão, Faro-Olhão, and Armona inlets. The residual flow flooding through Fuseta Inlet exits through Armona and Tavira inlets at ebb. At Cabanas Channel, the differences between flood and ebb indicate a negligible residual flow towards Tavira from Lacém Inlet (c. $5.4x10^4$ m^3, Fig. IV.4C), despite the opposite flow residual value observed at Lacém Inlet. Lacém Inlet is the smallest inlet of the system, with a shallow cross-section (c. 140 m^2, and a maximum depth of 1.5 m), where ADCP measurements along the spring tidal cycle were difficult to perform due to sand banks. On this basis, the flood/ebb discharge may be underestimated, especially at the beginning stages of the flood and at the peak ebb. In fact, although Lacém Inlet has a higher measured ebb discharge and a significantly longer ebb duration (Table IV.4), the inlet does not present a clear dominance, with mean and maximum U_{cs} being higher at flood (c. = 0.33 m/s and 0.52 m/s, respectively, Fig. IV.4C).

IV.4.2 Neap-tides

Results for neap-tides (Fig. IV.5A) indicate that inlets appear to work more independently during neap-tides than during spring-tides, characterised by a reduced magnitude of residual flows although still showing some important residual exchanges (Fig. IV.5C). The residual discharge and velocities of the Ancão Inlet are almost negligible and the mean flood/ebb velocities are low (c. 0.25 m/s, Fig. IV.5B). Here, the flood duration is longer and the inlet presents a slightly greater flood prism. Conversely, the mean ebb velocity is higher and the ebb duration shorter, with an offshore-directed residual (Fig. IV.5D and Table IV.4).

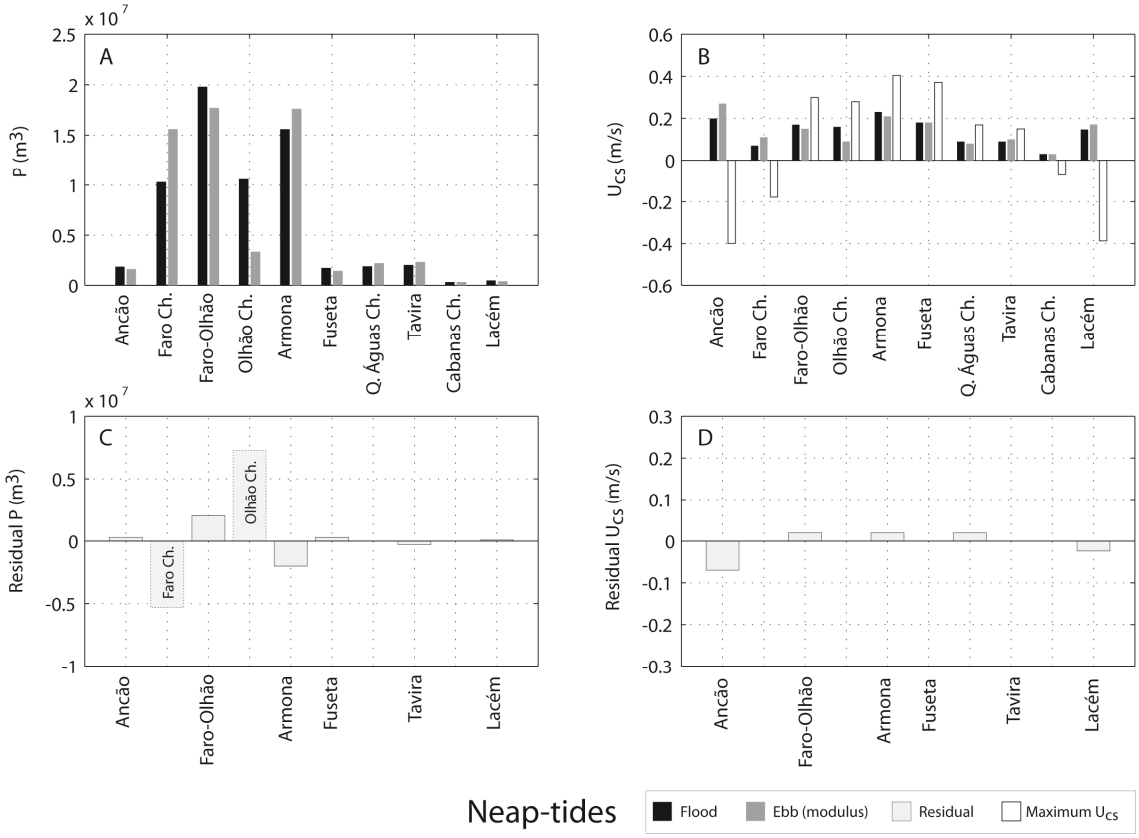

Figure IV.5 Ria Formosa inlets at neap-tides: (A) tidal prism; (B) mean cross-section velocities; (C) residual discharge; and (D) mean residual velocity. In all cases, positive values refer to flood and negative to ebb

Faro-Olhão Inlet also has an approximately equal flood/ebb prism, with a lower residual flow (c. 2.0x10^6 m^3/s, landward oriented, Fig. IV.5A and C) and a negligible residual *U* (Fig. IV.5D). The mean velocity is slightly higher at flood (residual of c. 0.02 m/s, landward oriented, Fig. IV.5C) and flood/ebb duration is approximately the same (Table IV.4). In this case, a higher mean flood velocity is associated with a longer flood duration and higher maximum U_{cs}. An examination of the adjacent channels of Faro-Olhão Inlet reveals some important behaviour (Fig. IV.5C, dashed grey bars). The Faro Channel ebb *P* is much higher, and duration much longer, than flood (Table IV.4), with mean velocity higher at ebb (Fig. IV.5B); conversely, for Olhão Channel, flood *P* and *U* are much higher (Fig. IV.5A and B) and duration longer (Table IV.4) than ebb, with mean velocity higher at flood (Fig. IV.5B). The observed behaviour seems to indicate channel preference according to whether the tide is flood or ebb, i.e., flood occurs mainly through Olhão Channel and ebb through Faro Channel, resulting in a recirculation pattern through the secondary channels that connect the two main navigable channels.

Armona Inlet ebb duration is longer than flood (Table IV.4), presenting a slight higher mean flood velocity. Both mean and maximum velocities are higher at flood, with a residual velocity directed landward (c. 0.02 m/s, Fig. IV.5C and 5D). The inlet presents a higher ebb prism, with a residual flow of c. -2.0x10^6 m^3/s, oriented offshore (Fig. IV.5C). The residual flows at Faro and Armona inlets (Fig. IV.5C, Table IV.4) indicate that these inlets maintain an inter-connected behaviour, with residual flowing from Faro-Olhão towards Armona Inlet, the same pattern observed at spring-tides.

Fuseta Inlet presents equal mean flood/ebb velocities and longer flood duration. However, the flood prism is higher than the ebb, with residual flowing from Fuseta to Tavira Inlet (Table IV.4 and Fig. IV.5C). Tavira Inlet presents a complementary inverse

behaviour to Fuseta Inlet: flood/ebb velocities are the same (Fig. IV.5A) and are associated with a longer ebb duration (Table IV.4), and the ebb prism is higher. Therefore, Fuseta and Tavira inlets demonstrate an inter-connected behaviour, showing a complementary circulation pattern, where a residual P flows towards Tavira Inlet. Quatro-Águas Channel measurements confirm the internal circulation between these two inlets, while Cabanas Channel presents equal mean flood/ebb velocities and prisms, although it has a longer ebb duration (Fig. IV.5A). Lacém Inlet at neap-tides presents a shorter ebb duration and higher mean and maximum ebb velocities (-0.17 and -0.39 m/s, Fig. IV.5B). Lacém Inlet also has a higher flood prism, which indicates the existence of some circulation from Lacém to Tavira Inlet, as supported by the residual flow observed at Cabanas Channel (Fig. IV.5C).

IV.5 DISCUSSION

Results from this study of the hydrodynamics of the Ria Formosa multiple-inlet system show that Ancão, Faro-Olhão, and Armona inlets together capture c. 90 % of the total prism. During spring-tides, the Faro-Olhão, Armona, and Ancão inlets account for c. 61%, c. 23%, and c. 8% of the total flow, respectively. During neap-tides, the Faro-Olhão and Armona inlets equally share the tidal prism (c. 45 % and c. 40 %, respectively), with Ancão Inlet having reduced importance. The Fuseta, Tavira, and Lacém inlets together transmit only c. 10 % of the total Ria Formosa tidal prism during both spring- and neap-tides.

At spring-tides, Ancão, Faro-Olhão, and Armona inlets are interconnected, showing a clear circulation pattern. The three inlets present ebb-dominated behaviour from a conventional viewpoint (higher mean ebb velocity is associated with shorter ebb duration), where the flood prism is considerably higher than the ebb prism at Faro-

Olhão Inlet but is lower than the ebb prism at Ancão and Armona inlets. In the case of Faro-Olhão Inlet, although mean velocities are higher at ebb than at flood, and ebb duration is shorter, the distortion of the velocity field produces higher maximum flood velocities. Therefore sediment transport is oriented strongly landward, dominating over both the weakly seaward residual velocity and the moderately distorted velocity field. Based on dredging reports and bathymetric charts, the net sediment entry through Faro-Olhão Inlet is $\cong 1.4 \times 10^5$ m^3/year (Pacheco et al., 2008), confirming the main inlet as a net importer of sand to the system (Salles, 2001).

A strong residual circulation from Faro-Olhão Inlet is directed towards Ancão and Armona inlets, during both spring- and neap-tides. Fuseta and Armona inlets also demonstrate a degree of interconnection, with residual flow from Fuseta towards Armona. Fuseta and Tavira inlets are similarly connected, with residual flowing from Fuseta (flood-dominated) towards Tavira (ebb-dominated). Despite these various interconnections, during neap-tides the inlets act more independently. The residual circulation is lower (mainly occurring between Faro-Olhão and Armona inlets), while an inner circulation pattern operates at the main Ria Formosa tidal channels (Faro and Olhão channels): the Olhão Channel acts mainly as a flood-dominated channel while the Faro Channel is responsible for the residual ebb towards the main inlet. In general terms, during neap-tides the degree of connection between the inlets is reduced because they cover a vast area and adjacent channels are too shallow to promote important hydraulic connections that lead to observable residual flows between them. As suggested by van de Kreeke et al. (2008), the morphology of the inner channels connecting the inlets can play an important role in inlet stability, by controlling the interconnections between the inlets. This can be particularly important for certain tidal conditions, where inlets can drain each sub-basin independently.

At spring-tides, a clear ebb dominance in single inlet terms (i.e., shorter ebb duration and higher mean and maximum ebb velocities) was verified at Ancão, Armona, and Tavira inlets and flood dominance (shorter flood duration and higher mean and maximum flood velocities) at Fuseta and Lacém inlets and at Olhão Channel. The other inlets and channels have larger/smaller prisms associated with higher/lower flow durations. At neap-tides, larger flood/ebb prisms were found to always correspond to longer flood/ebb durations. The results therefore support the idea (Salles et al., 2005) that, in contrast to single-inlet systems, the flood/ebb dominance concept and its application to infer stability cannot be generally applied to multiple-inlet systems.

Pendleton and FitzGerald (2005) showed that the area of the bay which contains most of P determines the overall flood/ebb dominance of a multiple-inlet system. Because Faro-Olhão Inlet is flood-dominated and Armona Inlet ebb-dominated, there is a contradiction in the tendency of the bay to either fill with sediment or maintain itself through self-flushing. The strong residual flow between Faro-Olhão and Armona inlets during spring-tides, and persisting through neap-tides, as well as the significant difference in prism distribution between neap-tides and spring-tides for both inlets, appears to be the key factor contributing to the maintenance of both inlets and to their short- to medium-term stability. As pointed out by van de Kreeke and Robaczewska (1993) and confirmed by Salles et al. (2005), it is the existence of residual flows between inlets, together with the magnitude and direction of the maximum velocity, that ultimately determines the flow and transport dominance in a given inlet, superceding the effects of tidal distortion. Within the present study, no general conclusion was reached regarding the unconditional stability of multiple-inlet systems, or regarding the role that residual circulation and non-linear inlet hydrodynamic interaction can play in inlet

stability. Although such a role seems evident, on the basis of enhancing the system flushing capability, the process needs to be further investigated.

Simulations performed by varying Faro-Olhão and Armona cross-sections (Salles, 2001) showed that when Armona Inlet experiences a reduction in its cross-sectional area, the hydrodynamic response is such that it tends to restore the original size: the seaward net flow and current, and the near-bed sediment transport, increase. Complementary simulations for tidal distortion (Salles, 2001) demonstrated that water surface distortion at Armona Inlet is dependent not only on changes in its cross-sectional area but also on disturbances at Faro-Olhão Inlet. It was also revealed in that study that Armona Inlet exhibits consistent ebb flow dominance and appears to be able to counteract disturbances. The ebb dominance at Armona Inlet as verified by the results of this study would tend to promote overall system stability by enhancing the system's flushing capacity. However, despite the ebb flow dominant behaviour of Armona Inlet during both spring- and neap-tides, and its apparent capacity to flush sediments and to counteract disturbances to its A_c, the inlet is narrowing. This means that instability may be caused by other events and processes, as discussed below.

The capacity of a back-barrier system to maintain multiple inlets depends largely on the sediment transport pattern in the vicinity of each inlet. If the littoral drift is strong, ebb shoals trap significant quantities of sand. The combined current-wave interaction during storm events forces morphological changes so that the inlet can move from an essentially ebb-tide dominated condition to a wave-dominated condition (Morris et al. 2001). During such events, the tide may not have the capacity to transport the material away from the inlet mouth area, and the inlet will accumulate sand due to the migration of the shoals to the shore. In determining the equilibrium of the A_c of an inlet, the basic premise is that the volume of sand transported to the inlet is constant and dependent on

the littoral drift, i.e., the influx of sand is balanced by the transport of sand out of the inlet by the ebb tidal currents (van de Kreeke et al., 2008).

In the case of Ria Formosa, retreat of the Armona tidal deltas has occurred as a direct consequence of tidal prism loss due to the opening of the Faro-Olhão Inlet (Andrade, 1990; Salles, 2001). This retreat has provided the major sediment source for the easternward extension of Culatra Island, and has contributed to the narrowing of the Armona Inlet (Vila-Concejo et al., 2002; Pacheco et al., 2008). Using a bathymetric chart from 1985 and assuming that the tide propagated equally and simultaneously at each inlet, Andrade (1990) quantified the spring tidal prism of Armona Inlet to be 48% of the overall Ria Formosa spring prism, while Faro-Olhão Inlet contributed with about 26%. This situation has now reversed completely, as shown by the values measured in this study (62% and 28% for spring-tides and 45% and 40% for neap-tides for Faro-Olhão and Armona inlets, respectively). The Armona Inlet had at the time (around 1985) two efficient channels of equal hydrodynamic importance, separated by a sand bank that today is part of Culatra Island. Currently, the flow is retrained to the eastern channel, close to Armona Island. The maximum amount of Armona Inlet width retreat was observed in the years immediately after the opening of Faro-Olhão Inlet (80 m/year, between 1955-1978), and has since decreased to approximately half that value during the last twenty years (Andrade, 1990).

An inlet system attempts to reach a state of dynamic equilibrium for a specific set of hydraulic conditions. If the hydraulic conditions are changed significantly, the system will attempt to attain a new state of dynamic equilibrium as dictated by the new conditions. Although Faro-Olhão Inlet is reaching stability regarding both A_c and adjacent coastline equilibrium (Pacheco et al., 2008), the continuing narrowing of Armona Inlet is dependent on the availability of sediment storage in the ebb-tidal delta,

which needs to be properly quantified. There is no evidence that Armona Inlet has yet stopped narrowing and therefore that the two major inlets of the system have reached stability. Despite the capacity of ebb currents at Armona Inlet for flushing sediments offshore, the influx of sand originating from large ebb-tidal deltas from previous hydraulic configurations will ultimately dictate whether both interconnected inlets will remain open. Because inlet stability is normally inferred from inlet hydraulics, derived empirical formulae do not take into account external controls, which can lead to erroneous interpretation of inlet hydraulics. The equilibrium volume of the ebb-tidal deltas needs to be known before relationships between inlets in a multiple-inlet system can be fully characterised.

IV.6 CONCLUSIONS

Salles (2001) and Salles et al. (2005) suggested that inlets in a multiple-inlet system can coexist, even if interconnected, by exchanging large portions of P between them, modifying the residual flow and, consequently, altering the sediment transport patterns. By combining a numerical simulation of the flow with a semi-empirical approach to inlet equilibrium, those authors forced variations on A_c and analysed the effect on tidal distortion, residual current, and net-sediment transport in a multiple-inlet system (Ria Formosa, Portugal). This study adds to that knowledge by presenting data on hydrodynamics and circulation patterns measured over a spring-neap tidal cycle in the Ria Formosa multiple-inlet system, deriving residual flows, and characterising the interconnections between inlets. The results show that the two main inlets are always interconnected, but transfer large portions of P between then, and drain the basin more independently for a portion of the neap-spring tidal cycle. The findings support the hypothesis proposed by other authors (Salles et al., 2005) that the capacity to exchange

large portions of prism, while maintaining independent behaviour for the majority of the neap-spring tidal cycle, can contribute to the stability of multiple inlets by altering the residual flow and, consequently, the transport capacity. This capacity can also be enhanced by the morphology of the channels connecting both inlets, or by the different amplitude or phases of the offshore tides at the inlets (van de Kreeke et al., 2008), although these dynamics require further research.

The two major and opposing interconnected inlets of the system, which are the main stabilised inlet (Faro-Olhão) and the natural and historically more persistent inlet (Armona), represent almost 90 % of the total prism of the Ria Formosa system. These inlets have large cross-sectional areas and a strong degree of interconnection. The prediction of the evolution of these two inlets would appear to rely on factors that cannot be approached using empirical equilibrium relations or be derived from inlet hydraulics. Residual flow between inlets can play an important role in enhancing stability, as can the morphology of the inner channels connecting both inlets. However, the capacity of an inlet to flush sediments during prevailing fair-weather conditions is not sufficient to counter the entry of sediment into the system during periods of storm activity or under intense wave-current interaction. The current-wave process during storms combined with the availability of sediment offshore, leads to the obstruction of inlet channels, affecting their hydraulic efficiency, eventually leading to inlet closure in the long term. The long-term equilibrium of sediment storage in the ebb-tidal deltas must be considered when analysing the possible equilibrium of multiple-inlet systems.

IV.7 REFERENCES

Andrade, C. F., 1990. O Ambiente Barreira da Ria Formosa, Algarve-Portugal. PhD Thesis, Universidade de Lisboa. 627 pp. (in Portuguese).

Aubrey, D.G., Speer, P.E., 1983. Sediment transport in a tidal inlet. Technical Report WHOI-83-20, Woods Hole Oceanographic Institution, Woods Hole, MA, 110p.

Aubrey, D.G., Speer, P.E., 1985. A Study of Non-Linear Tidal Propagation in Shallow Inlet/Estuarine Systems. Part I: Observations. *Estuar. Coast. Shelf Sci*. 21, 185-205.

Bakker, W.T., de Vriend, H.J., 1995. Ressonance and Morphological Stability of Tidal Basins. *Mar. Geol.* 126, 5-18.

Boon, J.D., and Byrne, R.J., 1981. "On Basin Hypsometry and the Morphodynamic Response of Coastal Inlet Systems." *Mar. Geol.* 40, 27-48.

Bruun, P., 1978. *Stability of Tidal Inlets*. Elsevier, Amsterdam, 506 pp.

Costa, M., Silva, R. and Vitorino, J., 2001. Contribuição para o estudo do clima de agitação marítima na costa Portuguesa. 2as Jornadas Portuguesas de Engenharia Costeira e Portuária in CD-ROM (in Portuguese).

de Vriend, H.J., Ribberink, J.S., 1996. Mathematical Modeling of Meso-Tidal Barrier Island Coasts, Part 2: Process-Based Simulation Models, in: P.L.-F. Liu, Ed.: Advances in Coastal and Ocean Engineering, 2. World Scientific, pp 151-197.

Dias, J.M.A. 1988. Aspectos geológicos do litoral algarvio. Geonovas (Lisboa), 10, 113-128 (in Portuguese).

Dean, R.G, Dalrymple, R.A., 2002. Coastal Processes with Engineering Aplications. Cambridge University Press, United Kingdom, ISBN 0-521-602750-0, 475pp.

Dronkers, J.J. 1986. "Tidal Asymmetry and Estuarine Morphology." Netherlands *J. Sea Res.* 20 (2/3), 117-131.

Escoffier, F.F., 1940. The stability of tidal inlets. Shore Beach 8, 114-115.

Escoffier, F.F., 1977. Hydraulics and Stability of Tidal Inlets. General Investigation of Tidal Inlets (GITI) Report 13, U.S. Army Engineer Waterway Experience Station, Vicksburg , MS, 72pp.

Friedrich, C.T. and Madsen, O.S., 1992. Nonlinear Diffusion of the Tidal Signal in Frictionally Dominated Embayments. *J. Geophy. Res*. 97, 5637-5650.

Friedrich, C.T., Aubrey, D.G., Giese, G.S., and Speer, P.E., 1993. "Hydrodynamic Modelling of a Multiple-Inlet/Barrier System. Insight into Tidal Inlet Formation and Stability", *in* Formation and evolution of multiple tidal inlets. Coastal and estuarine studies; 44. Aubrey, D.G., Giese, G.S. (eds.), American Geophysical Union, ISBN 0-87590-258-8, 235p, 95-112.

González-Castro, J.A., Ansar, M., Kellman, O., 2002. Comparison of discharge estimates from ADCP transect data with estimates from fixed ADCP mean velocity data, in: Proceedings of the ASCE-IAHR Hydraulic Measurement & Experimental Methods Conference, Estes Park, CO (CD-ROM).

González-Castro, J.A., Muste, M., 2007. Framework for Estimating Uncertainty of ADCP Measurements from a Moving Boat by Standardized Uncertainty Analysis. *J. Hydraul. Eng.,* 133(12), 1390-1410.

Jarret, J.T., 1976. Tidal Prism-Inlet area relationships. GITI Report, vol. 3. U.S. Army Corps of Engineers, Waterways Experiment Station, Vicksburg, MS.

Kraus N. C., and A. Militello, 1999: Hydraulic study of multiple inlet system: East Matagorda Bay, Texas. *J. Hydraul. Eng.*, 25, 224–232.

Liu, J.T. and Aubrey. D.G., 1993. "Tidal Residual Currents and Sediment Transport Through Multiple Tidal Inlets", *in* Formation and evolution of multiple tidal inlets. Coastal and estuarine studies; 44. Aubrey, D.G., Giese, G.S. (eds.), American Geophysical Union, ISBN 0-87590-258-8, 113-157.

Keulegan, G.H., 1967. Tidal flow in entrances. Water–level fluctuations of basins in communication with seas. Committee of Water Hydraulics, US Army Corp of Engineers, Technical Bulletin nº14, 89p.

Louters, T. and Gerritsen, F., 1994. The Riddle of Sands; a tidal system's answer to a rising sea level. National Institute for Coastal and marine Management Report RIKZ-90.040, 69p.

Morris , B.D., Davidson, M.A., Huntley, D.A., 2001. Measurements of the response of a coastal inlet using video monitoring techniques. *Mar. Geol*. 175, 251-72.

Newton, A., Mudge, S.M., 2003. Temperature and salinity regimes in a shallow, mesotidal lagoon, the Ria Formosa, Portugal. *Est. Coast. Shelf Sci.*, 57: 73-85.

O'Brien, M.P., 1969. Equilibrium Flow Areas on Inlets on Sandy Coasts. *J. Waterw. Harb. Div*. 95 (WW1), 43-52.

O'Brien, M.P., Dean, R.G., 1972. Hydraulics and Sedimentary Stability of Coastal Inlets. Proceedings of the 13th Conference on Coastal Engineering, Vancouver, Canada, ASCE, 761-780.

Oberg, K.A., Morlock, S.E., Caldwell, W.S., 2005. Quality-Assurance Plan for Discharge Measurements Using Acoustic Doppler Current Profilers. US. Geological Survey, Scientific Investigation Report 2005-5183, Reston, Virginia, 35pp.

Pacheco, A., Vila-Concejo, A., Ferreira, Ó. and Dias, J.M.A., 2007. Present Hydrodynamics of Ancão Inlet, 10 years after its Relocation. Proceedings of the Coastal Sediments '07 Conference. New Orleans, May 2007, 1557-1570.

Pacheco, A., Vila-Concejo, A., Ferreira and Ó., Dias, J.A., 2008. Assessment of Tidal Inlet Evolution and Stability Using Sediment Budget Computations and Hydraulic Parameter Analysis. *Mar. Geol.* 247, 104-127.

Pendleton, E.A. and FitzGerald, D.M., 2005, Comparison of the hydrodynamic character of three tidal inlet systems, *in* Knight, J., and FitzGerald, D., eds., Estuaries: J. Coast. Res. ISBN 978-1-4020-3296-7, Volume 8, Chapter 5, 83-100.

Pilkey, O.H., Neal, W.J., Monteiro J.H. and Dias, J.M.A., 1989. "Algarve Barrier Islands: a noncoastal-plain system in Portugal". *J. Coast. Res.* 5(2), 239-261.

Salles, P., 2001. Hydrodynamic Controls on Multiple Tidal Inlet Persistence. PhD Thesis, Massachusetts Institute of Technology and Woods Hole Oceanographic Institution, 272 pp.

Salles, P., Voulgaris, G. and Aubrey, D., 2005. Contribution of nonlinear mechanisms in the persistence of multiple tidal inlet systems. *Estuar. Coast. Shelf. Sci.* 65, 475-491.

Simpson, M.R., 2001. Discharge measurements using a broad-band acoustic Doppler current profiler, Open-File Report 01-1, US Geological Survey, Sacramento, CA, 123pp.

SonTek, 2000. Acoustic Doppler Profiler, Technical Documentation, San Diego, CA, SonTek/YSI, Inc. San Diego, CA, USA, 160p.

Soulsby, R.L., 1997. Dynamics of marine sands. A manual for practical applications. HR Wallingford Report SR 466, 142p.

Speer, P.E. and Aubrey, D.G., 1985. "A Study of the Non-Linear Propagation in Shallow Inlet/Estuarine Systems Part II: Theory", *Estuar. Coast. Shelf. Sci.* 21, 207-224.

van de Kreeke, J., 1985. Stability of tidal inlets – Pass Cavallo, Texas. *Estuar. Coast. Shelf Sci.* 21 (1), 33-43.

van de Kreeke, J., 1990. Multiple Tidal Inlets Be Stable? *Estuar. Coast. Shelf Sci.* 30: 261-273.

van de Kreeke, J., Brouwer, R.L., Zitman, T.J., Schuttelaars, H.M., 2008. The effect of a topography high on the morphological stability of a two-inlet bay system. *Coast. Eng.* 55, 319-332.

van de Kreeke, J., Robaczewska, K., 1993. Tide-Induced Residual Transport of Coarse Sediment; Application to the Ems Estuary. Netherland Journal of Sea Research, 31(3), 209-220.

Vila-Concejo, A., Matias, A., Ferreira, Ó., Duarte, C., Dias, J.M.A., 2002. Recent Evolution of the Natural Inlets of a Barrier Island System in Southern Portugal. *J. Coast. Res*. SI 36, 741-752.

Vila-Concejo, A., Ferreira, Ó., Matias, A., Morris, B.D., Dias, J.A., 2004. "Lessons from inlet relocation: examples from Southern Portugal". *Coast. Eng.* 51 (10), 967-990.

Vila-Concejo, A., Matias, A., Pacheco, A., Ferreira, Ó., Dias, J.M.A., 2006. Inlet hazard determination in the Ria Formosa barrier island system. *Cont. Shelf. Res.* 26 (9), 1045-1060.

Williams, J.J., Bell, P.S., Thorne, P.D., 2003. Field measurements of flow fields and sediment transport above mobile beds. *J. Geophy*. *Res.* 108, NO. C4, 3109, doi:10.1029/2002JC001336.

CHAPTER V

Application of Sediment Transport Models on a Multiple Inlet System

Abstract

Measurements spanning a spring tidal cycle of mean water levels, waves, near-bed flow turbulence and bedforms were obtained from the Ancão tidal inlet, Ria Formosa, Portugal. Well-established empirical formulae were used to estimate bedload, suspended load and total sediment transport rates. The results were found to compare favourably with available direct and indirect field observations of sediment transport rates. This approach was then applied in the other 5 tidal inlets of the Ria Formosa and a net annual sediment budget for the tidal inlet system was obtained. Although subject to a range of errors, the present results have helped to quantify net accretion/erosion and have enabled evaluation of both the flushing and by-passing capacity of tidal inlets in the system. In this respect the results are considered to contribute to improving understanding and prediction of tidal inlet morphodynamics, with practical application in a range of coastal engineering and coastal management areas concerned with navigation safety, coastal erosion, ecosystem health and water quality. It may be also applied to assess the long-term stability of single and multiple inlet systems, provided that estimates of sediment storage at ebb tidal deltas are available.

Keywords: tidal inlets; barrier islands; tidal currents; coastal morphology; sediment budget

V.1 INTRODUCTION

Tidal inlets are dynamic coastal features that play an important role in navigation, sediment supply to adjacent beaches and nutrient exchanges between back-barrier systems and the coastal zone (FitzGerald, 1996). Several authors have proposed conceptual or semi-empirical models that explain tidal inlet function and morphological evolution in terms of wave or tidal flow dominance (e.g. Oertel, 1972; Hayes, 1979; FitzGerald, 1996; FitzGerald et al., 2001; Morris et al, 2001, 2004). Other approaches advocate the use of qualitative conceptual models that are based on the historical evolution of inlet morphology (e.g. channel, ebb/flood shoals) and provide regional perspectives on interactions between beach processes and offshore areas (e.g. Kana and Stevens, 1992; Kana et al., 1999; Rosati and Kraus, 1999; Rosati, 2005; Elias and van der Spek, 2006; Pacheco et al., 2008). Despite progress in this area, no model is yet able to predict quantitatively the evolution of inlet morphology in the medium- to long-term and thus the need to consider inlet evolution in conceptual terms remains.

Quantification of sediment transport in tidal inlets is a fundamental requirement to support both conceptual and numerical modelling of tidal inlet function and evolution. Since field-based studies of sediment transport have the potential to quantify the magnitude and direction of net sediment transport, they may assist in identifying evolutionary trends for a single tidal inlet or a multi-inlet system. In this paper, field data are used in combination with a range of well-established semi-empirical formulae to estimate net sediment transport rates for the major tidal inlets in the Ria Formosa. These data include: a) high-frequency flow and water level data obtained from the Ancão tidal inlet; and b) boat-mounted Acoustic Doppler Current Profiler (ADCP) data obtained for complete tidal cycles (*c.* 12.5h) in the 5 other tidal inlets of the Ria Formosa during spring and neap-tide conditions.

V.2 FIELD SITE DESCRIPTION

The Ria Formosa is a multi-inlet barrier island system located in Southern Portugal (Fig. V.1). It comprises five islands and two peninsulas separated by six tidal inlets: two re-located inlets (Ancão and Fuseta), two artificially opened and stabilised inlets (Faro-Olhão and Tavira) and two natural inlets (Armona and Lacém). The embayment is characterised by large salt marshes, sand flats and a complex network of natural and partially dredged channels, covering 8.4 x10^7 m^2 (Andrade, 1990).

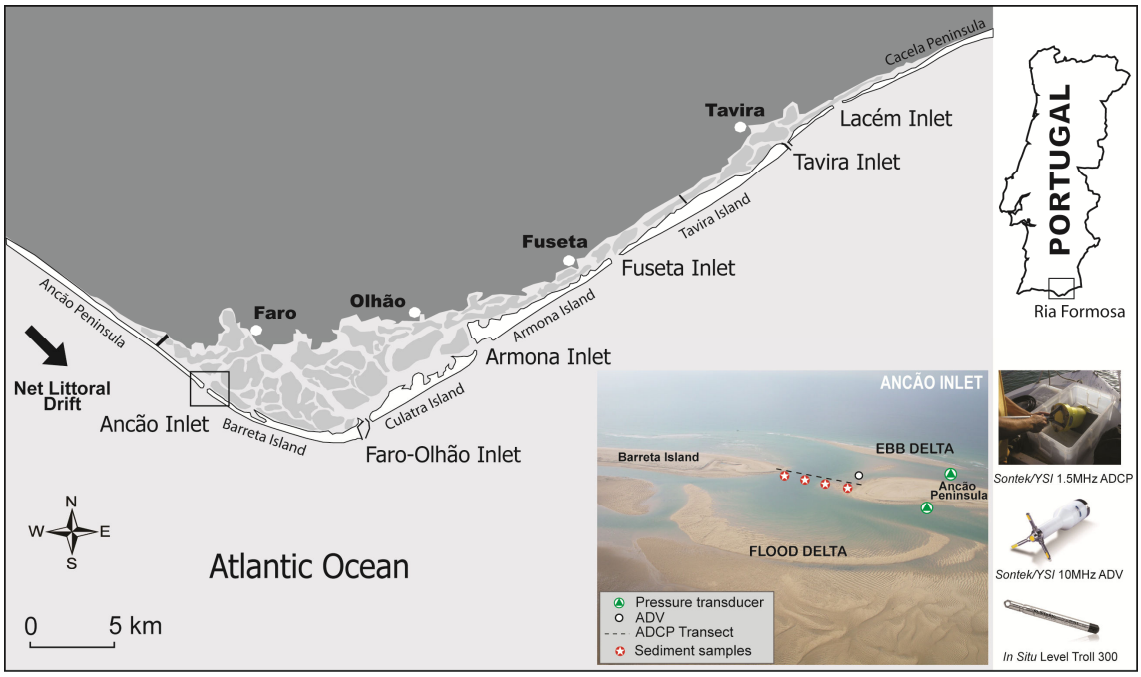

Figure V.1 Ria Formosa Multi-Inlet System, Southern Portugal, showing the Ancão tidal inlet, equipment deployment location and sampling positions

The tides in the area are semi-diurnal with typical average ranges of 2.8 m for spring tides and 1.3 m for neap tides. A maximum tidal range of 3.5 m can be attained during equinoctial tides. Harmonic analysis revealed M_2 as the dominant component with tides inside the lagoon being strongly distorted (Salles et al., 2005). Wave climate in the area is moderate to high (offshore annual mean significant wave height H_s~ 1 m and peak period T_p of 8.2 s, with storms characterised by H_s>3 m). Approximately 71% of

waves are from the W-SW, with *c.* 23% coming from the E-SE (Costa et al., 2001). Longshore currents in the area typically flow from west to east. Estimates of net annual longshore sediment transport obtained by various authors range between $1.0x10^5$ to $2.0x10^5$ m^3year^{-1} (Bettencourt, 1994). Measurements of longshore transport obtained along the updrift margin of the Ancão tidal inlet using fluorescent tracer sands gave eastward transport rates of approximately $1.3x10^5$ m^3year^{-1} for typical fair-weather conditions (Balouin et al., 2001).

V.3 METHODS

In order to provide suitable data for computation of bedload and suspended sediment transport, high-frequency measurements of flow turbulence were obtained in the Ancão tidal inlet close to the spring low-water line in October 2007 using an Acoustic Doppler Velocimeter-ADV (S*onTek/YSI* 10 MHz Ocean Probe) with an internal Pressure Transducer, PT (Fig. V.1). The ADV collected data at 25 Hz and operated in continuous burst mode (burst interval 1800 s and 30000 samples per burst) and for one complete tidal cycle. In addition, two *in situ* Level Troll 300 PTs were deployed on the seaward and lagoon sides of the Ancão tidal inlet to measure the difference in water level (pressure sensor accuracy of ± 0.2% and resolution of 0.005%, for full scale operation). These instruments were also located close to the spring low-water line and surveyed using a Differential Global Positioning System (DGPS) to determine their vertical and horizontal coordinates (± 5 mm). The PT internal clocks were synchronised and pressure data were recorded at 1 Hz. Pressure values were adjusted to account for local barometric pressure and corrected for depth attenuation of the wave-induced pressure signal (Bishop and Donelan, 1987). Measurements of vertical current velocity profiles were obtained across each inlet cross-section of the Ria

Formosa inlets, using a boat mounted ADCP (*SonTek/YSI* 1500 kHz) with bottom tracking, every hour during *c.* 12.5 hour spring and neap tidal cycles. Samples of bottom surficial sediment were also collected across each tidal inlet cross-section with a small grab sampler. In all cases datasets were obtained during fair-weather, SW wave conditions.

V.3.1 Bed sediment properties

Organic matter was removed from the grab samples using hydrogen peroxide and samples were weighed, washed, and oven-dried before being sieved at ½ ø intervals. Required grain-size parameters were computed according to the methodology described by Folk and Ward (1957) using the computer program GRADISTAT (Blott and Pye, 2001). Carbonate percentages were measured at ø intervals by weight loss on the addition of 10% HCl to dissolve shell fragments. Average grain diameters were then calculated for each channel cross-section. For the computation of suspended sediment, the median suspended grain diameter was obtained using:

$$\begin{aligned} d_{50,s}/d_{50} &= 1 + 0.011(\sigma_s - 1)(T_r - 25) \qquad for\ 0 < T_r < 25 \\ d_{50,s}/d_{50} &= 1 \qquad\qquad\qquad\qquad\qquad\qquad for\ T_r \geq 25 \end{aligned} \tag{V.1}$$

(van Rijn, 1984b), where d_{50} is the median grain size of the bed sediment, σ_s is a sorting parameter given by $\sigma_s = 0.5\,(d_{84}/d_{50} + d_{50}/d_{16})$ and T_r is a transport parameter defined here as $T_r = (\tau - \tau_{cr})/\tau_{cr}$, where τ is the time-averaged bed shear stress (see below) and τ_{cr} is the critical shear stress derived from the critical Shields $\theta_{cr} = \tau_{cr}\,g\,(\rho_s - \rho)\,d$, with $d = d_{50,s}$ for suspended and $d = d_{50}$ for bedload, ρ_s and ρ the grain and water density (ρ_s=2650 kgm^{-3} and ρ=1025 kgm^{-3} for seawater at 14ºC, salinity=35ppt, respectively) (Appendix V.1).

V.3.2 Bed Shear Stress and Bed Roughness

The ADV data were de-spiked and smoothed following standard procedures (Goring and Nikora, 2002). Zero-mean flow component time-series, u', v' and w', comprised of a time-varying, turbulent component, and a more regular, semi-sinusoidal component, attributable to the oscillatory flows imposed on the tidal currents by waves. The first-order wave-induced time-series u_w, v_w and w_w was effectively removed from the u', v' and w' time-series using a moving average filter (Williams et al., 2003a) to leave turbulence-only flow components u, v and w. The RMS wave-induced flow speed was calculated using $U_w = (\bar{u}_w^2 + \bar{v}_w^2)^{0.5} / \sqrt{2}$, where $\bar{u}_w$ and $\bar{v}_w$ are the wave variance values extracted from the PT time-series using a zero-crossing method combined with a Fast Fourier Transform (FFT) algorithm (Tucker and Pitt, 2001).

Time-averaged bed shear stress, τ, used here to parameterise the combined forces of lift and drag that are primarily implicated with the mobilisation and transport of sediments, was calculated using the Turbulent Kinetic Energy (TKE) and Reynolds Stress (RS) methods (Williams et al., 2003a). In the TKE method, τ is defined as:

$$\tau_{TKE}(z) = C\,\rho\,E(z) \qquad \text{(V.2)}$$

(Soulsby and Humphery, 1990), where C is a constant = 0.19 (Stapleton and Huntley, 1995), and the turbulent kinetic energy, E, at height z is defined as $E(z) = 0.5(\bar{u}^2 + \bar{v}^2 + \bar{w}^2)$, where $\bar{u}$, $\bar{v}$ and $\bar{w}$ are the variance of the turbulence-only time series. In the Reynolds stress method, τ is defined as:

$$\tau_{RS}(z) = \rho\,(-\overline{uw}^2 + -\overline{vw}^2)^{0.5} \qquad \text{(V.3)}$$

(Soulsby and Humphery, 1990) where $-\overline{uw}$ and $-\overline{ww}$ are the time-averaged Reynolds stresses. The time-averaged drag coefficient, Cd, at height z above the bed was obtained using:

$$Cd\ (z) = (\bar{\tau}/\rho)/U_{DA}{}^2 \tag{V.4}$$

(Williams et al., 2003a) where $\bar{\tau}$ is the mean local bed shear stress defined as $(\tau_{TKE} + \tau_{RS})/2$ and U_{DA} the depth-averaged current velocity, approximated using the empirical equation (Soulsby, 1997):

$$U_{DA} = \overline{S}(z)/(z/0.32h)^{1/7} \tag{V.5}$$

with $\overline{S}(z) = (\overline{U}^2 + \overline{V}^2)^{1/2}$, where $\overline{U}$ and $\overline{V}$ denote time-averaged values of U and V at height z, and h is the water depth.

The apparent bed roughness length, z_a, at height z was estimated using:

$$z_a = z \exp^{-[(k/\sqrt{C_d(z)})+1]} \tag{V.6}$$

where k is the von Kármán constant (=0.4).

The total time-averaged shear stress, τ_0, was also estimated using the simplified water slope method (Soulsby, 1997):

$$\tau_0 = \rho g\, hI\,. \tag{V.7}$$

where I is the water slope and g acceleration due to gravity.

The validity of this approach was examined using the two dimensional hydrodynamic numerical model XBeach (Roelvink et al., 2009). This was set up using the measured bathymetry and topography of the Ancão tidal inlet and was driven by the

measured gradients in tidal elevation imposed on its seaward and lagoon boundaries. In addition, standard JONSWAP wave spectra were imposed on the seaward boundary of the model, with characteristics similar to those prevailing during the measurements (i.e. $H_s = 1$ m and $T_p = 6$ s). While most model parameters were set to commonly used values (Roelvink et al., 2009), in this case the bed friction coefficient in the model (*'Cf'* in XBeach nomenclature) was adjusted until the depth-average current, U_{DA}, predicted by the model at the ADV location in the Ancão tidal inlet matched closely the measured value (i.e. within 3%). This term is equivalent to a depth-averaged drag coefficient, Cd_{DA}, and reflects the combined drag of sediment grains and bedforms. During the simulation period it was possible to match approximately predicted U_{DA} values with measured U_{DA} values using *'Cf'* = 0.005. However, in order to accurately simulate measured temporal changes in U_{DA} during the tidal cycle, multiple runs of XBeach were undertaken in which *'Cf'* was increased in incremental steps of 0.0002 between 0.002 and 0.015. The values of *'Cf'* providing the closest agreement between any given measured and simulated U_{DA} value were then identified.

Variability in bedform morphology is the result of a complex interaction between the bed, currents and unsteady shoaled waves of many frequencies and directions. In order to compute sediment transport it is necessary to quantify the drag of these bedforms to enable estimation of the skin friction component of bed shear stress that drives sediment transport. Houwman and van Rijn (1999) have established a useful relationship between the apparent bed roughness, $k_a = 30 z_a$, and the physical bed roughness, $k_s = 30 z_0$, in the form:

$$\frac{k_a}{k_s} = \exp\left(\gamma U_w / U_{DA}\right) \tag{V.8}$$

where $\gamma = 0.8 + \varphi - 0.3\varphi^2$, with φ being the angle between wave and current direction (in radians). In the present study, estimates of U_w were obtained from the ADV, U_{DA} and k_a derived from equations 5 and 6. Empirical relations between k_a and k_s were established for flood and ebb conditions. Here we only used ADV data with burst correlation coefficient values greater than 70 %. These empirical relationships express a wide range of situations, i.e., the instantaneous effect of wave-current interaction on the formation/destruction of bedforms through the tidal cycle.

V.3.3 Sediment transport

Estimates of the bed shear stress and apparent roughness were also obtained from the ADCP data. These data were rotated to align with the streamwise and spanwise directions and depth-averaged velocities were obtained for each 5 s velocity profile (or ensemble). The depth-averaged current velocity (U_{DA}) was obtained using:

$$U_{DA} = 1/h \int_0^h U(z)dz \tag{V.9}$$

(Soulsby, 1997), where $U(z)$ is the current speed at height z. The von Kármán-Prandtl equation (Soulsby, 1997) was then used to obtain estimates of τ and z_a:

$$U(z) = (\sqrt{\tau / \rho} / k) \ln(z / z_0) \tag{V.10}$$

Using this relationship and following linear regression of $U(z)$ on $\ln(z)$, an apparent roughness is obtained by $z_a = \exp(-c/m)$, where c is the intercept and m is

the slope. Using the above empirical relations between k_a and k_s, an estimate of z_0 was obtained. Using Eq. V.6, and replacing z_0 by z_a, the drag coefficient attributable to the bedforms is determined and then used to estimate the skin-friction component of shear stress, τ_s, by Eq. 4. The skin-friction shields parameter (θ_s) is then defined as:

$$\theta_s = \tau_s / g(\rho_s - \rho)d_{50} \tag{V.11}$$

For simplicity, other size fractions are not considered separately.

A unifying expression for the volumetric bedload transport rate (m^2s^{-1}), q_b, is given by:

$$q_b = \Phi\,[g(s-1)d^3]^{0.5} \tag{V.12}$$

(Soulsby, 1997), where Φ is the dimensionless bedload transport rate, with $d = d_{50}$. Here we apply four widely-used bedload formulae from Yalin (1964), van Rijn (1984a), Madsen (1991) and Nielsen (1992) to compute bedload transport rates for current-only conditions. These require estimates of the critical flow conditions necessary to initiate sediment transport. Both the bedload formulae and the methods used to estimate critical conditions are detailed in Appendix V.1.

The volumetric suspended transport rate, q_s, was derived from:

$$q_s = \int_{za}^{h} C(z)U_{DA} \tag{V.13}$$

where $C(z)$ is the suspended sediment concentration at height z and za the reference concentration. The value of $C(z)$ was derived from three different methods, considering two methods for current-only processes, assuming a linear (power law, C-PL) or

parabolic (Rouse profile, C-RP) increase of eddy diffusivity with depth, and one method for combined waves plus current situations (C-W). Using the ADV data, a statistically significant power-law relationship between q_s values obtained using different formulae and the parameter $U_{DA}\ d_{50,s}$ was obtained. The formulae used are detailed in Appendix 2. The method was first tested and validated at the Ancão tidal inlet and was then used to estimate q_s across all the inlets using as input parameters the U_{DA} values derived from the data collected with the ADCP and the sediment properties measured at each inlet (Table V.1).

Table V.1 Summary of sediment parameters from analysis of samples and thresholds of motion derived from empirical formulae

	Ancão	**Faro-Olhão**	**Armona**	**Fuseta**	**Tavira**	**Lacém**
d_{10} (mm)	0.52	0.40	0.35	0.51	0.09	0.27
d_{16} (mm)	0.59	0.46	0.41	0.59	0.21	0.31
d_{50} (mm)	0.88	0.86	0.61	0.98	2.88	0.48
d_{84} (mm)	1.38	5.19	1.08	2.10	6.29	0.81
d_{90} (mm)	1.64	6.22	1.39	3.06	20.70	0.97
Carbonates (%)	5	17	6	6	24	6
θ_{cr}	0.029	0.029	0.031	0.030	0.042	0.033
τ_{cr} (Nm^{-2})	0.421	0.410	0.302	0.468	1.933	0.256
General characteristics						
Ancão Inlet	Coarse sand, moderately well sorted					
Faro-Olhão Inlet	Varies from very coarse (margins, less sorted) to medium sand (centre, well sorted)					
Armona Inlet	Coarse sand, moderately sorted					
Fuseta Inlet	Very coarse sand, generally well sorted (finer and better sorted at channel centre)					
Tavira Inlet	Coarse sand (E margin) and fine gravel (W margin), both poorly sorted. Bedrock at channel centre					
Lacém Inlet	Medium sand (margins) to coarse sand (channel centre), well sorted.					

The resulting value of bedload, q_b, and suspended transport, q_s, computed using the above methods were used to define total transport, q_t, through a complete tidal cycle, in both spring- and neap-tidal conditions. In the convention used here, negative and positive q_t values are associated with ebb and flood tidal flow directions, respectively.

It should be borne in mind that q_t values obtained in this study are only estimates and are site-specific.

V.4 RESULTS

V.4.1 Bed Shear Stress and Bed Roughness

Fig. V.2A shows temporal changes and a clear time lag between water levels measured by the PTs over a period of *c.* 5 hours. Fig. V.2B shows temporal changes in the total shear stress obtained by the simplified water slope method (Eq. V.7) and the time-average shear-stress values (Eq. V.2 and V.3) derived from the ADV. Time-average (~1 s) values of U_{DA} and U_w are shown in Fig. V.2C and V.2 D, while $\overline{\tau}$ values are shown in Fig. V.2E and their components in Fig. V.2F. Maximum values of U_{DA} O (1.2 ms^{-1}) were measured during flood and ebb tides at the ADV location, over the range 0.10 m < h < and 2.22 m. Wave induced flow speeds averaged U_w O(0.25 ms^{-1}), increasing to U_w O(0.35 ms^{-1}), around flood peak.

Although showing the same general trends and magnitudes, TKE-derived values of $\overline{\tau}$ are always slightly higher than RS-derived values (Fig. V.2E), and have a lower variance. Both the RS and TKE methods fail to provide meaningful estimates of bed shear stress at the early stages of the ebb tide. It is thought that this result reflects boundary interference as a bedform migrated beneath the ADV and prevented the instrument from working. The current induced shear-stress is the main component of the mixed tide-wave dominated flow in the inlet, with instantaneous values in the range 0.7 Nm^{-2} to 4.9 Nm^{-2} (Fig. V.2F). This is approximately the same range of values as the mean current-wave instantaneous shear-stresses. Although waves induce generally lower instantaneous shear-stresses (0.3 Nm^{-2} to 1.1 Nm^{-2}), maximum instantaneous

shear stress values computed for combined current-wave processes, using the wave-boundary layer model (Fredsøe, 1984), were actually higher (2.2 Nm^{-2} and 6.5 Nm^{-2}).

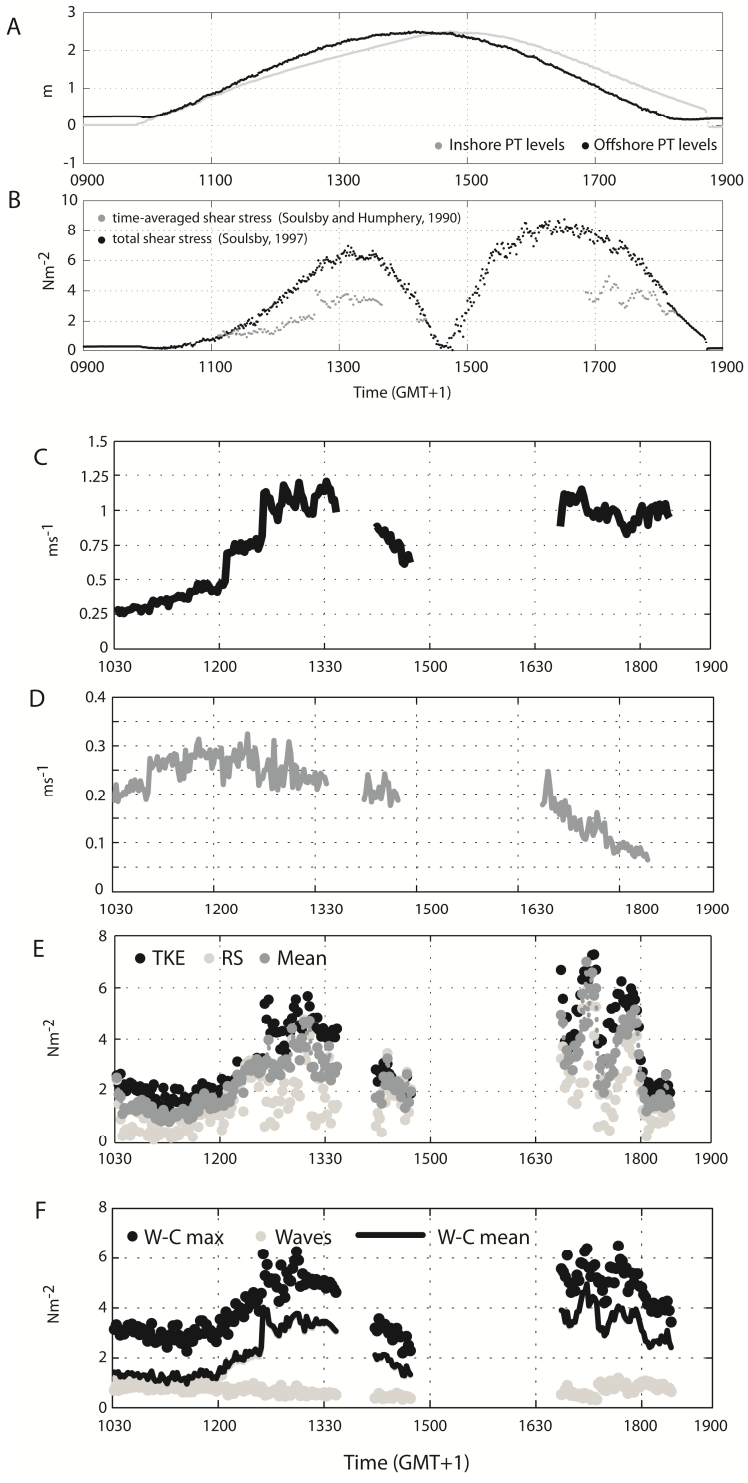

Figure V.2 Offshore/inshore pressure transducer levels (A); τ_0 (water slope method) and τ (mean of RS and TKE methods) (B); 1 s burst average values of U_{DA} (C); U_w (D); τ_{TKE} and τ_{RS} *(E);* and τ components (F)

Strong tidal currents $\overline{S}_{\max} O$ (1.9 ms^{-1}) in the Ancão tidal inlet resulted in the formation of a sequence of relatively long-crested bedforms, similar to mega-ripples, with their crests aligned approximately normal to the mean tidal flow direction (Fig. V.3A). Small current-wave generated ripples also formed, their length related (less than or equal) to near-bed orbital velocity. In order to examine the links between measured bed roughness and bed morphology, two different empirical equations were used to estimate ripples (Nielsen, 1992; van Rijn, 1993). These gave a mean ripple wavelength (λ_r =1.22 m) and heights (Δ_r = 0.23 m: Fig. V.3B and V.3C). These values are similar to the dimensions of the megaripples measured in the field (λ_r =1.7 m and Δ_r =0.16 m). Owing to the coarse nature of bed sediments, and their instability with the flow, the small ripples observed on the back of megaripples were not predicted by the empirical formulae.

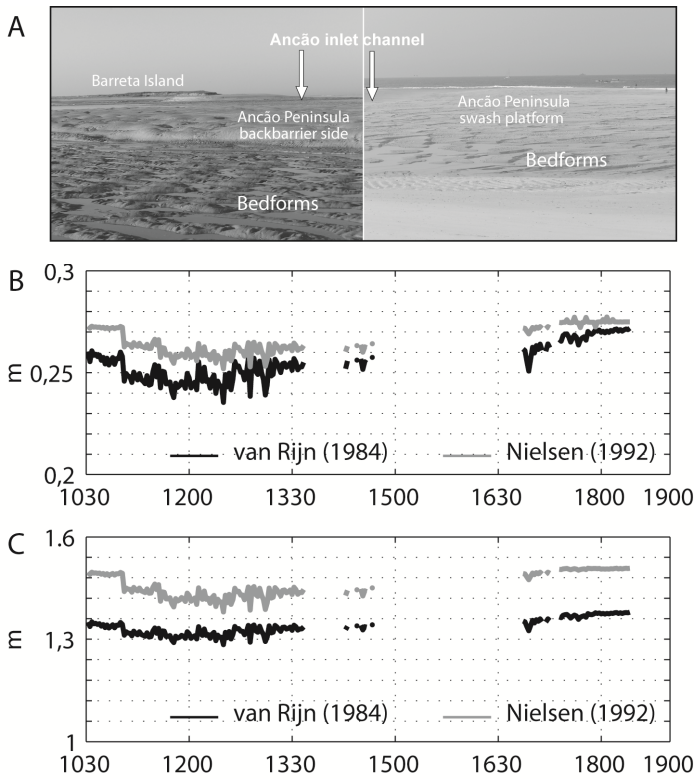

Figure V.3 Bedform morphology at the inner inlet channel, backbarrier side and at the updrift swash platform, Ancão Peninsula (A); height (A) and length (B) of bedforms determined empirically

Values of k_a and k_s are shown on Fig. V.4, where k_s values were determined based on two linear relationships for flood/ebb conditions derived from Eq. V.8 (Fig. V.4A).

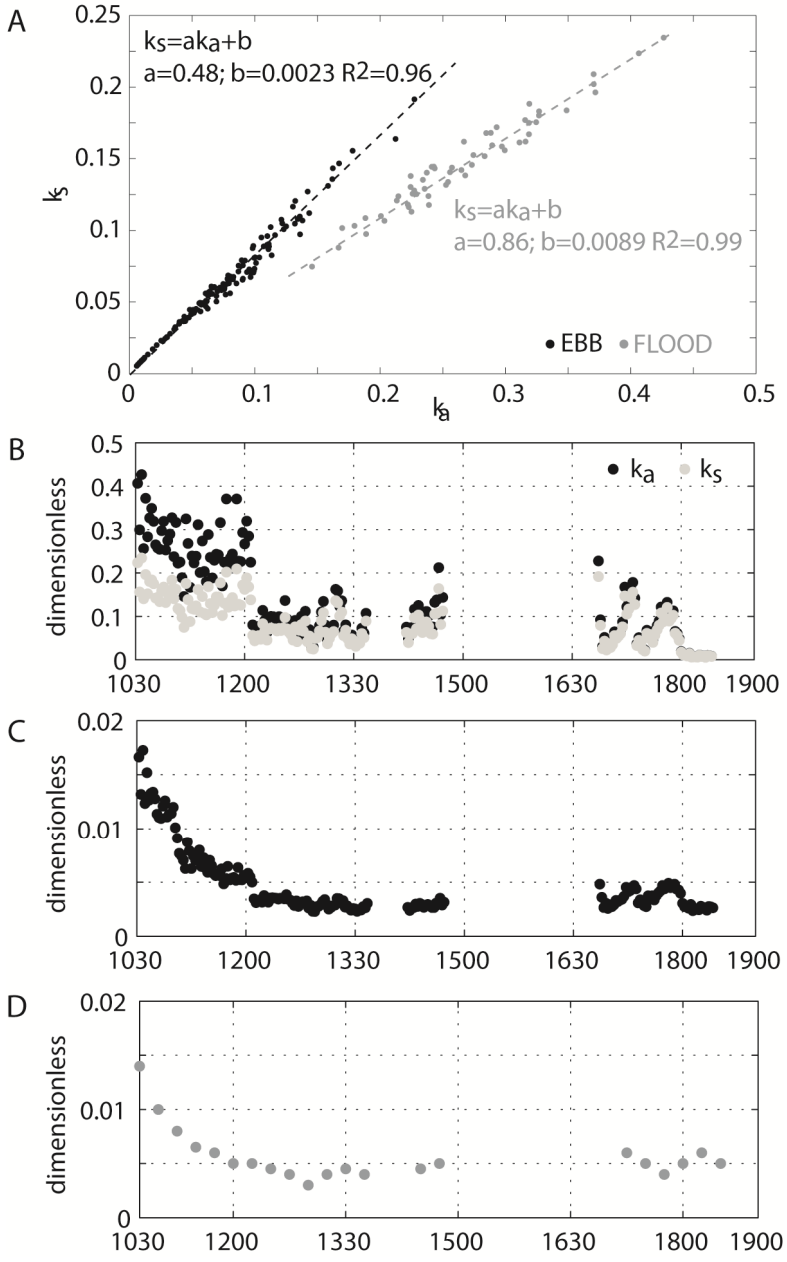

Figure V.4 Flood/ebb derived relations between k_a and k_s from Eq. 8 (A); 1 s burst average values k_a and k_s values (B); *Cd* (C); and *Cf* mean values determined by the XBeach (D)

The ratio between k_a / k_s ranges between 1.1 and 2.0 with a mean value of 1.4. Results indicate that U_w does not contribute significantly to mean U_{DA} (i.e. the ratio

U_w/U_{DA} ranges between 0.07 to 0.83 ms^{-1}, with a mean value of 0.34 ms^{-1}). Time-averaged k_s were found to be *c.* 0.088 m and thus similar to values measured in other studies over rough, mobile sediment beds (e.g. up to 0.1 m, van Rijn, 2007a). However, maximum k_s values of 0.23 m were obtained during peak flood tide flows and are probably related to dune-like features (Fig. V.4B). Computed values for k_a range from 0.006 m to 0.426 m, with a mean value of *O* (0.13 m) during the tidal cycle. Similar results are reported by Houwman and van Rijn (1999), who show that k_a is an almost constant value of 0.1 m U_w in the range 0.3-1.5 ms^{-1}.

Estimates of Cd, obtained from Eq. V.4, range between 0.005-0.015, with maximum values in the initial stages of the flood (Fig. V.4C). Those values can be compared with '*Cf* ' values obtained from the XBeach (Fig. V.4D). Although '*Cf* ' values are slightly higher, they reveal the same tendency, thus providing strong evidence that the water slope method gives a good estimate of total drag.

V.4.2 Sediment transport – the Ancão tidal inlet test case and its application

Samples of surficial bed sediments collected across the inlet cross-section using a grab had the following grain-size characteristics: d_{10}=0.52 mm, d_{16}=0.59 mm, d_{50}=0.88 mm, d_{84}=1.38 mm and d_{90}=1.64 mm (i.e., coarse sand). Suspended sediment grain-size was determined empirically using Eq. V.1. Theoretical threshold values of shear stress, τ_{cr}, and Shields parameter, θ_{cr}, were determined using the formulae detailed in Appendix V.1, summarised in Table V.1.

The suspended-sediment transport rate was obtained by multiplying the depth-averaged velocity by the mean suspended sediment concentration predicted by power law expressions (Fig. V.5). Analysing the coefficients obtained, it can be observed that

q_s correlates best with $\overline{U}d_{50s}$ to the power of *c.* 4. This is in agreement with other studies (e.g. Dyer, 1986). Peak values of suspended transport were *c.* 0.028 $kgm^{-1}s^{-1}$ during the peak flood in combined current-wave situations. Generally, average values for current-only and current-wave interaction lay between 0.01 and 0.015 $kgm^{-1}s^{-1}$, being slightly higher at during the flood tide and insensitive to the computation method.

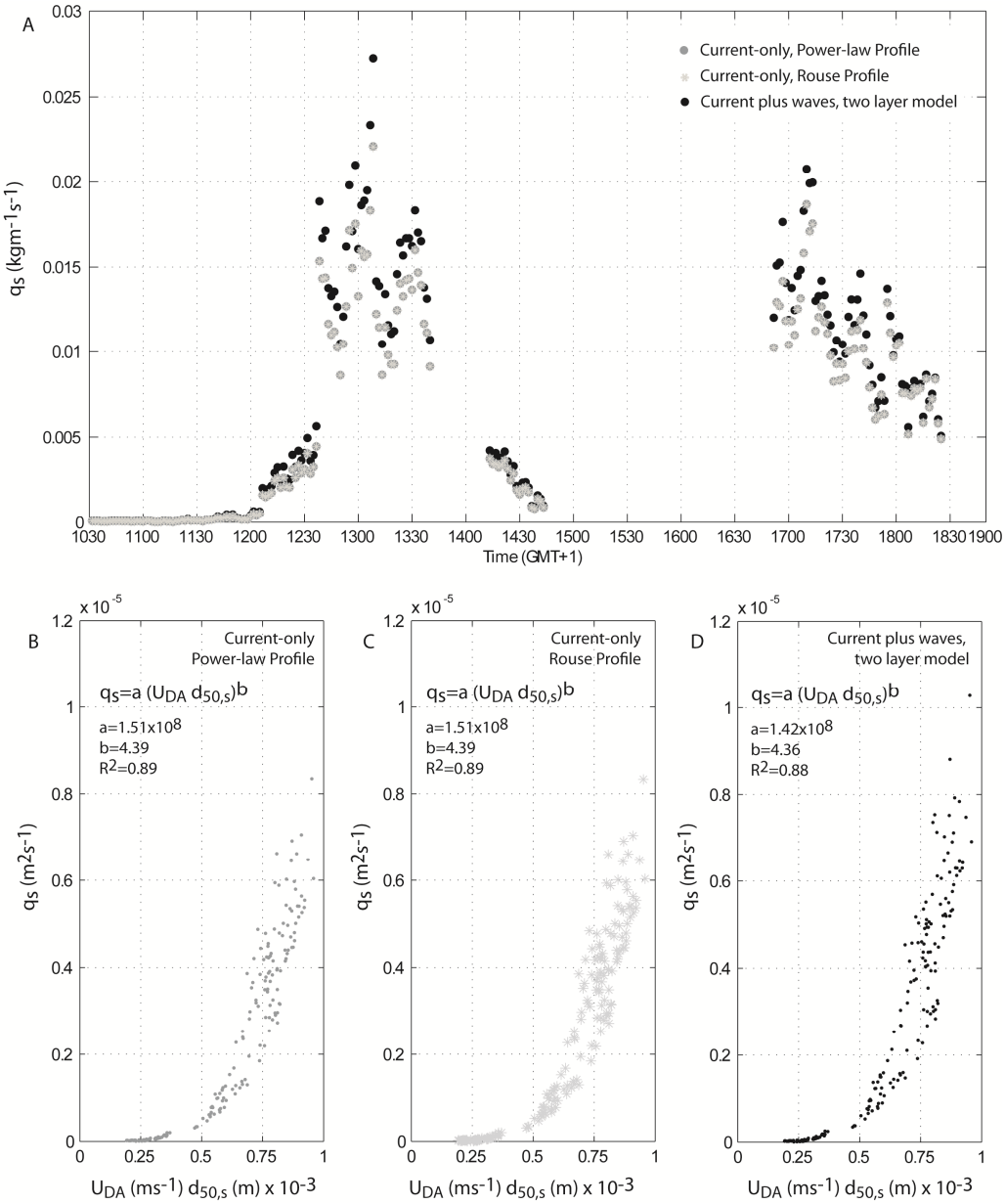

Figure V.5 Mass suspended sediment rate through the tidal cycle at Ancão tidal inlet (A) and volumetric transport rate as a function of the depth-average velocity for current-only processes with eddy diffusion varying linearly; parabolically (B) with the flow; and for the current-wave interaction (C)

Predicted net bedload and suspended transport produced by different methods are given in Fig. V.6, along with total net sediment transport rates for a spring-tidal cycle in Ancão tidal inlet. During the early stages of flood/ebb tide and when the tide falls to slack water, q_b < 0.25 kgm^{-1}s^{-1} (Fig. V.6B), which is coincident with U_{DA} < 0.6 ms^{-1} (Fig. V.6A). When that velocity is exceeded, q_s increases to values between 0.25-0.5 kgm^{-1}s^{-1}, with maxima > 0.75 kgm^{-1}s^{-1} coincident with U_{DA} > 1.5 ms^{-1}.Values of q_s present the same tendency (Fig. V.6C), although at a lower magnitude (approximately 10 % of bedload transport rates), i.e., when U_{DA} > 0.6 ms^{-1}, q_s range between 0.025-0.05 kgm^{-1}s^{-1}, with maxima > 0.075 kgm^{-1}s^{-1} when U_{DA} > 1.5 ms^{-1}.

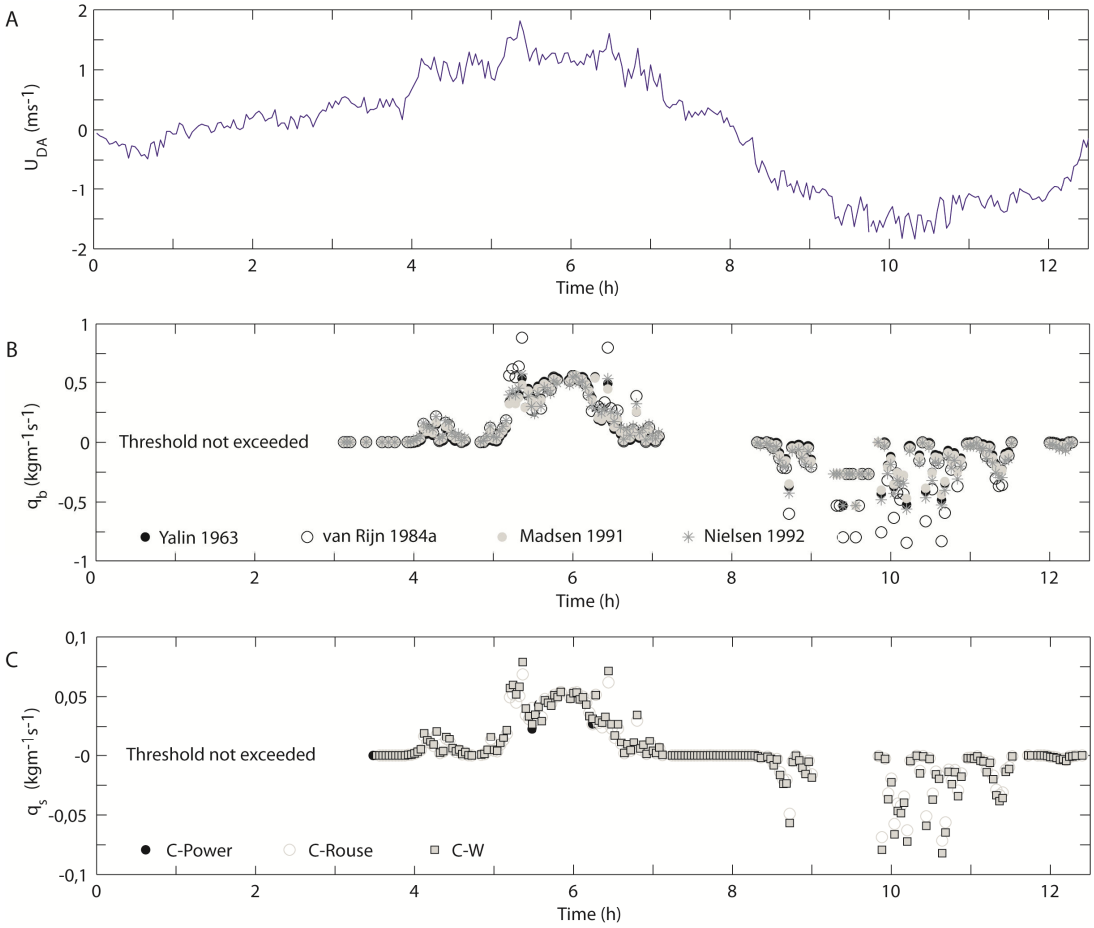

Figure V.6 Interpolated values of U_{DA} (A), q_b (B) and q_s (C) derived from the ADCP and sediment properties data for the spring-tide tidal cycle survey performed at Ancão tidal inlet

Integrated values of q_b and q_s through the tidal cycle are presented on Table V.2, with net sediment transport estimates obtained by the mean of the estimates given by different methods. The q_b methods differ by a maximum factor of 2, with van Rijn (1984a) method producing higher estimates. The value of $\overline{q_{b\ Ebb}}$ is approximately three times higher than $\overline{q_{b\ Flood}}$, resulting in $\overline{q_{b\ Net}}$ ~ -0.084±0.03 kgm^{-1}s^{-1}, i.e., net sediment export. Current-only and current-wave methods to derive q_s provide approximate values, resulting in $\overline{q_{s\ Net}}$ -0.011±0.001 kgm^{-1}s^{-1}, i.e., also sediment export. These values were then extrapolated to give annual volumetric transport rates, by assuming that mass concentration = sediment density (i.e. ρ_S=2650 kgm^{-3}), and multiplying the net rate by the cross-sectional transect width. For bedload, the volume is of the total settled bed material, including pore-water (i.e. porosity ε=0.4).

Table V.2 Estimates of mass (kgm^{-1}s^{-1}) and volumetric (m^{3}year^{-1}) transport rates using different models for bedload and suspended transport for a ADCP tidal cycle performed at Ancão tidal inlet during spring-tides

BED LOAD TRANSPORT	**Flood (kgm^{-1}s^{-1})**	**Ebb (kgm^{-1}s^{-1})**	**Net (kgm^{-1}s^{-1})**	**M^{3}year^{-1}***
Yalin (1964)	0.046	-0.114	-0.068	-1.57E+05
Van Rijn (1984)	0.071	-0.195	-0.124	-2.88E+05
Madsen (1991)	0.050	-0.115	-0.065	-1.51E+05
Nielsen (1992)	0.066	-0.144	-0.078	-1.81E+05
Mean	*0.058*	*-0.142*	*-0.084*	***-1.94E+05***
Standard deviation	*0.012*	*0.038*	*0.027*	*6.39E+04*
SUSPENDED TRANSPORT				
C-Rouse (Soulsby, 1997)	0.006	-0.017	-0.010	-1.33E+04
C-Power (Soulsby, 1997)	0.006	-0.017	-0.010	-1.33E+04
C-W (Soulsby, 1997)	0.007	-0.019	-0.012	-1.54E+04
Mean	*0.007*	*-0.018*	*,*	***-1.44E+04***
Standard deviation	*0.001*	*0.002*	*0.001*	*1.21E+03*

* For bedload, porosity (ε=0.4) is considered, i.e., volume of settled-bed material. The cross-sectional width is w=110 m, integrated transect value derived from the ADCP measurements

The same methodology, primarily validated for the spring-tide ADCP survey at Ancão tidal inlet, was then applied to the other inlets, for both spring and neap tidal cycles. Results of the annual volumetric transport rates are given for the Ria Formosa

inlets are presented in Fig. V.7. By estimating the average volumetric q_t during the neap to spring tidal cycle, the predicted transport rates are assumed here to represent volumetric transport occurring during fair-weather conditions and are representative of tidal amplitudes through the year. The estimates will be discussed in section V.5 in the light of existing knowledge of system dynamics.

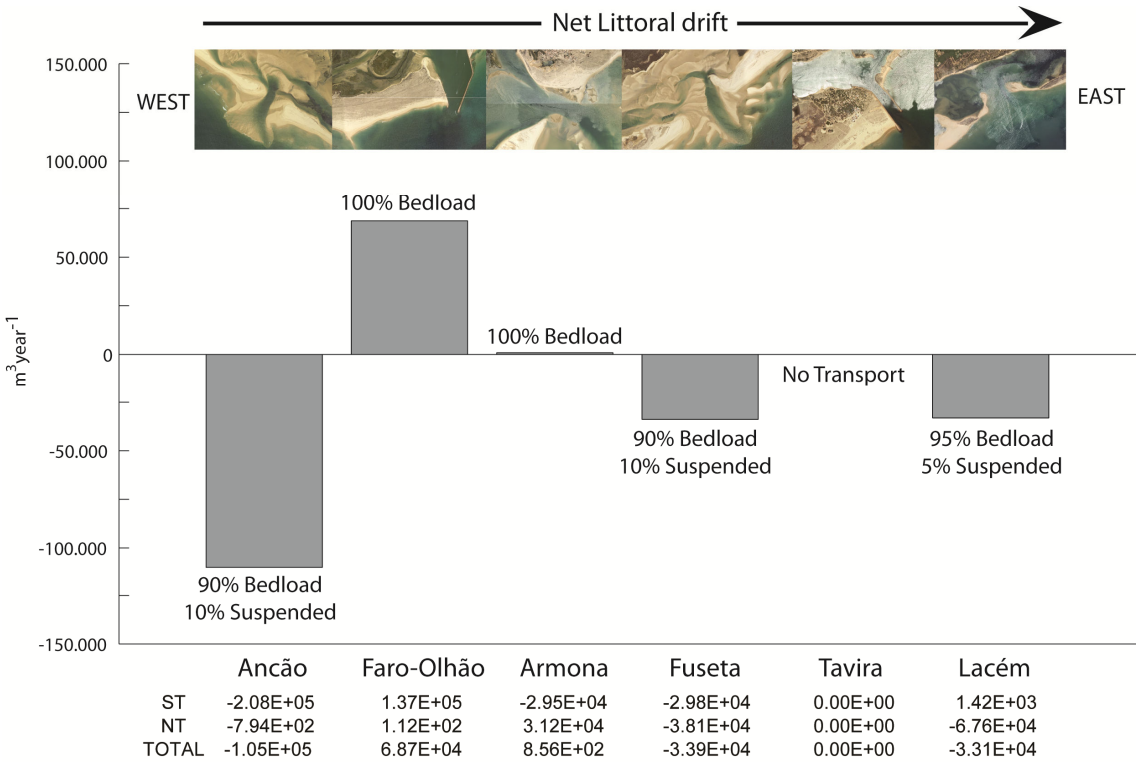

Figure V.7 Annual sediment transport estimates for the Ria Formosa inlets

The grain-size properties of surficial bed sediment samples across each transect are presented in Table V.1. All the inlet channels contain coarse sand, with medium-to-coarse, poorly-sorted sand in the adjacent channels. With the exception of the Tavira tidal inlet, more than 80% of the sediment is composed of terrigenous material (almost entirely quartz) with the remaining fraction being shell fragments. Entrainment thresholds, expressed as a critical Shields parameter and as a critical bed shear stress, are also presented in Table V.1.

V.5 DISCUSSION

V.5.1 Sediment transport in Ancão tidal inlet

Rates of bedload transport derived from measured bedform migration rates in Ancão tidal inlet by Williams et al. (2003a) on 28th February 1999 during fair-weather, spring tidal conditions range between 0.2 $kgm^{-1}s^{-1}$ to 0.4 $kgm^{-1}s^{-1}$, and were found to correlate linearly (R^2=0.865) to the mean of predicted values using various empirical formulae (van Rijn, 1984a; Madsen, 1991; Nielsen, 1992). The empirical methods used by Williams et al. to calculate bedload differed by a maximum factor of 3, similar to those obtained in the present study.

Acoustic measurements of suspended sediment transport rates obtained in the same study ranged between 0.01 $kgm^{-1}s^{-1}$ and 0.02 $kgm^{-1}s^{-1}$ and were essentially time-invariant. Estimates from empirical formulae (e.g. power law, Rouse profile) agree with the measured time-averaged and horizontal spatially-averaged profiles. Williams et al. (2003a) also showed that sediment resuspension events occurred only under wave crests, where wave-induced flow and mean current acts in broadly the same direction. The proportion of total sediment transport in the Ancão tidal inlet composed of suspended material was *c.* 30% of bedload transport (Williams et al., 2003a). The authors indicate that q_s is limited by the availability of fine sediment in the relatively coarse and well-sorted bed sediments of Ancão tidal inlet.

Our results confirm both the magnitude and trends measured previously at the site. Williams et al. (2003a) showed that the migrating mega-ripples and dune-like bed features observed at most locations in the inlet are responsible for the majority of bedload transport. Our data also indicate that, despite the presence of waves, the bulk of suspended sediment transport is accomplished by turbulent diffusion processes related to the strong tidal currents (*cf.* Williams et al., 2003a). There is almost no difference

between suspended sediment transport predicted by the current-wave boundary layer method and the two current-only methods. However, a measured increase in wave activity during the observational period resulted in enhancement of bedload transport, i.e. onshore directed, with maxima recorded during flood tide. Conversely, changes in hydraulic bed roughness between flood and ebb tides, as result of changing bed morphology due to the increase on the current speed, tended to enhance sediment transport offshore.

V.5.2 Application to the other inlets of the Ria Formosa

Total sediment transport rates, q_t, were extrapolated to obtain annual volumetric transport rates by multiplying the computed rates of sediment transport by the width of each transect. In Ancão tidal inlet, the net annual seaward sediment flux is estimated to be *c.* -1.00x10^5 m^{3}year^{-1}, approximately equal to the annual longshore sediment transport rate measured during fair-weather conditions at the updrift margin (*cf.* Balouin et al., 2001). This indicates that the ebb current is capable of flushing out sediments that enter the inlet during the flood tide. These seaward sediment movements are thought to be re-mobilised on the ebb shoal primarily by wave action and are transported in a net easterly direction (Vila-Concejo et al., 2002, 2004).

Application of the method to the Faro-Olhão tidal inlet results in a net annual sediment accumulation of *c.* 6x10^4 m^{3}year^{-1}, with sediment transport occurring solely as bedload. The computed value is approximately a third of the reported annual sediment entry into the system, when pre-dredging and post-dredging surveys are compared (the volume dredged in order to maintain channel navigability ≅ 1.4 x10^5 m^{3}year^{-1}).

Knowledge of sediment transport in the other inlets of the system is very scarce. Several authors suggest that, due to the deep scouring activity (up to 40 m in depth)

induced by engineering structures around Faro-Olhão tidal inlet, the offshore morphology of this inlet entrance provides a barrier to littoral drift in fair weather conditions (Andrade, 1990; Salles, 2001; Pacheco et al., 2008). Any sediment entering this inlet will therefore be transported to deeper areas and effectively removed from the littoral sediment system. Hence longshore littoral drift decreases east of the Faro-Olhão Inlet.

The balance between estimated annual q_t rates for spring and neap tide conditions at Armona tidal inlet approaches zero, with offshore/onshore transport during spring/neap tides, respectively. Armona tidal inlet was formerly the main inlet of the Ria Formosa, but following the opening of Faro-Olhão tidal inlet, Armona has gradually lost its hydraulic efficiency, resulting in a large reduction in its cross-sectional area (Pacheco et al., 2008; Pacheco et al., 2010). The inlet's hydrodynamics indicate that it is always ebb dominated. The two major inlets of the system, Faro-Olhão and Armona, represent almost 90% of the total tidal prism of the Ria Formosa system, where excess flood in Faro-Olhão ebbs through Armona, an interconnected sub-system especially active during spring-tides (Pacheco et al., 2010). Despite the capacity of ebb currents at Armona tidal inlet to flush sediments offshore (which seems to be enhanced during spring-tides), the results indicate influx of sand during neap tides. The origin of these sediments is thought to be from the remnants of large ebb-tidal deltas established in the past (Andrade, 1990; Salles, 2001).

Further east, the Fuseta and Lacém tidal inlets present the same export rates. Fuseta exports sediment through spring-neap tidal cycles, with values closer to 3.0×10^4 $m^3 year^{-1}$, similar to the recorded at spring-tide at Armona. Lacém, on the other hand, exports 6.0×10^4 $m^3 year^{-1}$ during neaps, with negligible onshore transport during spring tides. Bedload transport is predominant at both inlets. At Tavira tidal inlet, the combination of

the flow and sediment properties resulted in an overall net transport rate of zero. The sediments in the inlet channel (Table V.1) are very coarse, thus less mobile, and thresholds of motion were never exceeded. As a result, sediment exchange through the inlet is negligible in both directions, indicating an overall equilibrium between hydraulics and the bed, and/or the existence of a stratigraphic control (e.g. bedrock).

Although this study indicates the inlets might have the capacity to flush sediments offshore during prevailing fair-weather conditions, which is an indicator of multiple inlet persistence in the system (Salles 2001), the importation of significant quantities of sediments by onshore-directed wave-induced transport processes during storm events may obstruct the channels, affecting their hydraulic efficiency. A further important component of the sediment transport system in the Ria Formosa is longshore transport, which is usually directed at the ebb deltas and swash platforms of the outer inlet mouth (Williams et al., 2003b). However, consideration of this additional complexity in the sediment budget is beyond the scope of the present paper.

V.6 CONCLUSION

The present study has applied well-established empirical formulae, locally calibrated with high frequency current and water-level data, to estimate net bedload, suspended load and total transport in a multi-tidal inlet system. The methods applied focus on establishing robust relationships between bed roughness, bedload sediment transport and flow speed, as well as between suspended sediment transport and the depth-averaged velocity. The results obtained have been calibrated and verified at Ancão tidal inlet using measurements and a numerical model. The methodology has then been applied to the other inlets of the system to derive total net transport rates during complete spring and neap tidal cycles under fair-weather conditions. By quantifying

annual net sediment transport, this work has increased knowledge of sediment dynamics in multiple inlet systems and identified appropriate approaches to the prediction of sediment transport in these environments. The results have applications in coastal engineering and coastal management projects concerned with dredging and beach nourishment. The following conclusions can be drawn from this work:

Estimates of sediment transport, verified for the Ancão tidal inlet and extrapolated to give annual net transport rates, have enabled the establishment of a useful conceptual sediment transport model for fair weather conditions that can be applied to other inlets in the system. The model allows processes, such as sediment trapping, to be identified and has established the flushing capacity of the inlets in the Ria Formosa system. In doing so it has assisted in quantifying sediment transport rates and trends. The approach to prediction of sediment dynamics used here has accurately reproduced the magnitude and direction of sediment transport in the Ancão tidal inlet, as well as supporting the hypothesis that the main inlet of the system (Faro-Olhão tidal inlet) acts as a sediment sink in the system. Although making a number of simplifying assumptions, the results were found to represent, with reasonable accuracy, known processes and magnitudes of sediment transport for the inlets. However, owing to the problems of obtaining accurate measurements of sediment transport rates, the results presented here are site-specific and would require careful consideration if applied to other multiple inlet systems. Nevertheless, the approach appears to be robust and widely applicable.

Although the present work shows that, in fair-weather conditions, only Faro-Olhão tidal inlet imports sediment to the backbarrier, recent evolution of the system indicates rapid infilling rates and consequent narrowing of some inlets of the system. During storm events, or when increased wave activity is combined with flood currents, the inlets can import significant quantities of sand to the flood deltas. The amount imported

is thought to depend on the availability of sand offshore (i.e. on the ebb shoals and by the littoral drift). Despite the inlets' known capacity to redeposit sediments offshore under fair-weather conditions, net sediment influx can reduce the hydraulic efficiency of the channels. In this respect, if coupled with long-term quantification of ebb/flood delta volumes, the methodology presented here can be effectively used to calculate the medium- to long-term sediment budget. This has particular importance when attempting to understand sediment transport at inlet mouths, to quantify infilling rates and to define an optimal dredging volume. Together, these elements contribute to improving knowledge of inlet sediment dynamics, with broad application in a range of regional sediment management issues.

Appendix V.1: Estimation of critical flow conditions and bedload sediment transport

The critical Shields parameter, θ_{cr}, is defined as

$$\theta_{cr} = \frac{0.30}{1+1.2D_*} + 0.055[1-\exp(-0.020D_*)] \qquad \text{(V.A1)}$$

(Soulsby, 1997), with $D_* = (g(s-1)/\upsilon^2)^{1/3} d_{50}$, where s is the ratio of densities of grain and water (2.58) g is acceleration due to gravity (=9.81 m^2s^{-1}) and υ is the kinematic viscosity of water (=1.36x10^{-6} m^2s^{-1}).

The four bedload formulae used in the present study take the form

1) Yalin (1964)

$$\Phi = F_Y \theta_s^{0.5}(\theta_s - \theta_{cr}), \quad F_Y = 0.635/\theta_{cr}[1-(1/aT)\ln(1+aT)] \qquad \text{(V.A2)}$$

with $a = 2.45\theta_{cr}^{0.5} s^{-0.4}$ and $T = (\theta_S - \theta_{cr})/\theta_{cr}$

2) van Rijn (1984a)

$$\Phi = F_R\ \theta_s^{0.5}\left(\theta_s^{0.5} - \theta_{cr}^{0.5}\right)^{2.4},\quad F_R = (0.005/Cd^{1.7})(d/h)^{0.2} \tag{V.A3}$$

3) Madsen (1991)

$$\Phi = F_M(\theta_s^{0.5} - 0.7\theta_{cr}^{0.5})(\theta_s - \theta_{cr}),\ F_M = 8/\tan\phi_i \tag{V.A4}$$

where ϕ_i is the angle of grain repose in degrees.

4) Nielsen (1992)

$$\Phi = 12\ \theta_s^{0.5}\left(\theta_s - \theta_{cr}\right) \tag{V.A5}$$

Appendix V.2: Estimation of suspended sediment transport

Two equations used here to describe the vertical profile of suspended sediment, *C-Profile*, for current-only situations take a power law

$$C(z) = C_a(z/za)^{-b} \tag{V.A6}$$

and a parabolic (Rouse profile)

$$C(z) = C_a((z/za)(h - za/h - z))^{-b} \tag{V.A7}$$

form, where $C(z)$ is the suspended sediment concentration at height z, C_a is the reference concentration at height za, the exponent b is the Rouse number given by $b = w_s/(ku_*)$, where $u_* = (\tau_s/\rho)^{0.5}$. Values for C_a were obtained by taking the average of three different estimates of C_a from Smith and McLean (1977), van Rijn (1984b) and Zyserman and Fredsøe (1994).For natural sands the settling velocity is given by:

$$w_s = (\nu/d)[(10.36^2 + 1.049D_*^3)^{0.5} - 10.36] \tag{V.A8}$$

(Soulsby, 1997)

For combined waves plus currents situations the *C-Profile* was calculated using

$$C(z) = C_a\left(\frac{z}{za}\right)^{-b\max} \quad for\ za \le z \le z_w \tag{V.A9}$$

$$C(z) = C(z_w)\left(\frac{z}{za}\right)^{-bm} \quad for\ z_w < z \le h \tag{V.A10}$$

Soulsby (1997), where z_w is the wave boundary thickness, $z_w = (u_{*\max} T_s)/2\pi$, $u_{*\max}$ is the maximum bed friction velocity, T_s is the peak wave period, and $b_{\max}$ and b_m are the maximum and minimum Rouse numbers given by $b_{\max} = w_s / k u_{*\max}$ and $b_m = w_s / k u_{*m}$, where u_{*m} is the mean bed friction velocity. The values of u_{*m} and $u_{*\max}$ are given by $u_{*m} = (\tau_m / \rho)^{0.5}$ and $u_{*\max} = (\tau_{\max} / \rho)^{0.5}$, with $\tau_{\max}$ and τ_m as the maximum and mean bed shear-stress in a wave cycle. The values of $\tau_{\max}$ and τ_m were obtained from the ADV data, through the use of the analytical wave-current boundary layer model proposed by Fredsøe (1984).

V.7 REFERENCES

Andrade, C. F., 1990. O Ambiente Barreira da Ria Formosa, Algarve-Portugal. PhD Thesis, Universidade de Lisboa. 627p. (in Portuguese).

Balouin, Y., H. Howa, D. Michel. 2001. Construction of the swash platform associated with an ebb-tidal delta during fair weather conditions, The Barra Nova inlet, South Portugal. *J. Coast. Res*. 17, 4784–791.

Bettencourt, P., 1994. Les Environnements Sedimentaires de la Côte Sotavento (Algarve, Sud Portugal) et leur Évolution Holocéne et Actuelle. University Bordeaux I. 130p. (in French).

Bishop, C.T., Donelan, M.A., 1987. Measuring waves with pressure transducers. *Coastal Engineering* 11, 309–328.

Blott, S.J., Pye, K., 2001. GRADISTAT: a grain size distribution and statistics package for the analysis of unconsolidated sediments. *Earth Surf. Process. Landf.* 26, 1237-1248.

Costa, M., Silva, R., Vitorino, J., 2001. Contribuição para o estudo do clima de agitação marítima na costa Portuguesa. 2as Jornadas Portuguesas de Engenharia Costeira e Portuária in CD-ROM (in Portuguese).

Dyer, K.R., 1986. *Coastal and Estuarine Sediment Dynamics*. Wiley-Interscience, New York, 342p.

Elias, E.P.L., van der Spek, A.J.F., 2006. Long-term morphodynamic evolution of Texel Inlet and its ebb-tidal inlet (The Netherlands). *Mar. Geol.* 225, 5-21.

FitzGerald, D.M., 1996. Geomorphic Variability and Morphologic and Sedimentologic Controls on Tidal Inlets. *J. Coast. Res.* SI 23, 47-71.

FitzGerald, D.M., Kraus, N.C., Hands, E.B., 2001. Natural Mechanisms of Sediment Bypassing at Tidal Inlets. ERDC/CHL CHETN-IV-30, U.S. Army Enginner Research and Development Center, Vicksburg, MS., 10p.

Folk, R.L., Ward, W.C., 1957. Brazos River bar: a study in significance of grain size parameters. *J. Sediment. Petrol.* 27, 3-26.

Fredsøe, J., 1984. Turbulent boundary layer in wave-current motion. *J. Hydraul. Eng.* ASCE, 110, 1103-20.

Goring, D.G., Nikora, V.I., 2002. Despiking Acoustic Doppler Velocimeter Data, *J. Hydraul. Eng.* 128(1), 117-126.

Hayes, M.O., 1979. Barrier island morphology as a function of tidal and wave regime. In Leatherman, S.P., (Ed.), Barrier Islands: From the Gulf of St. Lawrence to the Gulf of Mexico. Academic Press, New York, N.Y., 1-27.

Houwman, K.T., van Rijn, L.C., 1999. Flow resistance in the coastal zone. *Coastal Eng*., 38, 261-73.

Kana, T.W., Stevens, F.D., 1992. Coastal Geomorphology and Sand Budgets Applied to Beach Nourishment. Proc. Coastal Engineering Practice '92, ASCE, VA, 29-44.

Kana, T.W., Hayter, E.J., Work, P.A., 1999. Mesoscale sediment transport at southeastern U.S. tidal inlets: conceptual model applicable to mixed energy settings. *J. Coast. Res.* 15(2), 303-13.

Madsen, O.S., 1991. Mechanics of cohesionless sediment transport in coastal waters. *Proc., Coastal Sediments*, ASCE, 15–27.

Morris , B.D., Davidson, M.A., Huntley, D.A., 2001. Measurements of the response of a coastal inlet using video monitoring techniques. *Mar. Geol*. 175, 251-72.

Morris, B.D., Davidson, M.A., Huntley, D.A., 2004. Estimates of the seasonal morphological evolution of the Barra Nova Inlet using video techniques. *Cont. Shelf. Res.* 24, 263-78.

Nielsen, I., 1992. Coastal Bottom Boundary Layers and Sediment Transport. World Scientific Publishing, Singapore, Advanced Series on Ocean Engineering, vol.4.

Oertel, G.F., 1972. Sediment transport on estuary entrance shoals and the formation of swash platforms. *J. Sediment. Petrol*. 42, 858–68.

Pacheco, A., Vila-Concejo, A., Ferreira Ó., Dias, J.A., 2008. Assessment of Tidal Inlet Evolution and Stability Using Sediment Budget Computations and Hydraulic Parameter Analysis. *Mar. Geol.* 247, 104-127.

Pacheco, A., Ferreira, Ó., Williams, J.J., Garel, E., Vila-Concejo, A., Dias, J.A., 2010. Hydrodynamics and Evolution of a Multiple-Inlet System. *Mar. Geol.* 274, 32-42.

Roelvink, J.A. Reniers A., van Dongeren, A., de Vries, J., McCall, R., Lescinski, J., 2009. Modeling storm impacts on beaches, dunes and barrier islands. Coastal Eng., 56(11-12), 1133-1152.

Rosati, J.D., Kraus, N.C., 1999. "Formulation of Sediment Budgets at Inlets". *Coast. Eng. Tech*. Note IV-15, 20p.

Rosati, J.D., 2005. Concepts in Sediment Budgets. *J. Coast. Res*. 21 (2), 307-322.

Salles, P., 2001. Hydrodynamic Controls on Multiple Tidal Inlet Persistence. PhD Thesis, Massachusetts Institute of Technology and Woods Hole Oceanographic Institution, 272 pp.

Salles, P., Voulgaris, G., Aubrey, D., 2005. Contribution of nonlinear mechanisms in the persistence of multiple tidal inlet systems. *Estuar. Coast. Shelf. Sci.* 65, 475-491.

Smith, J.D., McLean, S.R., 1977. Spatially averaged flow over a wavy surface. *J. Geophys. Res*., 82(12), 1735-46.

Soulsby, R.L., 1997. *Dynamics of marine sands. A manual for practical applications*. HR Wallingford Report SR 466, 142p.

Soulsby, R.L., Humphery, J.D., 1990. Field observations of wave-current interaction at the sea bed, in Water Wave Kinematics, eds A.Tørum and O.T.Gudmestad. Kluwer Academic Publishers, Dordrecht., 413-28.

Stapleton, R.L., Huntley, D.A., 1995. Seabed stress determination using the inertia dissipation method and turbulent kinetic energy method. *Earth Surf. Process. Landf.* 20, 807-815.

Tucker, M.J., Pitt, E.G., 2001. *Waves in Ocean Engineering*. Elsevier Ocean Engineering Book Series, Volume 5, Elsevier, Amsterdam, 521p.

van Rijn, L.C., 1984a. Sediment Transport, Part I: Bed Load Transport, *J. Hydraul. Eng*. 110(11), 1431-56.

van Rijn, L.C., 1984b. Sediment Transport, Part II: Suspended Load Transport, *J. Hydraul. Eng*. 110(11), 1613-41.

van Rijn, L.C. 1993. *Principles of Sediment Transport in Rivers, Estuaries and Coastal Seas*, Aqua Publications, Amsterdam, 614p.

van Rijn, L.C., 2007a. United view of sediment transport by currents and waves I: Initiation of motion, Bed roughness and Bed load transport. *J. Hydraul. Eng*,, ASCE, Vol. 133, No. 6, p. 649-667.

Vila-Concejo, A., Matias, A., Ferreira, Ó., Duarte, C., Dias, J.A., 2002. Recent Evolution of the Natural Inlets of a Barrier Island System in Southern Portugal. *J. Coast. Res*. SI 36, 741-752.

Vila-Concejo, A., Ferreira, Ó., Matias, A., Morris, B.D., Dias, J.A., 2004. "Lessons from inlet relocation: examples from Southern Portugal". *Coast. Eng.* 51 (10), 967-990.

Williams, J.J., Bell, P.S., Thorne, P.D., 2003a. Field measurements of flow fields and sediment transport above mobile beds. *J. Geophy. Res.* 108, NO. C4, 3109, doi:10.1029/2002JC001336.

Williams, J.J., O'Connor, B.A.O., Arens, S.M., Abadie, S., Bell, P., Balouin, Y., Van Boxel, J.H., do Carmo, A.J., Davidson, M., Ferreira, Ó., Heron, M., Howa, H., Hughes, Z., Kaczmarec, L.M., Kim, H., Morris, B., Nicholson, J., Pan, S., Salles, P., Silva, A., Smith, J., Soares, C., Vila-Concejo, A., 2003b. Tidal inlet function: field evidence and numerical simulation in the INDIA project. *J. Coast. Res*. 19(1), 189-211.

Yalin, M.S., 1964. Geometrical properties of sand waves. *J. Hydraul. Div.*, *Proc. ASCE*, 90 (HY5), 105-19.

Zyserman, J.A., Fredsøe, J., 1994. Data analysis of bed concentration of sediment. *J. Hydraul. Eng.* ASCE, 120(9), 1021-42.

CHAPTER VI

Long-term morphological impacts of the opening of a new inlet on a multiple inlet system

Abstract

In this study, the artificial opening of a new tidal inlet in an existing multiple inlet system is shown to significantly modify the adjacent nearshore and backbarrier morphology, as well as both updrift and downdrift shorelines. The study focuses on the dominant Faro-Olhão and Armona inlets in the Ria Formosa barrier island system of southern Portugal. The equilibrium state and future evolution of the system are inferred using a range of morphological and hydrodynamic indicators, including the evolution of the inlet cross-section, changes in tidal prism, and changes in the dimensions (length and area) of barrier islands. The results reveal how the morphology of an inter-connected two-inlet bay system and the adjacent coastlines have evolved following the artificial opening and stabilisation of Faro-Olhão inlet since 1929. A clear relationship between barrier island size, inlet cross-section/width, and tidal prism is demonstrated. Decadal time-scale changes in the tidal prism of the two inter-connected inlets are shown to be the main mechanism responsible for morphological change, and have resulted in the remobilisation of ebb-tidal delta sediments deposited during previous hydraulic configurations. These changes, in turn, have contributed to a narrowing of Armona inlet and an increase in the size of Culatra Island. The work highlights the importance of ebb-tidal deltas both as sand reservoirs and as conduits through which sand exchange between estuaries or lagoons and the open coast is regulated. It also shows the pivotal role of ebb-tidal deltas in trapping longshore-transported sediment and releasing it again during periods of increased wave activity. The findings have implications regarding the accurate assessment of the stability of multiple inlet systems.

Keywords: *ebb-tidal delta*, *tidal inlets*, *dynamic stability*, *Ria Formosa*, *Portugal*

VI.I INTRODUCTION

Given the dynamic nature of coastal barrier-inlet systems, changes occurring at one location due to natural processes or to anthropogenic activities frequently result in complex positive and negative feedbacks in sedimentary transport systems, which in turn bring about responses in one or more barrier-inlet elements. For example, once a new inlet is opened, its long-term evolution (over decadal time-scales) depends on the competing effects of waves and tidal currents that act to either close or widen the inlet, respectively (Swart and Zimmerman, 2009). Morphological changes in the areas adjacent to the new inlet take place over many years or even centuries and may extend far along the coast. In a multiple tidal inlet system, morphological adaptation to changes in hydrodynamic forcing and/or sediment supply is frequently profound and results in both short- and long-term impacts on water circulation and sediment transport through other inlets in the system.

When a new inlet is opened, sand is excluded from the longshore transport system and stored in an evolving ebb-tidal delta which attains an equilibrium volume after some time (Walton and Adams, 1976). Once the equilibrium volume is attained, sediment moving alongshore can then bypass the inlet by a variety of mechanisms. Until that condition is reached, it is expected that the downdrift shoreline will erode. Ebb-tidal deltas therefore have a significant impact on the downdrift coastal sedimentary budget, acting as 'valves' for the coastal sedimentary supply by regulating the sand exchange between estuaries or lagoons and the open coast, and also by trapping the alongshore-transported sediment (Hicks and Hume, 1997).

If the tidal prism is reduced at another inlet, the ebb-tidal currents will decrease in velocity and lead to a reduction in sediment supply to the ebb delta. As a result, the ebb-delta will erode (Dean, 1988). At the same time, the reduced ebb-tidal flow velocity

promotes more effective wave action and flood-tidal currents which act together to move ebb-delta sand onshore (Cleary and FitzGerald, 2003) in a process termed ebb shoal collapse (Kraus, 2006). This process results in the onshore migration of part of, or the entire, ebb shoal (Hansen and Knowles, 1988; Pope, 1991). The shape of the surface of the ebb-tidal delta also plays an important role in determining how wave energy is focused on adjacent coastal beaches and how waves propagate into the inlet. It therefore influences shoreline evolution along adjacent beaches and within the inlet (Buonaiauto and Kraus, 2003).

The objectives of this paper are to: (1) evaluate the morphological response of the coastline to the opening and stabilisation of an inlet in a multiple inlet system, where the inlet becomes the main inlet of the system; and (2) relate those changes to the inlet cross-section and tidal prism redistributions until a new system equilibrium is reached. The case study presented herein concerns the two main inlets of the Ria Formosa Barrier Island System: Faro-Olhão and Armona. The dataset couples the evolution of the inlet cross-section, changes in tidal prism, and changes in the dimensions (length and area) of barrier islands to give a regional perspective on the impacts that human intervention have had on the system. Specifically, the paper relates changes in the size of Culatra Island to the evolution of the cross-section of Faro-Olhão inlet towards equilibrium and to the narrowing of Armona inlet.

VI.2 STUDY AREA

VI.2.1 General characteristics

The Ria Formosa is a multi-inlet barrier system located in southern Portugal (Fig. VI.1A). It comprises five islands, two peninsulas separated by six tidal inlets, salt

marshes, sand flats and a complex network of tidal channels, covering an area of $8.4x10^7$ m^2 (Andrade, 1990).

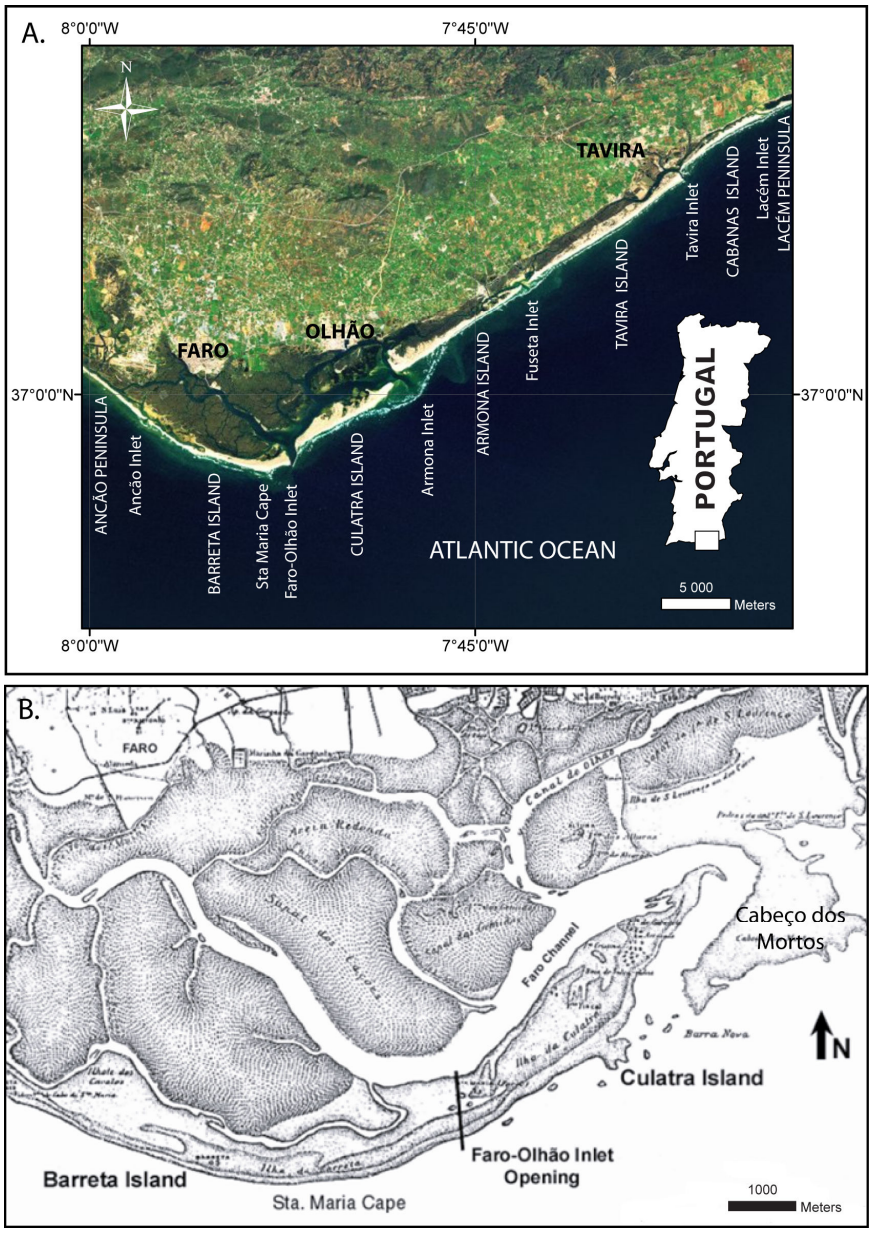

Figure VI.1 (A) Study area comprising the Ria Formosa multiple inlet system, southern Portugal (Google Earth, aerial photo from 2006). (B) Detail of the location of the artificially-opened Faro-Olhão Inlet (prior to opening, superimposed on a 1923 map, adapted from Esaguy, 1986).

The tides in the area are semi-diurnal with typical average astronomical ranges of 2.8 m for spring tides and 1.3 m for neap tides. A maximum tidal range of 3.5 m can be reached during equinoctial tides, and over 3.8 m with surge setup. Wave climate in the

area is moderate (an offshore annual mean significant wave height of H_s ~1 m and peak period, T_p, of 8.2 s, with storms characterized by H_s >3 m). Approximately 71 % of waves approach from the W-SW, with about 23 % coming from E-SE (Costa et al., 2001). The cuspate shape of the Ria Formosa system produces two areas differentiated in terms of exposure to wave action. The western flank, which is exposed to the dominant SW waves, is more energetic, while the eastern flank is directly exposed only to SE ('*Levante*') waves. Longshore currents in the area are from W to E. Littoral drift net values obtained by several authors (*see* Bettencourt, 1994) range from c. $1.0x10^5$ - $3.0x10^5$ m^3/year and c. $0.4x10^5$ - $1.5x10^5$ m^3/year, for the western and eastern flanks, respectively.

VI.2.2 Impacts of recent human intervention on the system

Faro-Olhão inlet, the main inlet of the Ria Formosa system, was artificially opened in 1929 at the location of the old Bispo inlet (Fig VI.1B), approximately 2 km E of Cape Santa Maria. Faro-Olhão inlet has subsequently been enlarged and stabilised, and its impact on the barrier island system and lagoon hydrodynamics has been very significant (Andrade, 1990). The most significant of these effects include a drastic reduction in the downdrift sediment budget, and a reduction in the width of Armona inlet (Salles, 2001). Sediment budget analysis by Pacheco et al., (2008) shows that the development of Faro-Olhão inlet has occurred in three phases (Fig. VI.2): (1) an initial phase of sediment retention (1929-1962), when the inlet started to capture longshore-transported sediment in order to build ebb and flood deltas, and the channel deepened as it evolved to achieve an equilibrium cross-section; (2) an intermediate stage (1962-1978), during which time both deltas accumulated sediments at approximately the same rate and major modifications occurred in both barriers, with Barreta Island accreting significantly and

further inlet scouring occurred; and (3) a recent stage (1978-2001), characterised by the evolution of both coastlines in response to the inlet's presence and by drastic intensification of scouring of the inlet gorge. The strong ebb-tidal currents from this inlet act as an effective barrier to longshore sediment transport, which enhances sand capture updrift of the western jetty, as enhances the retention capacity of the entire submarine strip between the beach and the breaker zone (Andrade, 1990; Pacheco et al., 2008).

Armona inlet is the oldest inlet of the system and was the main inlet of the system prior to the artificial opening of Faro-Olhão inlet, having maintained its present position for several centuries (Esaguy, 1984; Andrade, 1990; Salles, 2001, Fig. VI.3). Although its location is still stable, the inlet has become narrower after the construction of jetties at Faro-Olhão inlet (Fig. VI.2). The source of sediments contributing to this narrowing has been subject to some speculation, with hypotheses including: (1) bypassing of littoral drift through Faro-Olhão inlet; (2) sediment eroded from Culatra Island, immediately downdrift of Faro-Olhão inlet; and (3) local supply from the large ebb-tidal deltas of Armona inlet, which extend 1,500 m offshore. In a sediment budget analysis for Faro-Olhão inlet, Pacheco et al. (2008) showed that no significant inlet bypassing occurred, due principally to an increase in channel scouring. A further contributory factor concerns the location of the outer bar of the ebb-tidal delta in 8-10 m water depth. Pacheco et al. (2008) also showed that the amount of erosion occurring on the western half of Culatra Island is one order of magnitude lower than that measured along the eastern part of the island (Garcia et al., 2002). This evidence is sufficient to refute hypotheses 1 and 2 and, given the retreat of Armona inlet's deltas in response to tidal prism loss (Salles, 2001), hypothesis 3 may be a more likely explanation.

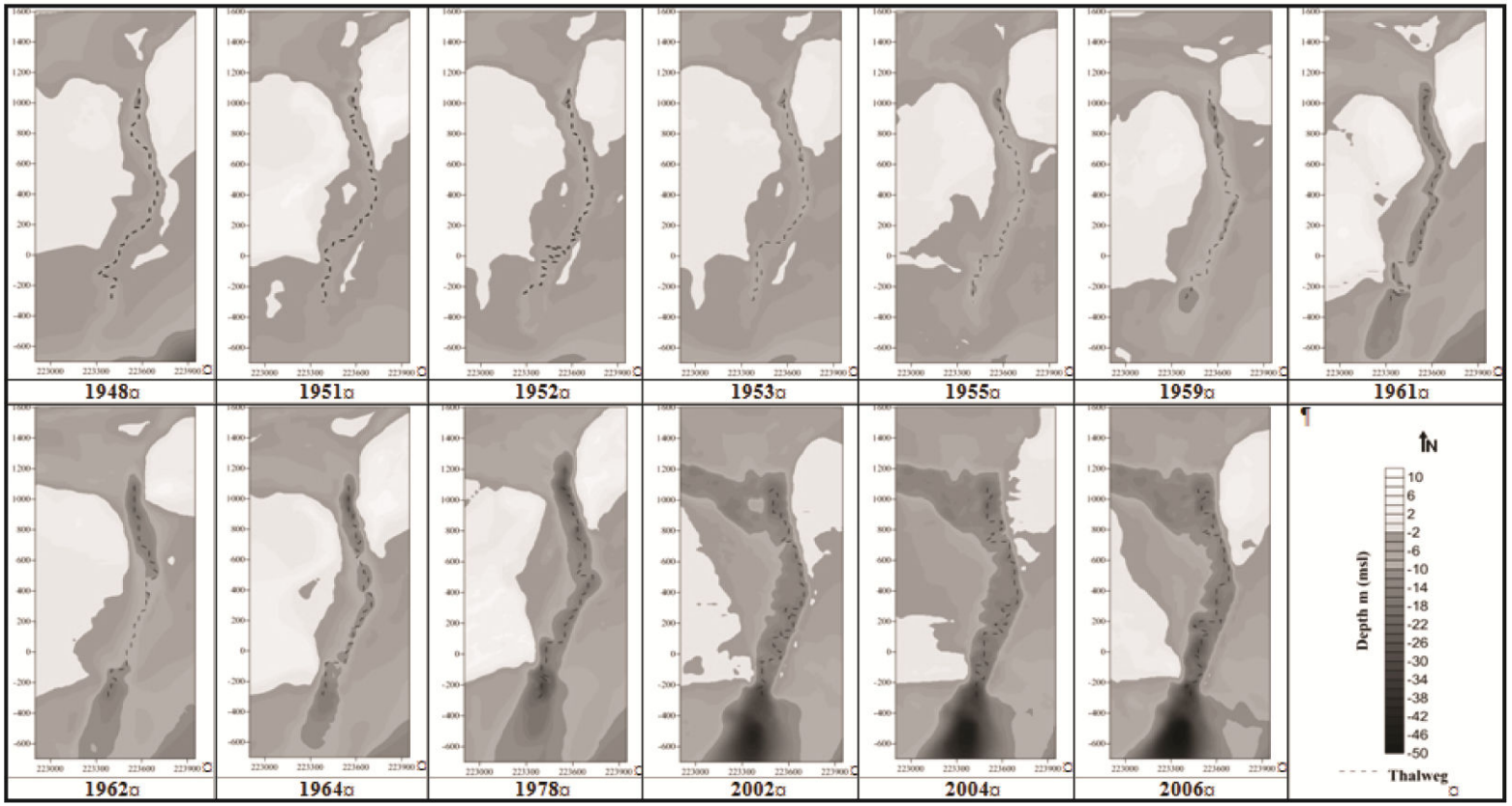

Figure VI.2 Faro-Olhão Inlet channel evolution from 1948-2006. Co-ordinate system: Datum 73, Portuguese Military Grid.

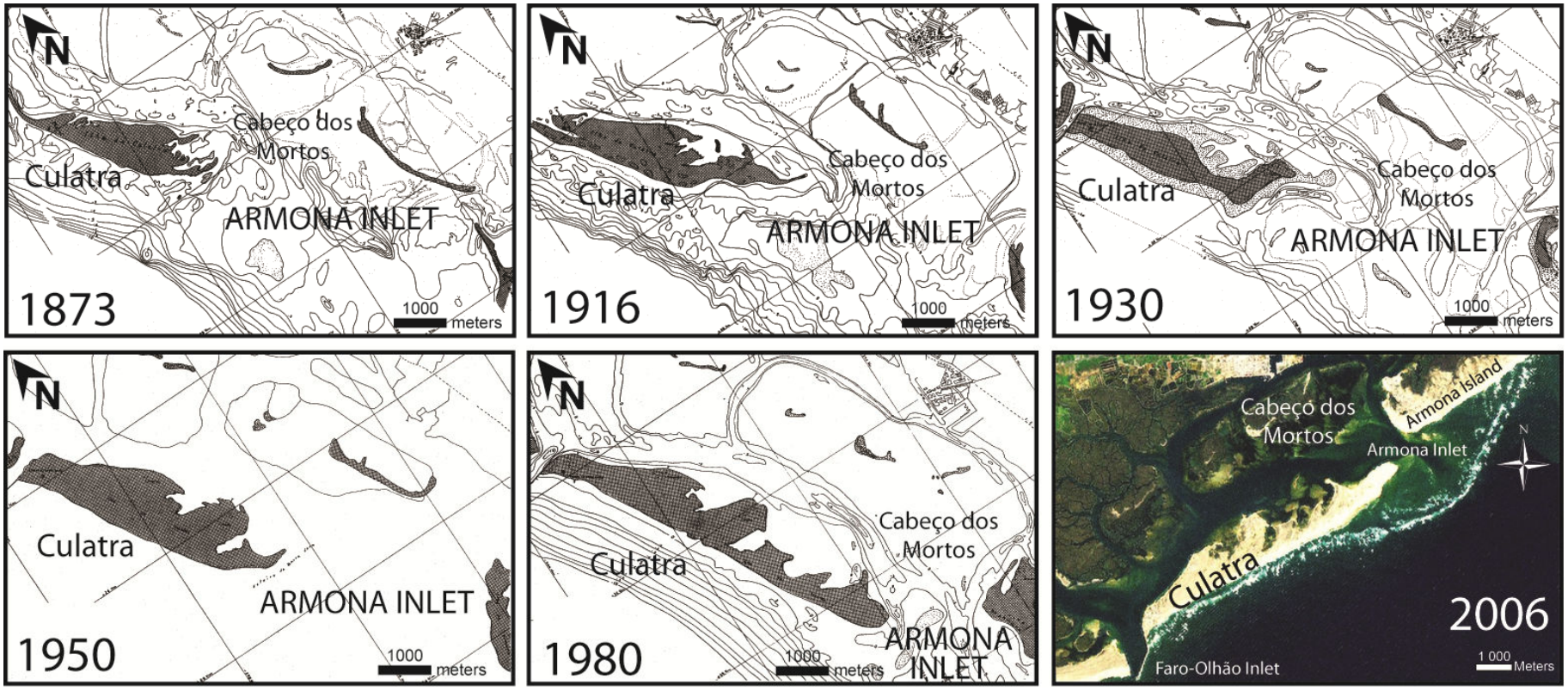

Figure VI.3. Armona Inlet evolution 1873-2006 (adapted from Esaguy, 1984).

VI.2.3 Recent hydrodynamic behaviour

Measurements of the tidal prism obtained for each inlet of the Ria Formosa reveal a clear circulation pattern between Faro-Olhão and Armona inlets (*cf.* Pacheco et al., 2010). The two inlets present ebb-dominated behaviour from a conventional viewpoint (i.e., higher mean ebb velocity is associated with shorter ebb duration). However, at Faro-Olhão inlet, the flood prism is considerably greater than the ebb prism. The sediment transport direction is strongly landward directed as evidenced by the regular dredging operations required to maintain channel navigability (*c.*140,000 m^3/year, Pacheco et al., 2008). In contrast, Armona inlet is always ebb-dominant and capable of flushing sediment seaward under fair-weather conditions, especially during spring tides. These two major inlets represent almost 90% of the total prism of the Ria Formosa system.

The interconnection between both inlets is particular active during spring tides, but is reduced during neap-tides when the inlets drain the basin more independently (Pacheco et al., 2010). Despite the capacity of ebb tidal currents at Armona inlet for flushing sediments offshore, the influx of sand originating from the large ebb-tidal deltas developed during past hydraulic configurations will ultimately dictate whether both interconnected inlets will remain open (Pacheco et al., 2010).

VI.3 METHODS

VI.3.1 The Evolution of Faro-Olhão Inlet

Digital terrain models of Faro-Olhão inlet were obtained from 14 bathymetric charts from the period 1948 to 2006. In order to analyse the evolution of the inlet channel, 107 cross-sectional profiles below mean sea level (MSL) were obtained at intervals along the inlet channel, with 25 of these being considered representative of the minimum

cross-section at the inlet gorge, i.e., the area of flow confinement at the jetties (Fig. VI.4A). Parameters such as minimum cross-section area (A_c), average channel cross-section (A_{avg}), mean channel depth (h_c), channel length (L_c) and hydraulic radius (R_H) were determined, following the recommendations of the *Coastal Engineering Manual* (Seabergh et al., 2006).

Considering inlet stability, Escoffier (1940, 1977) established the hydraulic relationship between the cross-sectional area of an inlet and the maximum spatially averaged cross-section velocity flow in an inlet during a tidal cycle to produce a stability curve. To obtain a stability curve for Faro-Olhão inlet, the maximum velocity (U_m) was estimated using the analytical method of Keulegan (1967) in the form:

$$K = (T / 2\pi a_0)(A_c / A_B)(2ga_0 / F)^{0.5} \quad \text{(VI.1)}$$

where K is a dimensionless parameter (termed the repletion coefficient), T is the tidal period, a_0 is the ocean tidal amplitude, A_c is the inlet cross-section area, A_B is the lagoon surface area, g is the acceleration of gravity, and F is the inlet impedance given by $F = k_{en} + k_{ex} + (2gn^2 L_c / h_c^{4/3})$, where k_{en} is the entrance loss coefficient, k_{ex} is the exit loss coefficient, n is the Manning coefficient, h_c is the mean channel depth, and L_c is the effective channel length. Here, hypsometric effects are ignored, so A_B, A_c, and R_H are constants. Keulegan (1967) established relationships between K and the following parameters: (i) the ratio of bay to ocean tidal amplitude (a_b / a_0); (ii) the tidal phase lag (ε); and (iii) the dimensionless maximum velocity (U_m'). The maximum velocity (U_m) through an inlet is related to U_m' as follows:

$$U_m = (U_m')(\sigma a_0)(A_B / A_c) \tag{VI.2}$$

where $\sigma = 2\pi / T$.

Keulegan's K can be related to ϕ parameters defined by the linear theory (Dean and Dalrymple, 2002):

$$K = \frac{\phi_2}{\phi_1^{0.5}(\phi_1^2 + \phi_2^2)^{1/4}} \tag{VI.3}$$

where the ϕ_2 dimensionless parameter is defined as:

$$\phi_2 = \frac{gA_c}{\sigma^2 A_B L_c} \tag{VI.4}$$

and ϕ_1 is derived from Eq. VI.3, with K and ϕ_2 first calculated from their definitions (Eq. VI.1 and VI.4). Then U_m is solved using the linear method:

$$U_m = \frac{2\phi_1 C_1 \sigma}{F} \tag{VI.5}$$

The values of K and U_m were computed using the linear theory approach (Dean and Dalrymple, 2002) to Keulegan (1967) and were used to generate the stability curve for Faro-Olhão inlet. Here the stability curve is interpolated and together with estimates of the equilibrium velocity (U_e), a sedimentary stability criterion derived from commonly used formulae is added for relating the tidal prism to cross-sectional area for dual jetties (Jarret, 1976). In this approach, the peak velocity U_m occurs at a critical value of A_c; if the actual A_c value is higher than the critical A_c value, the inlet is classified as being stable. The stability curve intersects U_e at two points. The point *a* is

in the unstable region, meaning that if A_c decreases then the inlet will close, i.e., the tidal flow through the inlet A_c is incapable of flushing incoming sediments; the point *b* located in the stable region means that any changes in A_c will promote velocity changes that will bring the A_c back to equilibrium.

VI.3.2 Evolution of Culatra Island

The evolution of Culatra Island was determined using measurements from aerial photos taken between 1947 and 2009. Sets of aerial photographs (Table VI.1) were geo-referenced using GIS software, and parameters such as total barrier island area and length were obtained for each available year. For consistency the high tide mark, clearly indicated by a strand line, was selected to identify the coastline position. Island length was measured between the point of attachment of Faro-Olhão inlet's eastern jetty and the most eastern dune crest. Using widely reported methods (e.g. Kraus and Rosati, 1998; Rosati, 2005), the mean and maximum errors in estimates of island area and length were calculated to be 10 % and 25 %, respectively (Pacheco et al., 2008).

VI.3.3 Evolution of Armona Inlet

Only three bathymetric maps were available for Armona inlet (1978, 1983, and 2004), and thus the methods applied to Faro-Olhão inlet could not be used in this case. Further, measured bathymetry only covered the navigable channel, thereby excluding important morphological features such as the ebb-tidal delta. The evolution of the inlet width was therefore obtained using a combination of available historical reports, aerial photography, and bathymetric charts (Table VI.1). Owing to data limitations, inlet width at MSL was estimated using a single cross-sectional transect located between the barrier islands at the location of minimum cross-section. In cases where aerial photography was

available, inlet width was also obtained at the minimum cross-section between the high tide marks, from one barrier to the other. The uncertainty on the inlet width measurements is related to errors on the geo-referencing process (±0.2 mm) and to errors in horizontal position from digitising the inlet width transect (±0.5 mm), which correspond to ±1.6 m and ±3.2 m, respectively, for 1:8000 scale aerial photography.

Table VI.1. Data and methods used to evaluate Culatra Island (area and length) evolution and Armona Inlet (width) evolution

Culatra Island			
Year	**Source**	**Area (m^2)**	**Length (m)**
1947	Aerial photography	2,851,970	4,530
1958	Aerial photography	3,028,904	4,800
1976	Aerial photography	3,225,772	5,500
1985	Aerial photography	3,303,086	5,979
2002	Orthophotomap	3,956,501	6,860
2005	Orthophotomap	3,958,788	7,077
2009	DTM Lidar Survey	3,772,941	7,020
Armona Inlet			
Year	**Source**	**Method**	**Width (m)**
1873	Esaguy, 1984	Bathymetry, MSL limits at inlet minimum A_c	4,300
1916	Esaguy, 1984	Bathymetry, MSL limits at inlet minimum A_c	3,850
1930	Esaguy, 1984	Bathymetry, MSL limits at Inlet minimum A_c	3,450
1950	Esaguy, 1984	Bathymetry, MSL limits at inlet minimum A_c	3,400
1958	Aerial Photography	Limits between high tide mark at inlet minimum A_c	2,700
1973	Esaguy, 1984	Bathymetry, MSL limits at inlet minimum A_c	2,000
1976	Bathymetry Survey	Bathymetry, MSL limits at inlet minimum A_c	1,575
1985	Aerial Photography	Limits between high tide mark at inlet minimum A_c	1,850
2002	Orthophotomap	Limits between high tide mark at inlet minimum A_c	640
2005	Bathymetry Survey	Bathymetry, MSL limits at inlet minimum A_c	610
2009	DTM Lidar Survey	MSL limits at inlet minimum A_c	610

VI.3.4 Data integration and analysis

In order to better assess the impact of opening Faro-Olhão inlet on Armona inlet, the A_c / P analysis described above required extending to include both inlets. However, the

analysis is limited by the data available, especially the lack of complete bathymetric charts of Armona inlet and its ebb tidal delta. This limitation prevents computation of Armona inlet's Escoffier curve and the evaluation of equilibrium areas.

In order to better understand the dynamics of Faro-Olhão inlet, its relationship to the temporal changes in tidal prism, the narrowing of Armona inlet, and the expansion of Culatra Island, historical changes in spring tidal prism for both inlets were obtained using three approaches/sources: numerical model output (ICN, 1999; Silva et al., 2002); empirical formulations (Andrade, 1990); and field data (Pacheco et al., 2010). Values for Faro-Olhão inlet cross-section, Culatra Island area, and Armona inlet width were linearly interpolated through time, and a relationship established between Faro-Olhão inlet cross-section and Armona inlet width and between Culatra Island area and Armona inlet width.

VI.4 RESULTS

The opening of Faro-Olhão inlet, its stabilisation by jetties, and the evolution of the channel towards equilibrium occurred between the end of engineering works in 1955 and the mid 1980s, when both channel (Fig. VI.4B) and minimum cross-section values stabilised (Fig. VI.4C). Despite the fact that the channel and minimum A_c values reached stability, there was an increase in scouring activity offshore. This is revealed by the digital terrain models (DTMs) from 2002, 2004, and 2006 (Fig. VI.2). Escoffier's curve (Fig. VI.5), produced using available hydrodynamic data (Table VI.2), shows that the inlet reached stability with respect to both hydrodynamic and sedimentary criteria. The minimum cross-section of Faro-Olhão inlet in 2006 lay in the stable region of the curve, on the right side of the inflexion point given by the critical A_c value (i.e., maximum U_m). This value coincides almost exactly with the stable root point, where

$U_m \sim U_e$. This evidence strongly suggests that the inlet is now stable in a morphodynamic sense.

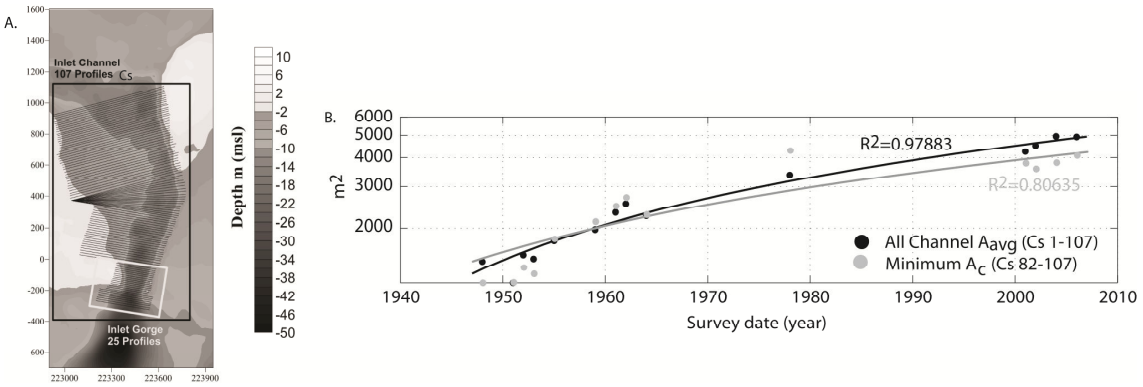

Figure VI.4. (A) Location of channel profiles measured and analyzed (B) channel evolution and (C) minimum cross-sectional evolution of Faro-Olhão Inlet from 1948-2006. Co-ordinate system: Datum 73, Portuguese Military Grid.

Figure VI.5. Escoffier's Curve (*sensu* Escoffier, 1977) for Faro-Olhão Inlet, where U_m is given by the linear approach (from Dean and Dalrymple, 2002) and U_e is from Jarret (1976).

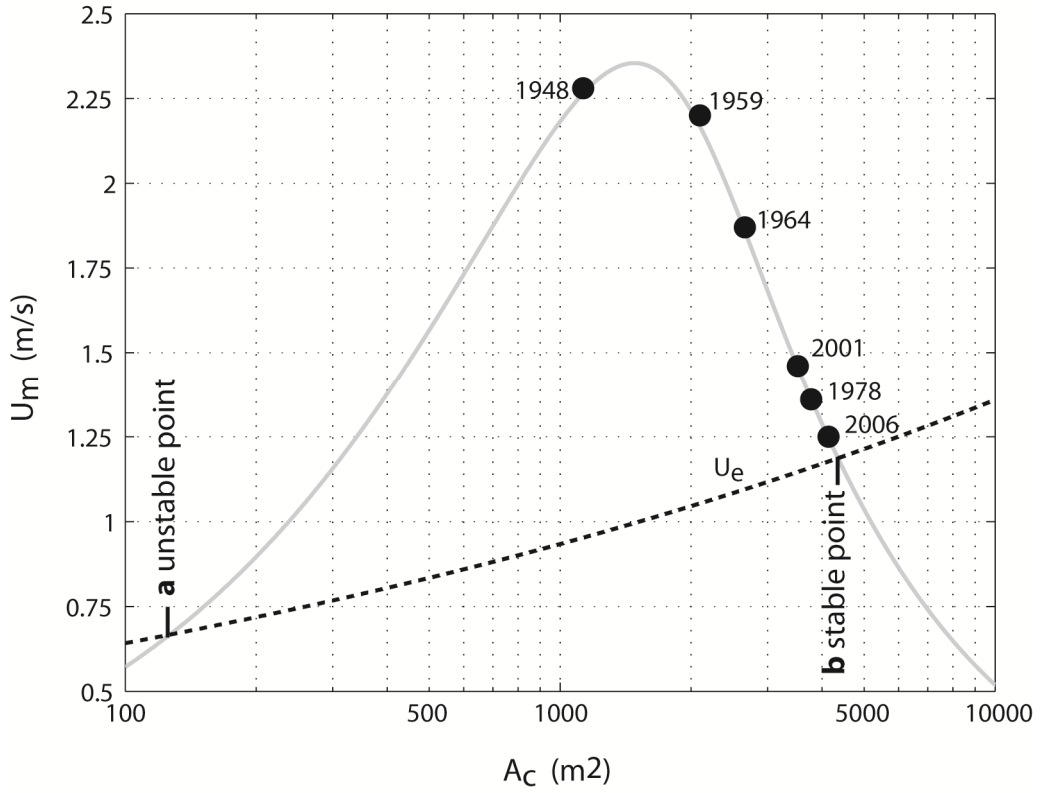

Table VI.2. Parameters used in the linear method (Dean and Dalrymple, 2002) approach to Keulegan (1967) for establishing an Escoffier (1977) curve for Faro-Olhão Inlet.

Hydraulic Criteria														
	1948	**1951**	**1952**	**1953**	**1955**	**1959**	**1961**	**1962**	**1964**	**1978**	**2001**	**2002**	**2004**	**2006**
A_c (m^2)	1146	1130	1333	1254	1813	2096	2423	2661	2215	4139	3772	3519	3780	4044
h_c (m)	-3.68	-3.61	-4.26	-4.04	-5.75	-6.68	-7.62	-8.48	-6.70	-13.05	-11.09	-10.42	-11.18	-11.86
L_c (m)	1937	1921	2371	1853	1901	1876	2111	1793	1855	2094	2000	2391	2381	2264
R_h	3.78	3.72	4.39	4.13	5.98	6.91	7.99	8.77	7.30	13.64	12.27	11.60	12.46	13.33
K	0.57	0.56	0.66	0.66	1.08	1.32	1.53	1.80	1.42	3.00	2.66	2.42	2.64	2.89
U_{max} (m/s)	2.38	2.38	2.31	2.44	2.35	2.20	2.00	1.87	2.14	1.25	1.38	1.46	1.36	1.28
a_b/a_0	0.52	0.52	0.59	0.59	0.82	0.89	0.93	0.96	0.91	0.99	0.99	0.99	0.99	0.99
General terms														
Manning's n = 0.016														
Entrance energy loss coefficient k_{en} = 0.25														
Exit energy loss coefficient k_{ex} = 1														
Tidal period (s) = 44,640														
Acceleration due to gravity (ms^{-2}) = 9.81														
Measured Tidal Prism (m^3) in 2006 (ADCP spring-tide flood prism) = 6.64E+07														
Ocean Spring Amplitude (m) = 1.25														
Bay Spring Amplitude (m) = 1.125														
A_b (m^2) = 2.9511E+07														

In the period from the opening of Faro-Olhão inlet to the present day, the length of Culatra Island has almost doubled (Table VI.1, Fig. VI.6). During this period, the length of the island increased by an average of *c.* 40 m/year, and its area by an average of *c.* 14,900 m^2/year. Values of Faro-Olhão inlet cross-section (A_c), Culatra Island area (A), and Armona inlet width (W) are presented in Fig. VI.7. Faro-Inlet minimum A_c changed significantly to about 1980, but since that time has presented a relatively stable value. However, Culatra Island continued increasing its dimensions (Table VI.1), while Armona inlet continued narrowing. Considering all the available data (from 1873 to 2009, Table VI.2), the rate at which Armona inlet has narrowed is approximately 30 m/year. Before the opening and stabilisation of Faro-Olhão Inlet (1873-1958), Armona inlet narrowed *c.* 20 m/year; this increased to *c.* 43 m/year after the engineering works had finished (1958-2009).

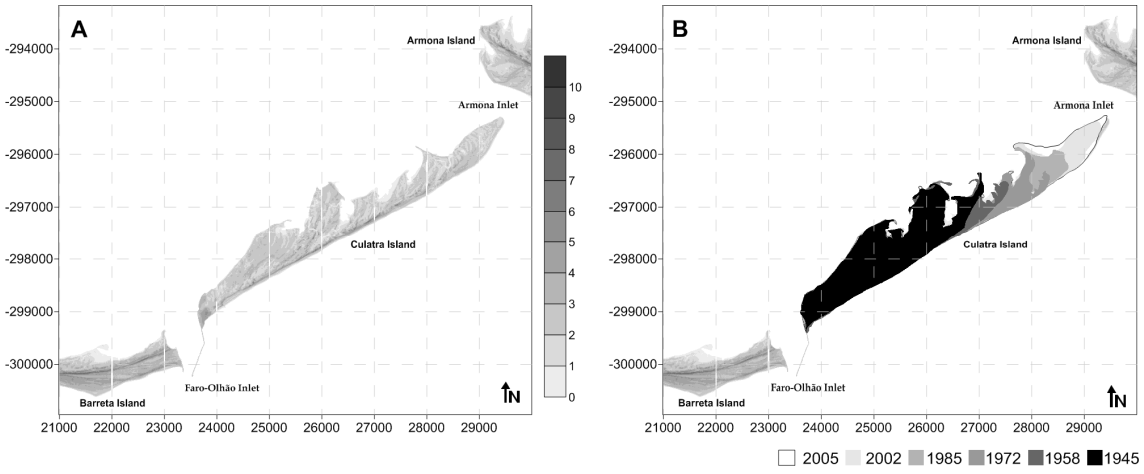

Figure VI.6. (A) Digital Terrain Models of Culatra Island (Lidar Survey, November 2009). (B) Culatra Island evolution from 1947-2009.

There appears to be an obvious relationship between the narrowing of Armona inlet, the cross-sectional increase of Faro-Olhão inlet, and the increase in size of Culatra Island. In order to examine the relationships further, the three datasets (Armona, Faro-

Olhão, and Culatra) were interpolated between equivalent periods, on which basis two relationships were established: (1) A_c versus W; and (2) A versus W (Fig. VI.8). The two curves show similar trends, with R^2 values of 0.76 and 0.91, respectively. Both relationships present an exponential behaviour from the mid-1980s to the present, coincident with increased scouring in the submarine gorge of Faro-Olhão inlet.

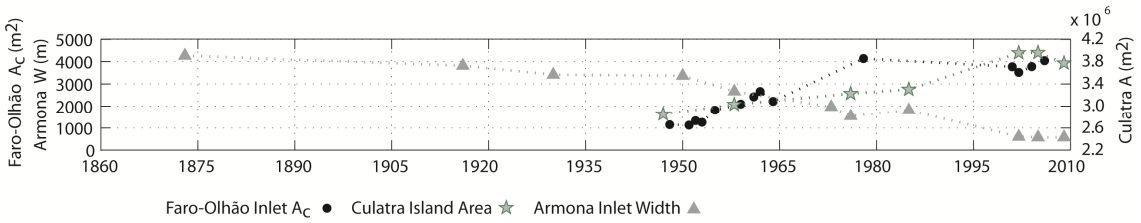

Figure VI.7. Evolution of Faro-Olhão Inlet cross-section A_c, Culatra Island area A, and Armona Inlet width W.

With respect to the tidal prisms (P) of Faro-Olhão and Armona inlets, temporal changes in P (Table VI.3) show that the former main inlet of the system, Armona, lost flow dominance to Faro-Olhão inlet between the 1970s and 1980s. The sum of P for both inlets measured in 2006 gives a total of *c.* 9×10^6 m^3. In general, the values obtained by numerical models (MOHID, http://www.mohid.com, and MIKE21, http://www.mikebydhi.com) slightly overestimate P. Values obtained by Andrade (1990) assume equilibrium conditions, which, as we observe from the evolution of A_c for Faro-Olhão inlet (Table VI.2, Figs. VI.4B, VI.4C, VI.5), were not achieved at that time (c. 1980). Considering the reduced importance of Ancão inlet in the interconnected hydrodynamic sub-system, and the relative stability of Armona inlet's width prior to the opening of Faro-Olhão inlet, it can be assumed that a volume approximately equal to the 2006 value of P formerly flowed through Armona inlet before Faro-Olhão inlet was opened. Today, P through Armona inlet represents *c.* 25% of the total original volume. This value can be directly compared with the evolution of Faro-Olhão A_c, by

computing the ratio between the two limits (2006 and 1948, Table VI.2), where A_{c1948} is *c.* 25% of A_{c2006}.

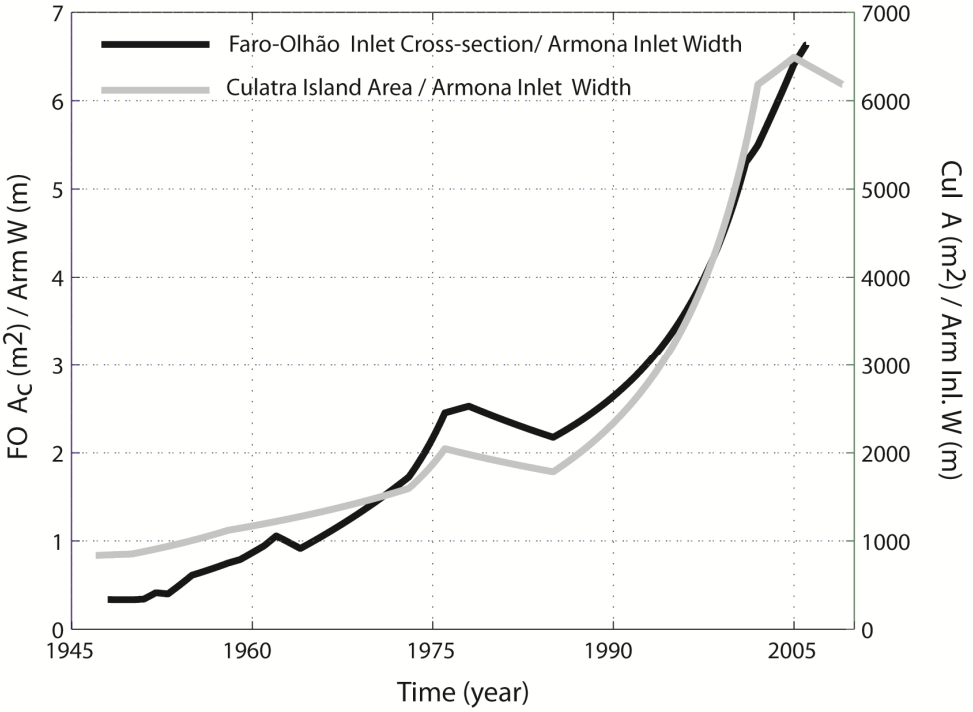

Figure VI.8. Ratio between Faro-Olhão Inlet Ac / Armona Inlet W and between Culatra Island A / Armona Inlet W.

Table VI.3. Compilation of Faro-Olhão and Armona inlets' spring tidal prisms through time, and the methods used for the calculations.

Year	Faro-Olhão Inlet	Armona Inlet	Source	Method
1970	$32x10^6$ m^3	$46x10^6$ m^3	Silva et al., 2002	MOHID, hydrodynamic model based on Navier-Stokes equations with Boussinesq and hydrostatic approximations
1980	$35x10^6$ m^3	$58x10^6$ m^3	Andrade, 1990	Jarret (1976) Tidal Prism/Cross-section equations
1990	$53x10^6$ m^3	$49x10^6$ m^3	Silva et al., 2002	MOHID, hydrodynamic model based on Navier-Stokes equations with Boussinesq and hydrostatic approximations
1996	$70\ x10^6$ m^3	$49x10^6$ m^3	ICN, 1999	MIKE 21, hydrodynamic model. Danish Hydraulic Institute (DHI) study for the Renewal Project, Ria Formosa Lagoon System
2001	$59x10^6$ m^3	$46x10^6$ m^3	Silva et al., 2002	MOHID, hydrodynamic model based on Navier-Stokes equations with Boussinesq and hydrostatic approximations
2006	$64x10^6$ m^3	$24x10^6$ m^3	Pacheco et al., 2010	ADCP tidal cycle measurements

VI.5 DISCUSSION

Since the artificial opening of Faro-Olhão inlet, Armona inlet has gradually lost its hydraulic efficiency, resulting in a large reduction in both its width and cross-sectional area. Although the latter could not be properly quantified due to the lack of complete bathymetric charts, the evolution of Faro-Olhão inlet A_c (Fig. VI.4C, Table VI.2), and the overall tidal prism flow through both inlets, indicates that the reduction represented about 75% of its initial value prior to the opening of Faro-Olhão inlet. Armona inlet previously had two well-defined channels divided by a large sand bank called "Cabeço dos Mortos" (Fig. VI.3) which linked both ebb and flood tidal deltas. Although the whole ebb tidal delta could not be fully reconstructed from the bathymetric charts available (Fig. VI.3, years 1873, 1916, and 1930), it is thought to have had similar or larger dimensions than the flood delta, due to the historic ebb-dominance behaviour of the inlet (Andrade, 1990; Salles, 2001; Salles et al., 2005).

The opening of Faro-Olhão inlet, its stabilisation, and the scouring process related to the evolution of A_c towards stability, greatly reduced the flow through Armona inlet, resulting in a shift in tidal prism dominance from Armona to Faro-Olhão. Tidal inlets, particularly when not constrained by jetties, have very high longshore sediment transport trapping capabilities (Fontolan et al., 2007). For an inlet such as Armona, which used to have a flow of ~9×10^6 m^3, the subsequent flow reduction of about 75% resulted in an oversupply of sediment. Ebb-tidal current loss over the shoal allowed waves and flood tidal currents to push the shoal landward. This in turn provided the sediment necessary to enlarge Culatra Island and to reduce the width of Armona inlet. Further, whenever a new sand spit has been built by longshore sediment transport across the mouth of Armona inlet, it has been immediately incorporated into Culatra Island through the formation of vegetated dune ridges (Garcia et al., 2002). This process led to

the progressive extension of Culatra Island and to the narrowing of Armona inlet, and peaked between the 1980s and 2000 (Fig. VI.7). This occurred at the same time as extensive scouring of Faro-Olhão inlet and its resulting extension offshore.

A clear relationship exists between the evolution of Faro-Olhão and Armona inlets (Fig. VI.8). Previous studies have demonstrated that Faro-Olhão inlet prevents sediment bypassing (Pacheco et al., 2008), and the present study has added further knowledge regarding the local sediment budget by showing that the source of Culatra Island's enlargement is directly related to the recession of Armona inlet's deltas. Tidal prism exchange between interconnected inlets is therefore the main mechanism for morphological changes in this coastal sector. The data also indicate that the cross-section of Faro-Olhão inlet has reached stability (Figs VI.4C and VI.5), that the dimensions of Culatra Island have stabilised (Table VI.1, Fig. VI.6), and that the width of Armona inlet is now essentially constant (Table VI.1, Fig. VI.5).

The area has also been affected significantly by the interception of longshore sediment transport by Faro-Olhão inlet. Erosion rates on Culatra Island are currently $<1x10^4$ m^3/year (Pacheco et al., 2008), and are concentrated immediately downdrift of the east jetty of Faro-Olhão inlet. This constitutes about 10 % of minimum net annual littoral drift in the area (Bettencourt, 1994). Recent data on the evolution of Culatra Island suggest that the coastline has reached stability and that processes acting on the island are mainly cross-shore, with erosion/accretion balanced through the winter/summer seasons and a zero net change in volume (Garcia et al., 2002; Pacheco et al., 2008). The contribution of the net longshore drift to the increase in size of Armona inlet's ebb tidal delta can therefore be considered negligible. Armona inlet also bypasses sand downdrift, and there is no evidence to suggest erosion downdrift of Armona Island. Although Armona inlet has narrowed, the minimum channel cross-section has a current

maximum depth of *c.*10 m (MSL), and a total A_c of 3,000 m^2, a value obtained from the bottom-tracking of the Acoustic Doppler Current Profiler (ADCP) during the 2007 spring-tide survey at high-tide peak. In 1983, based on one of the few available bathymetric maps of the inlet channel, the maximum depth was also *c.*10 m (MSL), and A_c was 4,700 m^2 for a channel length of 1,850 m. Although the inlet has narrowed significantly, it continues to maintain a well-defined, navigable channel (Fig. VI.3).

Recent work on multiple inlet systems (Brouwer, 2006; Brouwer et al., 2008; van de Kreeke et al., 2008) shows that such systems can have several stable equilibrium states, provided that the interaction between inlets is weak. The authors of those studies argue that the equilibrium of multiple inlet systems depends on the degree of connectivity in the basins drained by each inlet. Through numerical simulations, the studies were able to conclude that no stable configuration exists for large wetted cross-sectional areas over topographic highs, approaching the situation of a single lagoon. In other words, if inlet interconnection is strong in multiple inlet systems, one of the inlets will eventually close because the system will tend to behave as a single system. In the case of Faro-Olhão/Armona inlets, the interaction is permanent and strong, although variable through the tidal cycle. Flooding through Faro-Olhão inlet ebbs though Armona inlet. The flushing capacity of Armona inlet is therefore enhanced by its ebb dominance, while Faro-Olhão inlet is always flood-dominated and is a net sediment importer to the system.

VI.6 CONCLUSION

This study has shown how the morphology of an interconnected two-inlet bay system and the adjacent coast in the Ria Formosa, southern Portugal, has evolved after the artificial opening and stabilisation of one inlet. The morphological indicators chosen

reveal the progression of the analysed coastal sector towards stability. The study contributes to our understanding of the equilibrium of multiple inlets with respect to the impacts of anthropogenic activities. In addition, it provides insights into the future evolution of the system which may assist coastal management and planning.

The clear relationships between barrier island dimensions, inlet cross-section/width, and tidal prism demonstrate the importance of ebb-tidal deltas in maintaining the equilibrium of these systems. This equilibrium condition depends to a large extent on the ebb delta sediment reservoir and on the sediment transport capacity of waves during moderate and extreme storm events. Despite the strong interconnection between the two inlets studied, the main inlet (Faro-Olhão) is flood-dominated and imports sediment to the system, enhancing the ebb and flushing capacity of the other interconnected inlet (Armona). Morphological and hydrodynamic indicators presented in the study suggest that equilibrium may be attained in a two-inlet bay system.

Cross-sectional channel areas at inlet entrances are known to adjust generally to local hydrodynamic conditions and to sediment availability. However, the evidence presented within this study raises questions about how to best evaluate the stability of such complex coastal systems. A ‘stable’ inlet does not necessarily imply that the cross-section of that inlet is constant through time and remains equal to the equilibrium flow area. Quantification of the ebb tidal delta volume is necessary for evaluating multiple inlet stability, especially after significant changes in the hydrodynamics of such systems. Because the transport of significant amounts of sediment, especially during storm events, can reduce the hydraulic efficiency of the inlet channels, further research is needed to assess sediment storage in ebb deltas and to discover how that sediment can be mobilized by increased wave activity. In a recent review of the morphodynamics of tidal inlet systems by Swart and Zimmerman (2009), the authors argued that a full

evaluation of the stability of inlet systems requires a detailed coupling of nonlinear dynamics in the backbarrier area, the inlet, and the ebb-tidal delta, including the effect of waves over the delta and in the adjacent coastal zone, especially their role in stirring and transporting the sediment. The case study presented here supports the need for this approach and highlights a requirement to accurately quantify sediment transport over the ebb shoal of Armona inlet in order to establish a better understanding of the dynamic behaviour of the two main inlets of the Ria Formosa system.

VI.7 REFERENCES

Andrade, C. F., 1990. *O Ambiente Barreira da Ria Formosa*, Algarve-Portugal. PhD Thesis, Universidade de Lisboa. 627 p.

Bettencourt, P., 1994. *Les Environnements Sedimentaires de la Côte Sotavento (Algarve, Sud Portugal) et leur Évolution Holocéne et Actuelle*, University Bordeaux I. 98 p.

Brouwer, R.L., 2006. *Equilibrium and stability of a double inlet system*. M.Sc theses Department of Civil Engineering, Delft University of Technology, 81 p.

Brouwer, R.L., Zitman, T.J., Shuttelaars, H.M., van de Kreeke, J., 2008. Effects of amplitude differences on equilibrium and stability of a two-inlet bay system. In Dohmen-Janssen and Hulscher, editors, *River, Coastal and Estuarine Morphodynamics 2008*, London, 2007. RCEM 2007, Taylor & Francis, 33-40.

Buonaiuto, F.S., Kraus, N.C., 2003. Limiting slopes and depths at ebb-tidal shoals. *Coast. Eng.* 48, 51-65.

Cleary, W.J., FitzGerald, D., 2003. Tidal Inlet Response to Natural Sedimentation. Processes and Dredging-Induced Tidal Prism Changes: Mason Inlet, North Carolina. *J. Coast. Res.* 19 (4), 1018-1025.

Costa, M., Silva, R. and Vitorino, J., 2001. Contribuição para o estudo do clima de agitação marítima na costa Portuguesa. *2as Jornadas Portuguesas de Engenharia Costeira e Portuária*, CD-ROM.

Dean, R.G., 1988. Sediment Interaction at Modified Coastal Inlets: Processes and Policies, Hydrodynamics and Sediment Dynamics of Tidal Inlets. *Lecture Notes on Coastal and Estuarine Studies*, D.G. Aubrey and L. Weisher, eds., Vol. 29, Springer – Verlag, New York, NY, 1988, 412-439.

Dean, R.G, Dalrymple, R.A., 2002. *Coastal Processes with Engineering Applications*. Cambridge University Press, United Kingdom, ISBN 0-521-602750-0, 475 p.

Dean, R.G, Walton, T.L., 1973. Sediment transport processes in the vicinity of inlets with special reference to sand trapping. In: CRONIN, L. E.(Ed.), *Estuarine Research*,Vol. 2, Academic Press, New York, 129-149.

Esaguy, A.S., 1984. *Ria de Faro "Barra da Armona", Evolução 1873-1983*. Direcção Geral de Portos Internal Report, 5 p.

Esaguy, A.S., 1986. Ria *de Faro, Barra de Faro-Olhão. Evolução 1955-1985.* Direcção Geral de Portos Internal Report, 10 p.

Escoffier, F.F., 1940. The stability of tidal inlets. *Shore and Beach,* 8, 114-115.

Escoffier, F.F., 1977. *Hydraulics and Stability of Tidal Inlets. General Investigation of Tidal Inlets* (GITI), Report 13, U.S. Army Engineer Waterway Experience Station, Vicksburg , MS, 72 p.

FitzGerald, D.M., 1996. Geomorphic Variability and Morphologic and Sedimentologic Controls on Tidal Inlets. *J. Coast. Res.* SI 23, 47-71.

Fontolan, G., Pillon, S., Delli Quadri, F., Bezzi, A., 2007. Sediment storage at tidal inlets in northern Adriatic lagoons: Ebb-tidal delta morphodynamics, conservation and sand use strategies. *Estuar. Coast. Shelf. Sci.* 75, 261-277.

Garcia, T., Ferreira, Ó., Matias, A., Dias, J.A.. Recent evolution of Culatra Island (Algarve-Portugal). *Proceedings of Littoral 2002*, The Changing Coast. Porto-Portugal, 289-294.

Hansen, M., Knowles, S.C., 1988. Ebb-tidal delta response to jetty construction at three South Carolina inlets, in *Hydrodynamics and Sediment Dynamics of Tidal Inlets*, D.G. Aubrey and L. Weishar, eds., Lecture Notes on Coastal and Estuarine Studies 29, Springer, 364-381.

Hicks, D.M., Hume, T.M., 1997. Determining Sand Volumes and Bathymetric Change on an Ebb-tidal Delta. *J. Coast. Res*. 13 (2), 407-416.

ICN, 1999. Instituto da Conservação da Natureza. Estudo Ambiental do Projecto "Requalificação do Sistema Lagunar da Ria Formosa", Relatório Final da 1ª Fase, Vol. 1 memória descritiva, 223 p.

Jarret, J.T., 1976. *Tidal Prism-Inlet area relationships*. GITI Report, vol. 3. U.S. Army Corps of Engineers, Waterways Experiment Station, Vicksburg, MS.

Kraus, N. C., 2006. Coastal inlet Functional Design: Anticipating Morphological Response, *Proceedings Coastal Dynamics '06* CDROM, ASCE, 14p.

Kraus, N.C., Rosati, J.D. 1998. Estimation of uncertainty in coastal-sediment budgets at inlets. *Coast. Eng. Tech. Note*, IV-16, 12p.

Keulegan, G.H., 1967. Tidal flow in entrances. Water–level fluctuations of basins in communication with seas. *Committee of Water Hydraulics*, US Army Corp of Engineers, Technical Bulletin nº14, 89p.

Mason, J.E., 1986. *Morphologic Evolution of a Relocated Mesotidal Inlet: Captain Sam's Inlet, South Carolina*. Technical Report, Dept. Geol., University South Carolina, 149p.

O'Brien, M.P., 1969. Equilibrium Flow Areas on Inlets on Sandy Coasts. *J. Waterw. Harb. Div*., 95 (WW1), 43-52.

Pacheco, A., Vila-Concejo, A., Ferreira and Ó., Dias, J.A., 2008. Assessment of Tidal Inlet Evolution and Stability Using Sediment Budget Computations and Hydraulic Parameter Analysis. *Mar. Geol.,* 247, 104-127.

Pacheco, A., Ferreira, Ó., Williams, J.J., Garel, E., Vila-Concejo, A., Dias, A., 2010. Hydrodynamics and Equilibrium of a Multiple-Inlet System. *Mar. Geol.,* 274, 32-42.

Pope, J., 1991. Ebb delta and shoreline response to inlet stabilization, examples from the southeast Atlantic Coast, *Proc. Coastal Zone '9*1, ASCE, 643-654.

Rosati, J.D., 2005. Concepts in Sediment Budgets. *J. Coast. Res.,* 21 (2), 307-322.

Salles, P., 2001. *Hydrodynamic Controls on Multiple Tidal inlet Persistence*. PhD Thesis, Massachusetts Institute of Technology and Woods Hole Oceanographic Institution, 272p.

Salles, P., Voulgaris, G. and Aubrey, D., 2005. Contribution of nonlinear mechanisms in the persistence of multiple tidal inlet systems. *Estuar. Coast. Shelf. Sci.* 65, 475-491.

Seabergh, W.C. 2006. Hydrodynamics of Tidal inlets. In: Demirbilek, Z. (editor), *Coastal Engineering Manual*, Part II, Coastal Hydrodynamics, Chapter II-6, Engineer Manual 1110-2-1100, U.S. Army Corps of Engineers, Washington, DC, 73p.

Silva, J.R.A., Leitão, P.C., Braunschweig, F., Neves, R., 2002. Ria Formosa 3D hydrodynamic model. A contribution for the understanding of the Faro-Olhão Inlet processes. *Proceedings of Littoral.* 2002, 197-207.

Swart, de H.E., Zimmerman, J.T.F., 2009. Morphodynamics of Tidal Inlet Systems. *Annu. Rev. Fluid Mech*., 41: 203-229.

van de Kreeke, J., 1992. Stability of Tidal Inlets; Escoffiers Analysis, *Shore Beach* 60(1), 9-12.

van de Kreeke, J., Brouwer, R.L., Zitman, T.J., Schuttelaars, H.M., 2008. The effect of a topography high on the morphological stability of a two-inlet bay system. *Coast. Eng.,* 55, 319-332.

Walton, Jr., T.L., Adams, T.L., 1976. Capacity of Inlet Outer Bars to Store Sand. *Proc. of the 15th Coastal Engineer Conference*, ASCE, Vol. 2, 1919-1937.

CHAPTER VII

General conclusions

VII.1 SUMMARY

The opening of tidal inlets and subsequent readjustment of the tidal prism are responsible for significant changes along adjacent coastlines, especially in multi-inlet systems. This process is more evident when jetties are involved in inlet stabilisation, because they disrupt natural inlet migration patterns and impact the overall sediment budget of the coastal cells involved. The Ria Formosa multi-inlet system, like other inlet systems, has been subjected to several anthropogenic activities with marked effects on the neighbouring coast. The Faro-Olhão Inlet's opening provides an informative case study of the associated and unpredictable effects of anthropogenic intervention, which in this example caused pronounced sediment scouring, the narrowing of Armona Inlet and the growth of Culatra Island.

No previous study has made a convincing attempt to develop inlet history based on sediment budget calculations and to link this to inlet parameters. The analysis of inlet channel evolution and cross-sectional area with respect to the progression towards inlet geometric stability can be of great value in understanding sediment patterns. If the inlet cross-section is not in dynamic equilibrium, the cells comprising the inlet budget area are also out of dynamic equilibrium and therefore will undergo changes until equilibrium is achieved between the adjacent coast, deltas and inlet channel area.

Throughout this thesis, both historical and present hydrodynamic and sediment transport patterns were analysed. Methods for quantifying hydrodynamic and sediment transport patterns were presented, based primarily on data acquired using high frequency acoustic equipment, and by applying well established methodologies and empirical formulae to calculate tidal prism and net sediment transport quantities. Methodologies presented throughout the thesis can be applied generally to multiple-inlet systems around the world.

The analyses demonstrated that combining inlet hydraulic analysis with detailed sediment budget analysis can help to interpret sediment pathways and assign approximate values to their magnitudes. Throughout Chapter II, new sediment budget concepts developed by Rosati (2005) are applied with an emphasis on uncertainty calculations. Instead of using longshore sediment transport rates and computing several "representative budgets", the approach taken in this thesis considers the rate of longshore transport as unknown and unchanging, thereby coupling the balanced budget obtained with inlet parameter analysis in order to understand sediment pathways and accretion/erosion tendencies within each coastal cell. Analysis of uncertainty, a central element of modern data treatment, plays an important role both in avoiding over-interpretation of data and in highlighting how the sediment budget could become better constrained in the future.

For the case-study analysed, the Faro-Olhão Inlet, the sediment budget reveals that the inlet is only just reaching equilibrium. Although its cross-sectional area reached equilibrium around 1978, observed stability is related to jetties and a stratigraphy control that prevents further deepening, and not to the achievement of dynamic equilibrium. The intense scouring process occurring in the inlet offshore area continued after 1978, and was responsible for redistributing sediments in the inlet area and adjacent coast. This redistribution implies several possible sediment transport paths. The most likely path, as interpreted from the sediment budget computations, appears to be the loss of sediment to the offshore area as a result of the seaward progression of the scouring process.

In terms of progress in the use of data processing methods, this thesis presented a statistical evaluation of two theoretical fitting methods - logarithmic and power law - commonly used to extrapolate velocities to unmeasured areas of a vertical profile, such

as near-bottom velocities, which can then be applied to estimate bed-friction velocities used in sediment transport formulae. The work is presented in Chapter III and was motivated by the increasing use of boat-mounted ADCPs to measure discharge and sediment transport estimates. Analysis of covariance (ANCOVA) was used to test the models' performance when applied to velocity data collected with ADCPs. The logarithmic law model proved to be more robust across different velocities and channel morphologies and should be adopted as the preferred method for extrapolating velocity profiles when using boat-mounted ADCPs in confined channels and at inlet entrances. Both models consistently produce better simulations in inlets with larger cross-sectional areas, where turbulence scales are more attenuated due to spatial averaging.

Hydrodynamic measurements, especially inlet tidal prism quantification, proved to be essential when it came to inferring the stability of the overall system, understanding inlet circulation patterns and evaluating their influence on the pathways and magnitude of sediment transport. By presenting data on hydrodynamics and circulation patterns measured over a spring-neap tidal cycle in the Ria Formosa multiple-inlet system, the data showed that the Faro-Olhão and Armona inlets - which represent almost 90% of the total prism of the system - are always interconnected, but transfer large portions of tidal prism between them and drain the basin more independently for a portion of the neap-spring tidal cycle.

At spring-tides, Ancão inlet and the two main inlets are interconnected, showing a clear circulation pattern. The three inlets present ebb-dominated behaviour from a conventional viewpoint (higher mean ebb velocity is associated with shorter ebb duration), although the flood prism is considerably higher than the ebb prism at Faro-Olhão Inlet but is lower than the ebb prism at Ancão and Armona inlets. At neap-tides, larger flood/ebb prisms were always found to correspond to longer flood/ebb durations.

The results therefore support the idea (Salles et al., 2005) that, in contrast to single-inlet systems, the flood/ebb dominance concept cannot be generally applied to multiple-inlet systems.

Recent work on multiple inlet systems (Brouwer, 2006; Brouwer et al., 2008; van de Kreeke et al., 2008) shows that the equilibrium of multiple-inlet systems depends on the degree of connectivity between the basins. Through numerical simulations, those studies were able to conclude that if inlet interconnection is strong in multiple inlet systems, one of the inlets will ultimately close because the system will behave as a single basin. This present thesis revealed that Faro-Olhão and Armona inlets are strongly interconnected, although this interconnection is variable through the tidal cycle. The findings support the hypothesis proposed by other authors (Salles et al., 2005) that the capacity to exchange large portions of prism, while maintaining independent behaviour for the majority of the neap-spring tidal cycle, can contribute to the stability of multiple inlets by altering residual flow and, consequently, transport capacity. The prediction of the evolution of these two inlets would appear to rely on factors that cannot be approached using empirical equilibrium relationships or derived from inlet hydraulics.

Quantification of sediment transport in tidal inlets remains a fundamental requirement for both conceptual and numerical modelling of tidal inlet function and evolution. Since field-based studies of sediment transport have the potential to quantify the magnitude and direction of net sediment transport, they may assist in identifying evolutionary trends for a single tidal inlet or a multi-inlet system. Through Chapter V, the use of well-established empirical formulae, locally calibrated with high-frequency current and water-level data, allowed net sediment transport to be derived for the Ria Formosa. By quantifying annual net sediment transport, this work has increased

knowledge about sediment dynamics in multiple inlet systems and identified appropriate approaches for the prediction of sediment transport in these environments. The approach has accurately reproduced the known magnitude and direction of sediment transport through the tidal inlets of the Ria Formosa, supporting the hypothesis that the main inlet of the system, Faro-Olhão Inlet, acts as a sediment sink in the system. Although mean velocities are higher at ebb than at flood, and ebb duration is shorter, the distortion of the velocity field produces higher maximum flood velocities (see Chapter IV). Therefore sediment transport at Faro-Olhão Inlet is oriented strongly landward, dominating over the weakly seaward residual velocity and the moderately distorted velocity field.

The model allows processes, such as sediment trapping, to be identified and flushing capacity to be established. If coupled with long-term quantification of ebb/flood delta volumes, the method proved to be useful in calculating medium- to long-term sediment budgets. This has particular importance when attempting to understand sediment transport at inlet mouths, to quantify infilling rates and to define an optimal dredging volume. Together, these elements contribute to improved knowledge of inlet sediment dynamics, with broad application in a range of regional sediment management issues.

Finally, in Chapter VI, the impacts of the opening of an inlet on a multiple inlet system are analysed. Focusing on the two main inlets of the Ria Formosa system in Portugal - the Faro-Olhão and Armona inlets - the equilibrium and future evolution of the system are inferred from morphological indicators. The dataset couples the evolution of the inlet cross-section, changes in tidal prism, and changes in the dimensions (length and area) of barrier islands to give a regional perspective on the impacts that human intervention has had on the system. The methods presented can be applied to other multiple-inlet systems. In the case of Ria Formosa, retreat of the

Armona tidal deltas has occurred as a direct consequence of tidal-prism loss due to the opening of the Faro-Olhão Inlet. Ebb-tidal current-loss over the shoal allowed waves and flood currents to push the shoal landward, contributing sediment to expand Culatra Island and narrow the Armona Inlet.

Throughout Chapter II, sediment budget analysis demonstrated that Faro-Olhão Inlet is impermeable to sediment bypassing (longshore transport). The work developed in Chapter VI augmented this sediment budget model, showing that the source of Culatra Island's growth is directly related to the recession of Armona Inlet's deltas. Tidal prism exchange between interconnected inlets is therefore the main mechanism for morphological changes in this coastal sector. The study also concludes that littoral drift in the area has been reformulated due to the blockage of the Faro-Olhão Inlet. Present erosion rates on Culatra Island are negligible, indicating that the coastline has reached stability. Beach processes occurring through the island are mainly cross-shore, with erosion/accretion balanced through the winter/summer seasons and a zero net exchange of volume. The contribution of net longshore drift to the increase in size of Armona Inlet's ebb tidal delta can therefore be considered negligible. Armona Inlet also bypasses sand downdrift, and there is no evidence from coastal evolution to suggest erosion downdrift of Armona Island. Although Armona Inlet has narrowed, it continues to maintain a well defined, navigable channel.

Despite the Armona Inlet's demonstrated capacity to redeposit sediments offshore under fair-weather conditions, a capacity enhanced by its ebb dominance (Chapter IV and V), a significant amount of sediments stored in the ebb tidal delta from previous hydraulic configurations can be transported onshore by increased wave activity. This net sediment influx can reduce the hydraulic efficiency of the channels. Analysis of the morphological evolution of the interconnected two-bay system and adjacent coast since

the artificial opening and stabilisation of one inlet demonstrated importance of ebb-tidal deltas in maintaining the equilibrium of these systems.

VII.2 RECCOMENDATIONS FOR FURTHER WORK

Although the evolution of cross-sectional area is a valuable parameter with which to analyse the locational/geometrical stability of an inlet, it should be complemented with analysis of other external controls. Existing formulae, widely used to infer inlet stability, relate cross-sectional area to the tidal prism and include terms to represent wave energy versus sediment storage on the ebb-tidal delta. Such formulae should be reviewed with a view to including other variables (e.g. stratigraphy controls) and to making them more adaptable in their application.

Annual variations of longshore transport rates can affect the morphology and therefore equilibrium of the inlets and adjacent coastlines. These values are normally considered to remain constant through the year and are used on decadal sediment budget computations, which can render the interpretation of morphology and sediment transport paths more difficult. This factor should be better studied and included in the various models of coastal morphology.

Residual flow between inlets can play an important role in enhancing stability, as can the morphology of the inner channels connecting both inlets, although these dynamics require further research. Also, the capacity of an inlet to flush sediments during prevailing fair-weather conditions is not sufficient to counter the entry of sediment into the system during periods of storm activity or under intense wave-current interaction. The current-wave process during storms, combined with the availability of sediment offshore, leads to the obstruction of inlet channels, affecting their hydraulic efficiency and eventually leading to inlet closure in the long term. The long-term

equilibrium of sediment storage in the ebb-tidal deltas must be considered when analysing the possible equilibrium of multiple-inlet systems.

Following van de Kreeke et al. (2008), who showed that depending on the length and friction factor of the inlet channels there can be stable configurations, the causes and conditions that determine those equilibrium conditions are not clear and must be better studied. A full evaluation of the stability of inlet systems requires a detailed coupling of nonlinear dynamics in the backbarrier area, inlet and ebb-tidal delta, including the effect of waves over the delta and in the adjacent coastal zone and especially their role in stirring and transporting the sediment. A robust evaluation of the stability of the two main inlets of the Ria Formosa system can only be fully achieved by quantifying sediment transport over the ebb shoal of Armona Inlet. Finally, unless net longshore transport is negligible, it would be wise to emplace rigorous long-term monitoring of sediment bypassing processes prior to the opening of a new inlet in any coastal barrier system.

VII.3 REFERENCES

Brouwer, R.L., 2006. Equilibrium and stability of a double inlet system. M.Sc theses Department of Civil Engineering,DelftUniversity of Technology, 81 pp.

Brouwer, R.L., Zitman, T.J., Shuttelaars, H.M., van de Kreeke, J., 2008. Effects of amplitude differences on equilibrium and stability of a two-inlet bay system. In Dohmen-Janssen and Hulscher, editors, *River, Coastal and Estuarine Morphodynamics 2008*, pages 33-40, London, 2007. RCEM 2007, Taylor & Francis.

Rosati, J.D., 2005. Concepts in Sediment Budgets. J. Coast. Res. 21 (2), 307-322.

Salles, P., Voulgaris, G. and Aubrey, D., 2005. Contribution of nonlinear mechanisms in the persistence of multiple tidal inlet systems. *Estuar. Coast. Shelf. Sci.* 65, 475-491.

van de Kreeke, J., Brouwer, R.L., Zitman, T.J., Schuttelaars, H.M., 2008. The effect of a topography high on the morphological stability of a two-inlet bay system. *Coast. Eng.* 55, 319-332.